INVESTIGATIONS OF BOUNDARY LAYER PHENOMENA USING A NEW METHOD OF OBSERVATION

Thesis Presented By

ALLAN ALEXANDER NICOL
A.R.T.C.

for the Degree of

Doctor of Philosophy

University of Edinburgh

October 1958

C O N T E N T S

C O N T E N T S (Contd.)

PREFACE

This research was carried out under the joint supervision of Dr. M.A.S. Ross, Department of Natural Philosophy, University of Edinburgh, and Professor W.H.J. Childs, Department of Physics, Heriot Watt College.

The experimental work was conducted in co-operation with Mr. J.G. Burns, who was responsible for the early work on the vane and who developed a mathematical theory for its natural frequencies.

SYMBOLS

x - Distance from leading edge of flat plate

y - Distance from surface of plate

z - Distance at right angles to x and y and measured from centre of flat plate

U_o - Mean free stream velocity

U - Mean velocity at point in the boundary layer in the direction x

V - Mean velocity in the direction y

u_1 - Component of total velocity in the x direction

v_1 - Component of total velocity in the y direction

u - Instantaneous x component of velocity fluctuation

v - Instantaneous y component of velocity fluctuation

u' - Root Mean Square value of x component of turbulent velocity fluctuation

v' - Root Mean Square value of y component of turbulent velocity fluctuation

w' - Root Mean Square value of z component of turbulent velocity fluctuation

P - Mean pressure at some point in the boundary layer

p - Instantaneous pressure fluctuation produced by disturbance

p_1 - Component of total pressure

C_r - Wave velocity

β_r = $2\pi f$, where f is the frequency

α = $\frac{2\pi}{\lambda}$, where λ is the wavelength

β_i - Amplification coefficient

ρ - Density

μ - Viscosity

ν = $\frac{\mu}{\rho}$ Kinematic Viscosity

SYMBOLS (Contd.)

q - Dynamic pressure

δ - Boundary layer thickness

δ^* - Boundary layer displacement thickness

$\delta^* = 1.72\sqrt{\frac{x}{U_o}}$ for Blasius velocity distribution

$R = \frac{U_o \delta^*}{\nu}$ - Reynolds number

$R_x = \frac{U_o x}{\nu}$ = x-Reynolds number

$R = 1.72\sqrt{Rx}$ for Blasius velocity distribution

L = Scale of u' fluctuations

The symbols given here are those occurring regularly throughout this research. Wherever any single expression has occurred in the text, the symbols used have been defined then and there.

INTRODUCTION

This thesis is a study of the boundary layer on a flat plate, using a new method of observation. The boundary layer, and in particular, the laminar region, has been examined using a new device, which takes the form of a small vane. This vane is freely hinged and suspended at its leading edge, lies vertically in the xz plane, and its dimensions are of the same order as the wavelengths of the disturbances, to which it is expected to respond. Such an instrument responds only to v fluctuations of velocity and is uninfluenced by those of u and w.

The ultimate aim of the research programme is to use the vane in the transition and turbulent regions, and attempt to obtain information on the formation of turbulence. Before

the vane can be put in the turbulent region, however, its own performance has to be ascertained, by investigating relatively well known phenomena in the laminar region, and this forms the subject of the thesis.

CHAPTER 1

THE BOUNDARY LAYER: TRANSITION AND TURBULENCE

1.1. The Boundary Layer

When a fluid flows past a solid boundary, the part of it in contact with and nearest to the boundary is retarded by virtue of its viscosity. It is this part that is termed the boundary layer, the concept being due to L. Prandtl, 1904.

In this thin layer the velocity of the fluid increases from zero at the wall (no slip) to its full free stream value, which corresponds to external frictionless flow. Broadly speaking the boundary layer can be divided into three sections, the laminar, transition and turbulent regions, occurring in that order, with increasing Reynolds number. The equations governing the flow in the laminar region, which is smooth and undisturbed, were originally solved by Blasius, 1908, and more recently, with a high degree of accuracy by L. Howarth, 1938. Excellent experimental agreement has been obtained by Nikuradse, 1942. As the Reynolds number increases, the flow becomes more disturbed, momentum changes take place at right angles to it, and as a result, the velocity distribution over a cross-section of the boundary layer is much more uniform for turbulent than for laminar flow.

1.2. Laminar Separation Theory.

Various theories have been proposed regarding the nature of transition from laminar to turbulent flow. One of the earliest was that of G.I. Taylor, 1936. His theory was that transition was caused by separation, either momentary or permanent in the laminar region, due to the varying pressure gradients accompanying turbulence in the flow outside the boundary layer. Thus transition should be governed by the Karman-Polhausen parameter for laminar separation. For isotropic turbulence such as occurs in the wake of a grid, Taylor was able to relate the Karman-Polhausen parameter to the measurable free stream quantities, scale and intensity. He was therefore able to relate the pressure forces causing intermittent separation to free stream quantities. Taylor evolved the relation $\left[\frac{u'}{U_0} \left(\frac{x}{L} \right)^{\frac{1}{5}} \right]$ as the parameter which determines the Rx value at which the boundary layer becomes turbulent. Taylor confirmed that this parameter does control transition with fairly large values of free stream turbulence on flat plates, spheres and elliptic cylinders. This theory has met with objections, the main one being that separation has not been shown to be a necessary condition for transition.

1.3. The Method of Small Disturbances.

About the same time as Taylor put forward his theory Tollmien (1931) and Schlichting (1933), presented a purely theoretical solution which assumed small disturbances in the flow. As a result of this theory it was suggested that transition was governed by the frequency, rather than the magnitude, of the disturbance. Since this theory is now accepted, a brief review of the mathematics and most important results would be useful at this stage.

In this method only disturbances which are compatible with the equations of motion are admitted, and their application to the case of two-dimensional mean flow is considered. Further simplifications include that the mean velocity U depends only on y , i.e. U = f(y) whereas V is assumed zero everywhere, i.e. V = 0.

Upon this flow is assumed a two-dimensional disturbance, which is a function of time as well as space and is represented by,

$$u = f_1(x,y,t)$$
$$v = f_2(x,y,t) \qquad (1)$$

The full Navier-Stokes equations for three-dimensional flow are,

$$\rho\frac{\partial u_1}{\partial t}+u_1\frac{\partial u_1}{\partial x}+v_1\frac{\partial u_1}{\partial y}+w_1\frac{\partial u_1}{\partial z}=X-\frac{\partial p_1}{\partial x}+\mu\left(\frac{\partial^2 u_1}{\partial x^2}+\frac{\partial^2 u_1}{\partial y^2}+\frac{\partial^2 u_1}{\partial z^2}\right)$$

$$\rho\frac{\partial v_1}{\partial t}+u_1\frac{\partial v_1}{\partial x}+v_1\frac{\partial v_1}{\partial y}+w_1\frac{\partial v_1}{\partial z}=Y-\frac{\partial p_1}{\partial y}+\mu\left(\frac{\partial^2 v_1}{\partial x^2}+\frac{\partial^2 v_1}{\partial y^2}+\frac{\partial^2 v_1}{\partial z^2}\right)$$

$$\rho\frac{\partial w_1}{\partial t}+u_1\frac{\partial w_1}{\partial x}+v_1\frac{\partial w_1}{\partial y}+w_1\frac{\partial w_1}{\partial z}=Z-\frac{\partial p_1}{\partial z}+\mu\left(\frac{\partial^2 w_1}{\partial x^2}+\frac{\partial^2 w_1}{\partial y^2}+\frac{\partial^2 w_1}{\partial z^2}\right)$$

$$\frac{\partial u_1}{\partial x}+\frac{\partial v_1}{\partial y}+\frac{\partial w_1}{\partial z}=0 \qquad (2)$$

On substituting the components of total velocity,

$$u_1=U+u\ ,\quad v_1=v\ ,\quad p_1=P+p$$

and reducing to two dimensions, neglecting the differential coefficients and products of disturbance velocities, the Navier-Stokes equations become,

$$\frac{\partial u}{\partial t}+U\frac{\partial u}{\partial x}+v\frac{\partial U}{\partial y}=\nu\left(\frac{\partial^2 U}{\partial y^2}+\frac{\partial^2 u}{\partial x^2}+\frac{\partial^2 u}{\partial y^2}\right)-\frac{1}{\rho}\left(\frac{\partial P}{\partial x}+\frac{\partial p}{\partial x}\right)$$

$$\frac{\partial v}{\partial t}+U\frac{\partial v}{\partial x}=\nu\left(\frac{\partial^2 v}{\partial x^2}+\frac{\partial^2 v}{\partial y^2}\right)-\frac{1}{\rho}\left(\frac{\partial P}{\partial y}+\frac{\partial p}{\partial y}\right) \qquad (3)$$

and the equation of continuity is

$$\frac{\partial u}{\partial x}+\frac{\partial v}{\partial y}=0 \qquad (4)$$

If it is considered that the mean flow itself satisfies the Navier-Stokes equations, then by subtracting from equation (3) the corresponding Navier-Stokes equation for $u = v = p = 0$, the following two equations are obtained in terms of the disturbances only,

$$\frac{\partial u}{\partial t} + U\frac{\partial u}{\partial x} + v\frac{\partial U}{\partial y} = \nu\left(\frac{\partial^2 u}{\partial x^2} + \frac{\partial^2 u}{\partial y^2}\right) - \frac{1}{\rho}\frac{\partial p}{\partial x} \qquad (5a)$$

$$\frac{\partial v}{\partial t} + U\frac{\partial v}{\partial x} = \nu\left(\frac{\partial^2 v}{\partial x^2} + \frac{\partial^2 v}{\partial y^2}\right) - \frac{1}{\rho}\frac{\partial p}{\partial y} \qquad (5b)$$

$$\frac{\partial u}{\partial x} + \frac{\partial v}{\partial t} = 0 \qquad (6)$$

The pressure terms can be eliminated by differentiating (5a) with respect to y, and (5b) with respect to x and subtracting. The result is a linear homogeneous equation in u and v.

$$\frac{\partial^2 u}{\partial y\,\partial t} + U\frac{\partial^2 u}{\partial x\,\partial y} + \frac{\partial U}{\partial y}\frac{\partial u}{\partial x} + v\frac{\partial^2 u}{\partial y^2} + \frac{\partial v}{\partial y}\frac{\partial U}{\partial y} - \frac{\partial^2 v}{\partial x\,\partial t} - U\frac{\partial^2 v}{\partial x^2}$$

$$= \nu\left(\frac{\partial^3 u}{\partial x^2\,\partial y} + \frac{\partial^3 u}{\partial y^3} - \frac{\partial^3 v}{\partial x^3} - \frac{\partial^3 v}{\partial y^2\,\partial x}\right) \qquad (7)$$

Since it has been assumed that the perturbation

is two dimensional, then it is possible to introduce a stream function $\psi(x,y,t)$ such that

$$u = \frac{\partial \psi}{\partial y} \qquad v = -\frac{\partial \psi}{\partial x} \tag{8}$$

The stream function representing a single oscillation of the disturbance is assumed to be of the form

$$\psi(x,y,t) = \phi(y) e^{i(\alpha x - \beta t)} = \phi(y) e^{i\alpha(x-ct)} \tag{9}$$

where $\phi(y)$ represents the initial amplitude of the stream function which depends only on y, $\alpha = \frac{2\pi}{\lambda}$ where λ is the wavelength and t is the time. Since β and hence c are generally complex quantities, equation (9) may be written

$$\psi = \phi(y)\, e^{i[\alpha x - (\beta_r + i\beta_i)t]} = \phi(y) e^{[i\alpha(x-(c_r+ic_i)t]}$$

where β_r, the real part, is the angular velocity or $2\pi f$ (f is the frequency) and β_i, the imaginary part, is the coefficient of amplification or damping depending on whether it is positive or negative.

Hence

$$u = \frac{\partial \psi}{\partial y} = \phi'(y)\, e^{i(\alpha x - \beta t)} \tag{10}$$

$$v = -\frac{\partial \psi}{\partial x} = -i\alpha \phi(y) e^{i(\alpha x - \beta t)}$$

and when these values are substituted into equation (7) the result is

$$(U-c)(\phi''-\alpha^2\phi)-U''\phi = \frac{i\nu}{\alpha}\left(\phi''''-2\alpha^2\phi''+\alpha^4\phi\right) \tag{11}$$

Equation (11) is a homogeneous linear differential equation of the fourth order with a general solution of the form

$$F = C_1\phi_1 + C_2\phi_2 + C_3\phi_3 + C_4\phi_4 \tag{12}$$

where ϕ_1, ϕ_2, ϕ_3, ϕ_4 are the particular solutions and C_1, C_2, C_3, C_4 are the constants of integration.

The evaluation of the four particular solutions of the general stability equation is an extremely difficult task and will only be outlined here. H. Schlichting 1951 provides a full discussion of the theory.

The method consists of finding two solutions ϕ_1 and ϕ_2 from the so-called frictionless stability equation, i.e. equation (11) with the right-hand side terms neglected when R is large.

i.e. $$(U-c)(\phi''-\alpha^2\phi)-U''\phi = 0 \tag{13}$$

The coefficients ϕ_3 and ϕ_4 are now deduced from a new subsidiary equation, which itself is deduced from the full equation (11), retaining only the most important

viscous term. The particular solutions ϕ_3 and ϕ_4 take into account the essential influence of viscosity on the disturbances and their purpose is to enable all four of the boundary conditions to be satisfied, the non-viscous solutions ϕ_1 and ϕ_2 being capable of satisfying only two.

The result which is of greatest interest to this present research is presented as Fig. 1. The axes are non-dimensionalized and are essentially frequency against x distance along the plate. Any disturbance with a frequency falling inside the enclosed loop will be amplified and disturbances falling outside the loop will be damped. Therefore a disturbance, of a particular frequency, as it travels down the plate, will first be damped, then amplified as it crosses the neutral stability curve and then damped again. From this theory it was assumed then, that eventually the amplitude of the amplified disturbances became so great as to effect transition from laminar to turbulent flow.

This result predicted then that transition was caused by disturbances inside the boundary layer, whereas with the older theory of G.I. Taylor, transition was attributed to finite disturbances in the flow outside the boundary layer.

The decision as to which of the two theories should be adopted had to be left to experiment.

Boundary layer flow along a flat plate was first investigated experimentally by J.M. Burgers, 1924. Later H.L. Dryden, 1934, 1939, and his colleagues undertook a very thorough and careful investigation of this type of flow. During the course of those investigations extensive data on the velocity distribution were carefully plotted with the aid of hot wire anemometers in terms of space coordinates and time. However these particular experiments failed to show the existence of neutral or amplified oscillations of the type predicted by Tollmien's theory.

1.4. Experimental Verification of the Theory of Small Disturbances.

Eventually in 1940, H.L. Dryden assisted by G.B. Schubauer and H.K. Skramstad undertook an extensive experimental programme of investigation into the phenomenon of transition from laminar to turbulent flow. They attached great importance to the effect of free stream turbulence and by using screens and honeycombs they achieved the extremely low and never previously attained value of $\frac{u'}{U_o} = 0.02$. The stream was then used to investigate the boundary layer on a flat plate at zero incidence and great care was taken to ensure that the pressure gradient was as nearly zero as possible. Finally Schubauer and Skramstad

1947, verified beyond all doubt the existence of the so-called boundary layer oscillations. Using hot wire equipment, they observed the amplification of the natural oscillations causing transition. As the transition region was approached the amplitude of the oscillations became extremely large, and at the point of transition the regular fluctuations transformed abruptly into irregular fluctuations of high frequency which are characteristic of turbulent flow.

With the aid of this experiment, they were also able to show that when the free stream turbulence is raised above 1%, then transition is caused directly by the random disturbances, and that no selective amplification of sinusoidal disturbances takes place. In so doing, Schubauer and Skramstad discovered the reason for the failure of previous researchers to observe the laminar oscillations.

Even more important than detecting the natural laminar oscillations they were able to detect the growth or decay of controlled artificial disturbances, introduced into the boundary layer. Using a very thin vibrating ribbon of variable frequency, they were able to inject a disturbance of any particular frequency into the boundary layer, and by following its progress downstream, verified completely the neutral stability curve. The agreement with the theoretical curve of Tollmien and Schlichting is shown in Fig. 2.

Another interesting result emerging from the research of Schubauer and Skramstad is that shown in Fig. 3. The critical Reynolds number of transition increases considerably as the intensity of turbulence is decreased. A maximum value of $R_x = 3 \times 10^6$ is reached at an intensity of 0.1%. This demonstrates the existence of an upper limit to the critical Reynolds number.

Following this excellent confirmation of the theory, C.C. Lin, 1945, revised the theory of stability and the calculations of W. Tollmien and H. Schlichting, and showed that agreement existed at all essential points, the main difference being a slight shifting of branch 2 of the curve.

From their results Schubauer and Skramstad formulated a new theory of transition, and used the analogy of the formation of turbulence from a free vortex sheet. The boundary layer first becomes wave-like, and eventually discrete eddies appear, as is usually assumed for a vortex sheet. These eddies in themselves are very unstable and eventually decay into turbulence. This decay is gradual, the random turbulent motion only occurring part of the time. This explanation seems to fit their quantitative data better than the explanation of intermittent separation. In the oscillograms presented by Schubauer and Skramstad, of hot-wire output downstream of the vibrating ribbon,

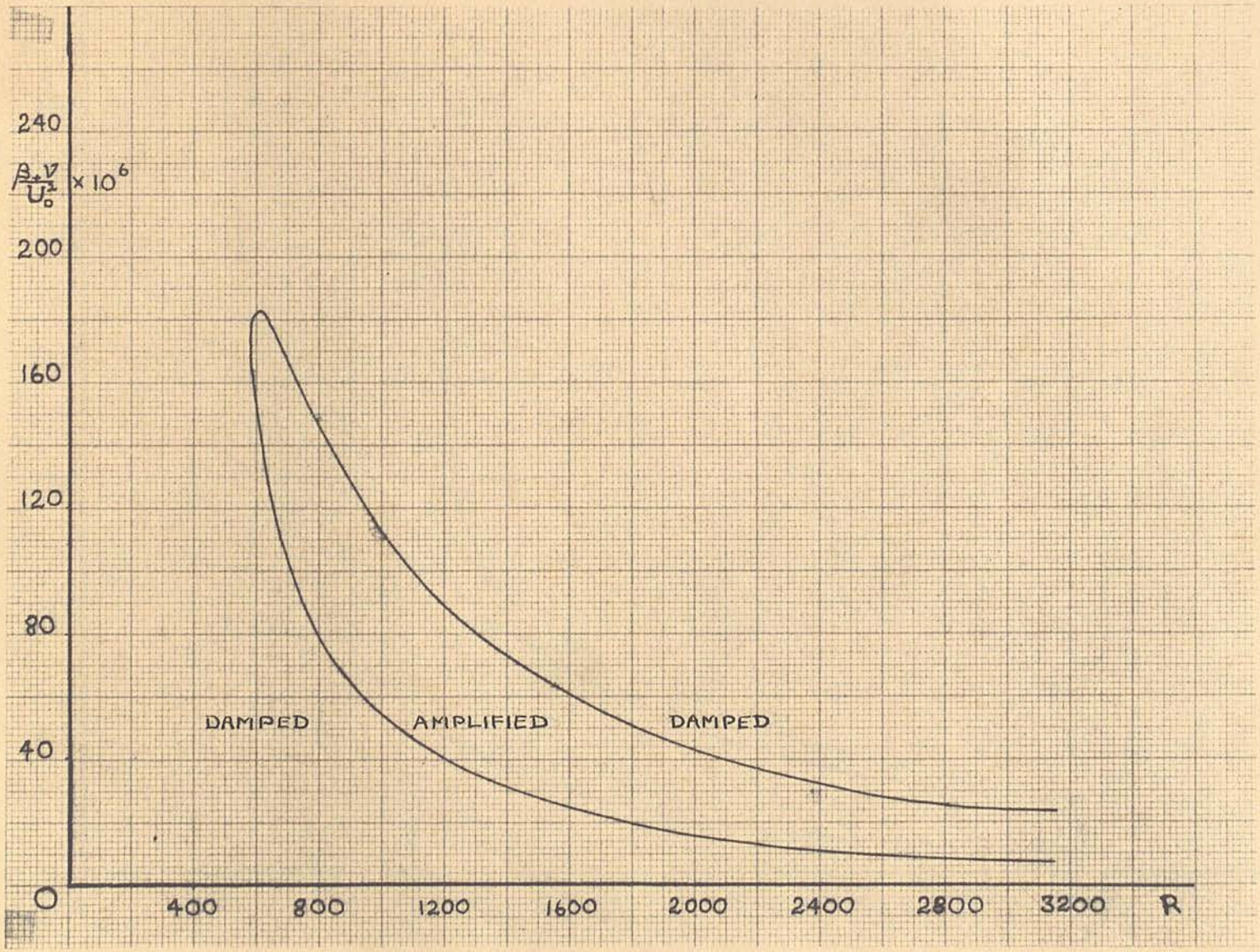

FIG.1 Theoretical Neutral Stability Curve according to Schlichting.

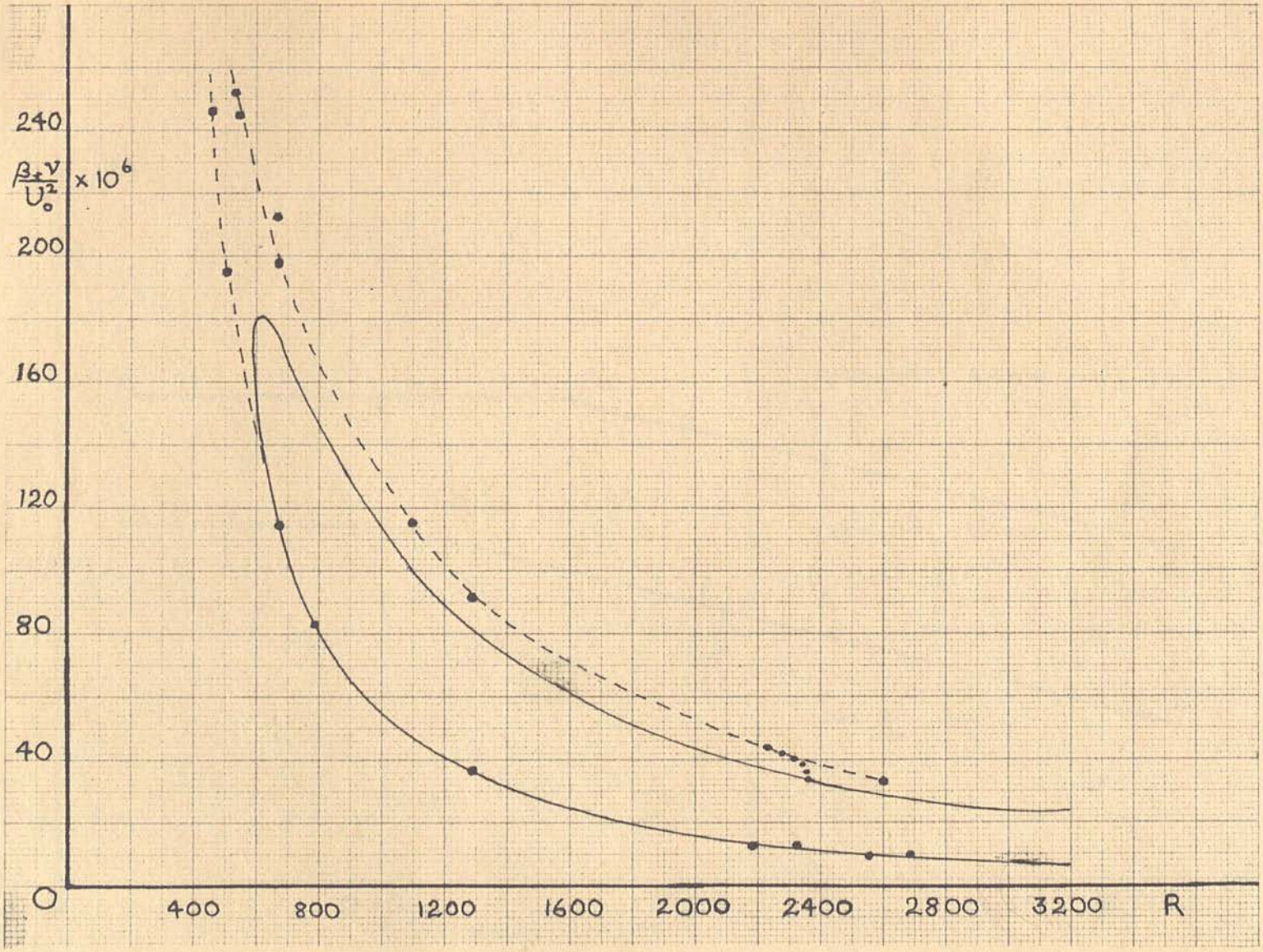

FIG.2 Experimental Verification of Neutral Stability Curve by Schubauer and Skramstad.

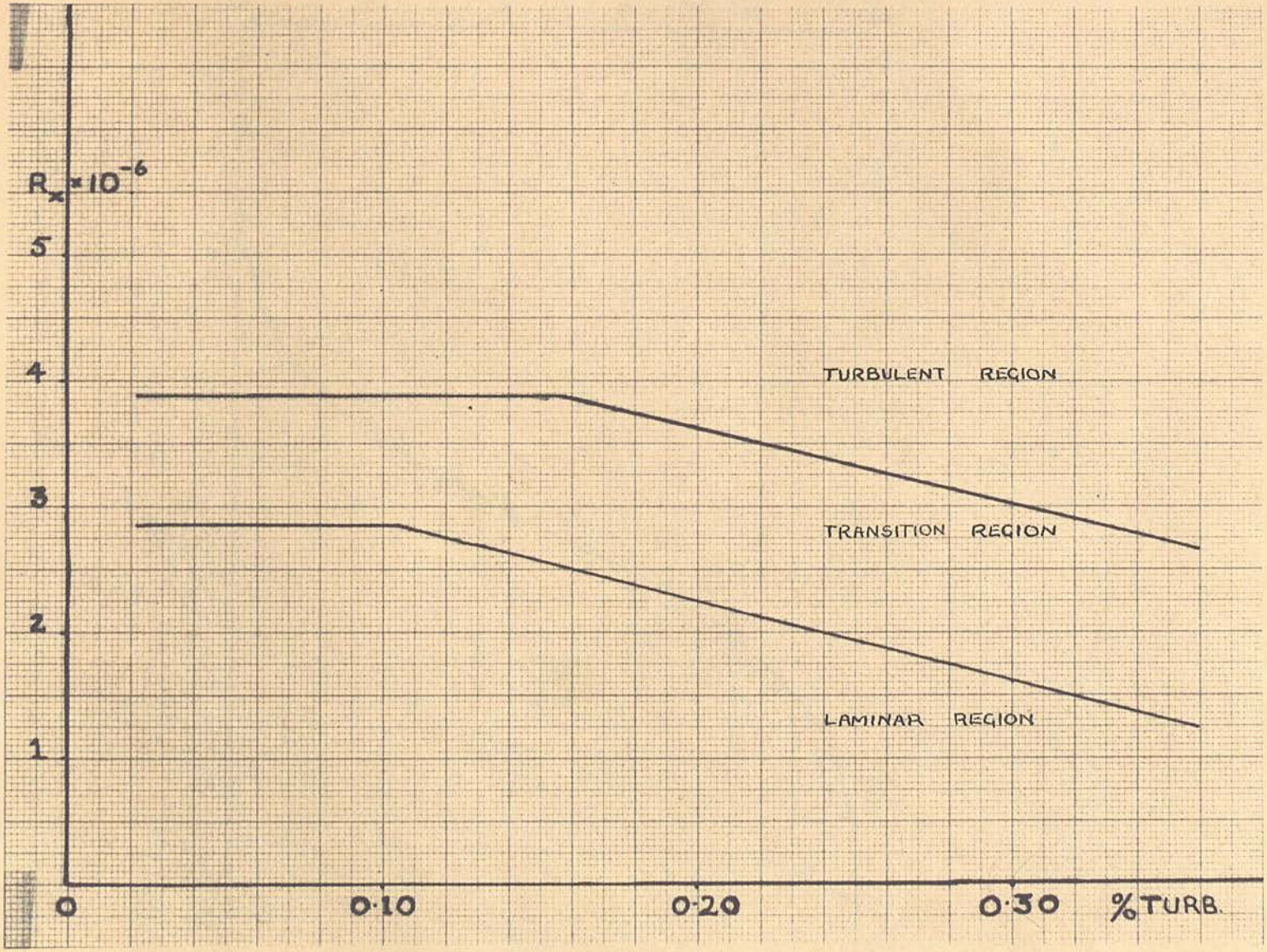

FIG.3 Effect of Turbulence on x-Reynolds Number of Transition.

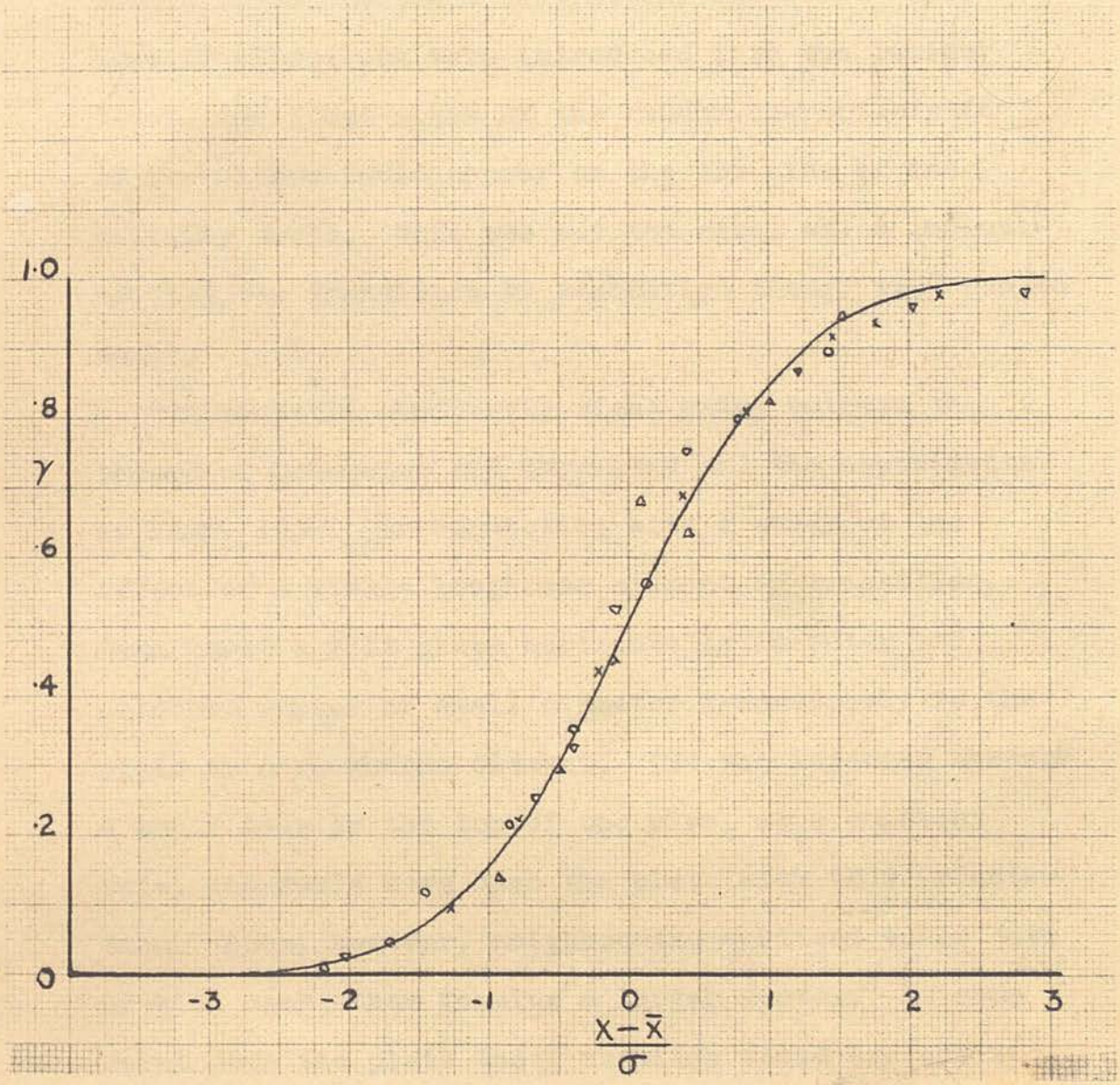

FIG.4 Intermittency Factor, γ, in Transition Regions.

the first turbulent 'bursts' observed in the laminar layer were not confined to the low velocity part of the cycle. If the turbulent 'bursts' were truly caused by intermittent separation, one would expect that if vibrations were introduced into the laminar layer, the first signs of the random characteristic of turbulence would appear on the low side of the velocity cycle. This was not the case, which indicated that the transition by separation theory was open to doubt.

A probable similarity might exist between the theory of Schubauer and Skramstad and the experiments of Hama, 1953. In connection with a study of the effect of a single roughness element on transition, Hama towed a flat plate horizontally in water and attached a pipe of small diameter transversely to the plate as a roughness element. Dye was injected through a small hole in the top of the pipe, at a constant rate, and would move down the plate with this orientation. Soon, however, neighbouring vortices would join up with each other forming a larger vortex. At some point down the plate these vortices would explode and the motion become random. Although conditions behind a roughness element are totally different from those in a boundary layer, some similarities might exist in the manner in which both motions become turbulent.

1.5. Formation of Turbulence

One further approach to the problem is that taken by Emmons, 1951. In an observation on a water table analogy to supersonic flow, Emmons observed boundary layer transition. It could easily be seen that the thin layer of water, when it became turbulent, was considerably changed in appearance with either transmitted or reflected light. Emmons noted that transition is not a clearly defined phenomenon, but is rather an intermittent process. He points out that by virtue of disturbances carried into the layer by outside turbulence, plate roughness, vibration etc., the laminar layer is disturbed. When these disturbances reach a certain value, a turbulent burst occurs. The turbulent 'spot' moves along with the fluid and gradually fans out, making turbulent all before it. From this theory then the farther one moves down the plate, the greater percentage of the time the particular point under observation will be turbulent. Transition should therefore be defined in terms of the percentage of time any particular spot is turbulent, and this fraction is termed the intermittency factor γ.

G.B. Schubauer and P.S. Klebanoff, 1955, plotted γ for several cases where conditions leading to transition were varied. The lengthsof the regions were different in all cases but the distributions were similar. In order to obtain a common basis of

comparison, Gaussian integral curves were fitted to the cases separately and the standard deviation σ was determined for each case. All could then be represented on a common scale in units of σ, and when superimposed at the point $\gamma = 0.5$ they appear as shown in Fig. 4. Here x is the distance from the leading edge of the plate $\bar{x}$ being the distance to the point where $\gamma = 0.5$. The curve is a Gaussian integral curve and values of σ range from 0.3 to 0.8 feet.

In this report Schubauer and Klebanoff also tried to find experimental support of the concept that transition occurred abruptly along an irregular line. This line was considered to surge upstream and downstream, and to separate the laminar flow from the turbulent flow.

They introduced a 'spot' of turbulence into the boundary layer by means of a spark discharge, and followed its progress downstream with the aid of hot-wires. This 'spot' of turbulence was found to fan out, and grow three-dimensionally. Furthermore the oscillograms of the turbulence bursts propagated by the spark, very closely resembled those of natural turbulence, i.e. a turbulent burst began with an abrupt increase in velocity and its ending was followed by a slow velocity decrease. By using two hot-wires in conjunction with each other, they were able to

observe the passage of a spot of turbulence, and from this they concluded that a transition region consists of patches of turbulence going downstream.

The transition region can now be considered as having two parts. (1) The initial breakdown of laminar flow due to a perturbation, and (2) the growth of turbulence into the surrounding laminar region. Local breakdowns may be expected to have a random nature, since the high amplitude isolated peaks from which the breakdowns are formed, are themselves randomly distributed over the xz-plane.

A complete bibliographical review of the boundary layer is given by H.L. Dryden, 1955.

1.6. Summary

In conclusion it can be said, that at low levels of turbulence, laminar oscillations play an integral part in transition. A disturbance is amplified until the amplitude of a peak in the wave train is sufficiently large to cause breakdown, and a turbulent spot results. This turbulent spot grows as it is convected downstream, to be joined by other similar patches of turbulence, until the boundary layer is fully turbulent.

However, as the free stream turbulence gets

progressively greater then the laminar oscillations contribute less and less toward transition. For a free stream turbulence level of 1.0% it has been shown that the laminar oscillations play no part at all in transition. As the turbulence is increased, the percentage of total energy centred around the amplified frequency decreases considerably, and the extreme purity of the oscillation is lost. The frequency spectrum is also much more uniform.

Quantitatively speaking, the situation governing the formation and development of turbulent spots into fully developed turbulent regions, may be said to be understood. The outstanding problem now remaining to be solved, is that concerning the sudden redistribution of energy when a turbulent spot is formed. An examination of the oscillograms of Schubauer and Skramstad shows that the frequency of the laminar oscillations is relatively low, about 60 c/s, whereas the frequency of the turbulent spots is of the order of 1000 c/s. How is this redistribution of energy effected?

It was with a view to eventually solving this problem that the idea of the vane was conceived. This instrument would respond to v fluctuations and it was hoped that after its potentialities had been assessed, by initially investigating relatively well established phenomena (by hot wire methods) in the

laminar region, to examine the transition and turbulent regions. By having an instrument of this type, it might be possible to use it as a mechanical filter to examine the turbulent spectra. In this way frequencies hitherto undetected by hot wire apparatus may be exposed.

CHAPTER 2

CONSTRUCTION AND CALIBRATION OF THE TUNNEL

2.1.1 Description and Construction of the Tunnel

From the conclusions of the previous chapter it was evident that if the most favourable conditions were to be obtained for the research programme, then a low or fairly low turbulence tunnel was required.

The choice of wind tunnel is a modified National Physical Laboratory design and is of the single pass type, the tunnel room itself being used for the return flow. This is a reputedly low speed, 100 ft./sec., low turbulence tunnel, and it was hoped to reduce the turbulence still further by the insertion of screens. As modifications extra settling lengths are included after the inlet and contraction sections. The purpose of the extra sections is to allow the air stream to settle before it reaches the working section, thereby giving an improvement in the turbulence level. A detailed account of this is given at the end of this chapter. Photographs of the actual tunnel are shown in Figs. 5 and 6.

From a consideration of the cross-sectional areas of the room and the tunnel, the velocity of the return flow is estimated to be of the order of 2 or 3 ft./sec., and as the incidental instruments and benches are either kept out of the way or placed symmetrically

about the room, the return flow is relatively undisturbed.

2.1.2. Inlet Flare and Honeycomb Straightener

The contours of the inlet flare are designed so that the air is drawn in smoothly, and that no separation occurs at the walls. A honeycomb straightener is placed a few inches from the curved part of the flare, where the radial component of the inflow is small, and serves to remove most of the residual swirl in the air, due to the fan. It is made of 4" long, $\frac{3}{8}$" hexagonal section brass tubes soldered together. The Reynolds number for the straighteners, calculated for a windspeed at entry of about 30 ft./sec., is approximately 10^4. Since the critical Reynolds number for laminar flow along a plate falls between 10^5 and 5×10^6, then no turbulent wake is to be expected from the straighteners. The only possibility of a turbulent wake occurring, being if the approaching streamline is not parallel to the axis.

2.1.3 Screens, Contraction and Diffuser

Situated behind the straightener is the turbulence reducing screens section. This part of the tunnel was built so that it afforded easy access to

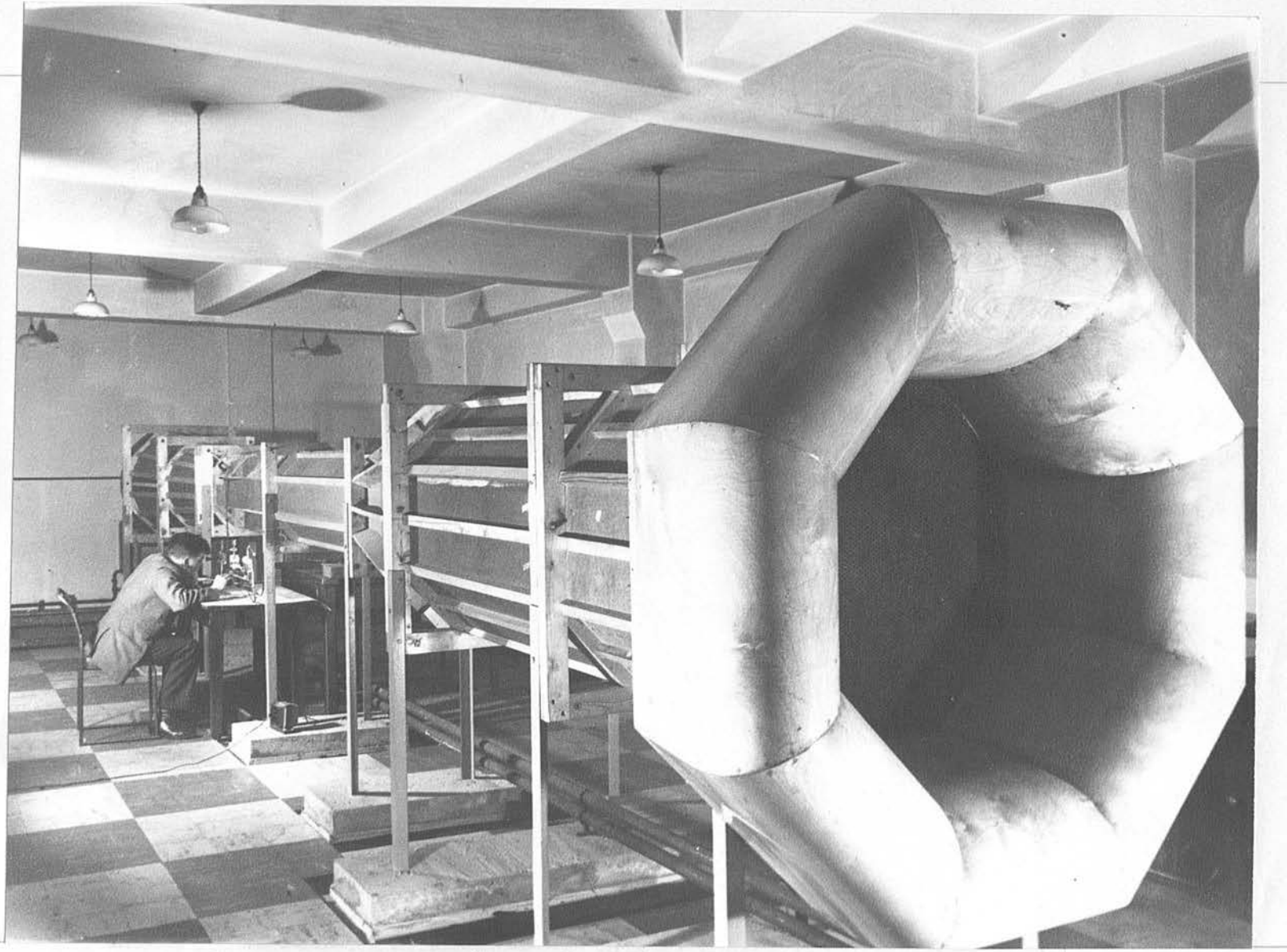

FIG.5 The Wind Tunnel Viewed from the Inlet Flare.

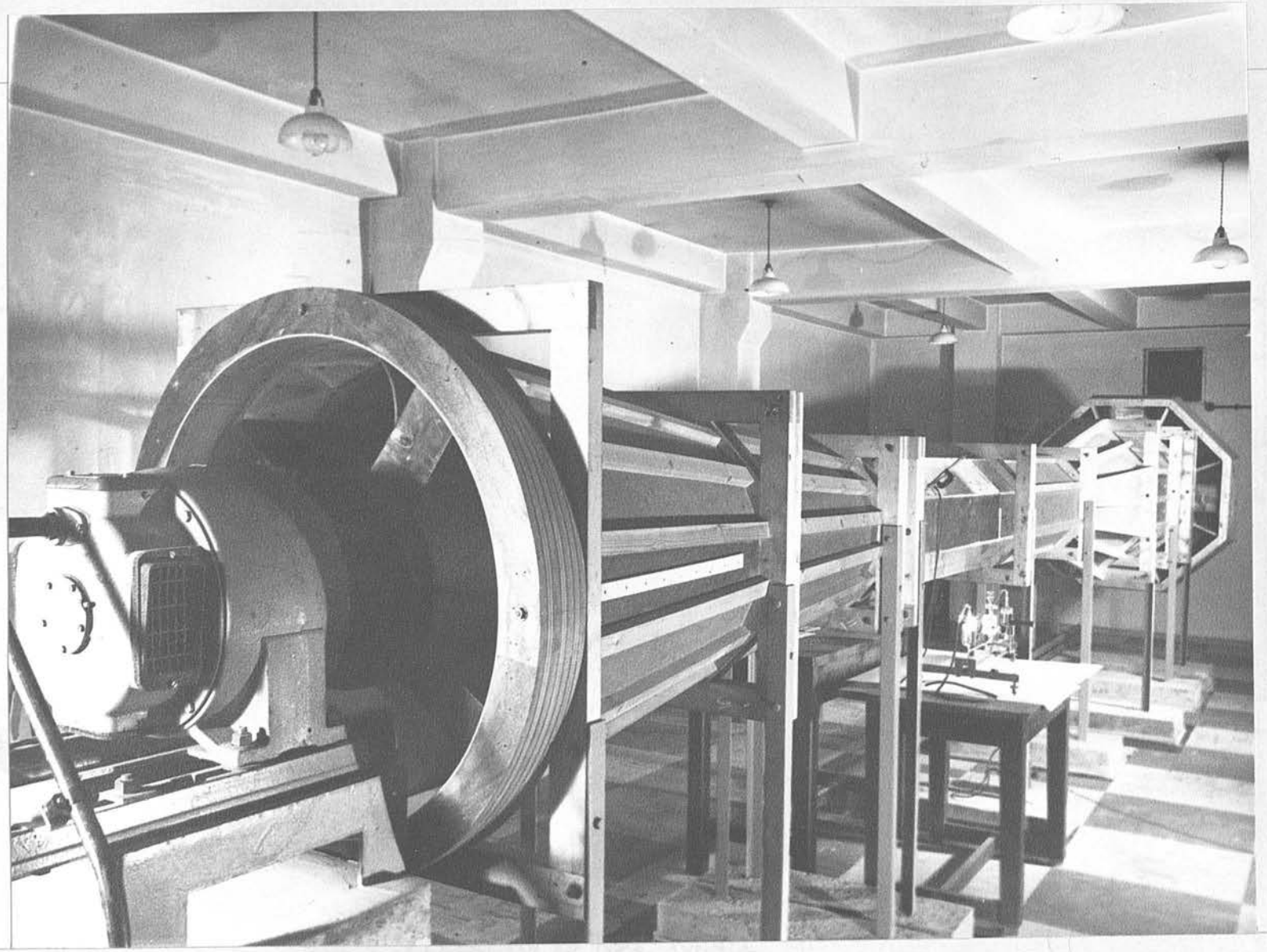

FIG.6 The Wind Tunnel viewed from Diffuser Outlet.

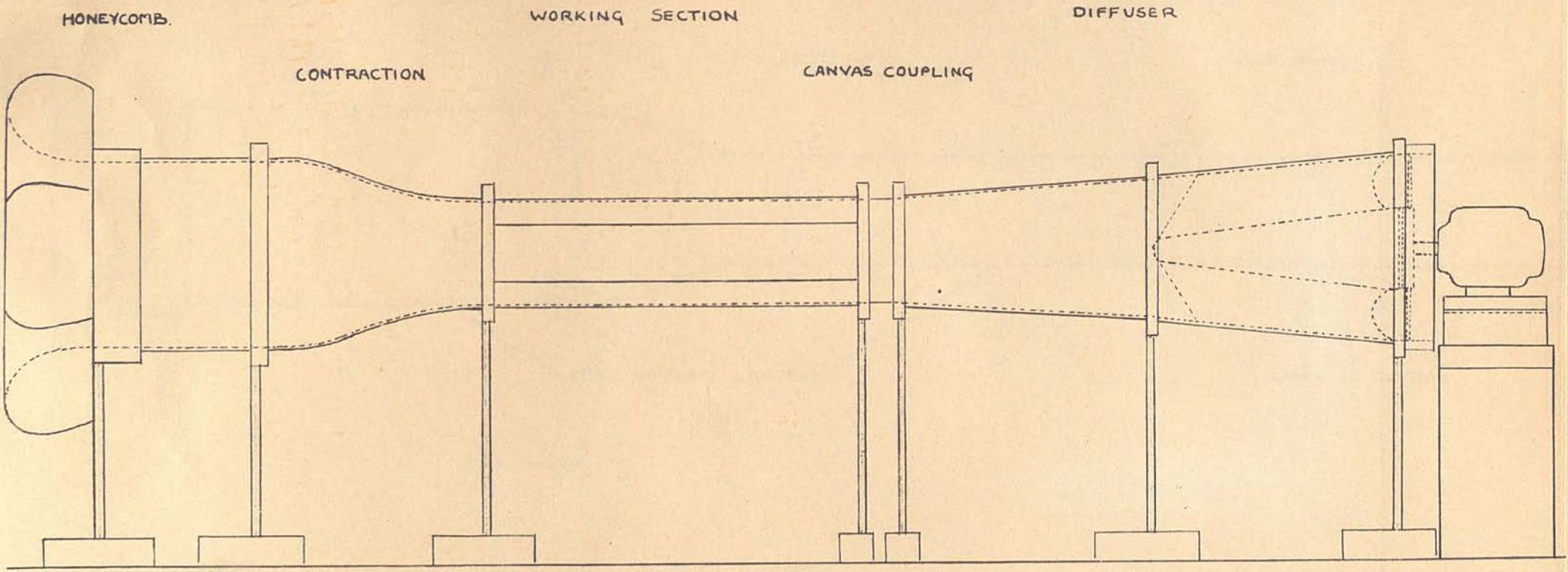

FIG.7 ELEVATION OF N.P.L. TUNNEL

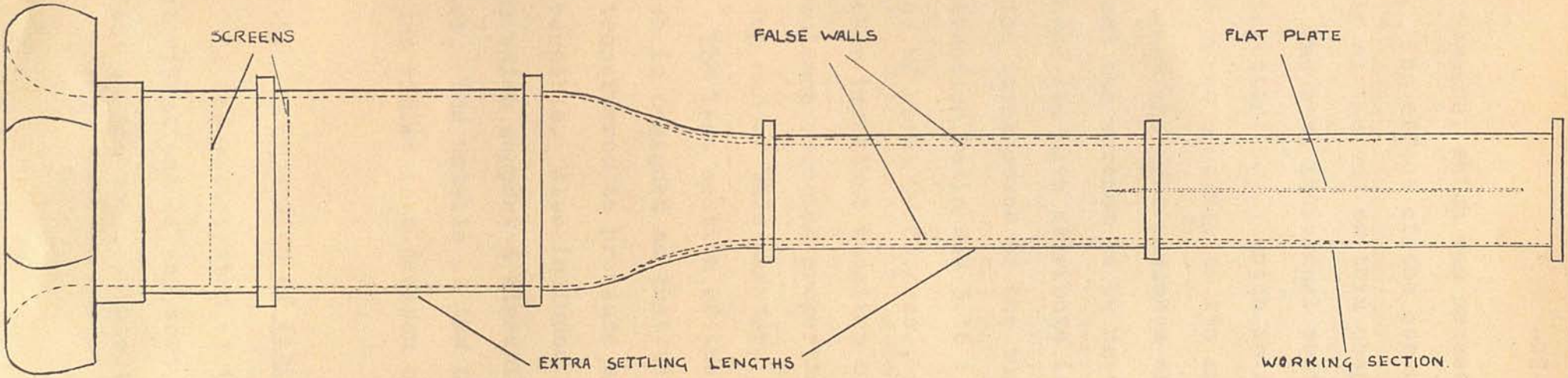

FIG.8 PLAN VIEW OF ACTUAL TUNNEL

the screens, which was necessary for cleaning purposes etc. The effect of the screens will be discussed fully at the end of this chapter.

The next individual section of the tunnel is the contraction cone, which is designed to increase the wind speed smoothly to its maximum value in the working section. The presence of the contraction also allows the screens to be used more effectively, and perhaps its main attribute is the beneficial effect on the total power of the tunnel. In this case the contraction ratio was 3.16 : 1 giving a maximum speed of about 90 ft./sec., in the working section. Another important function of the contraction is its turbulence reducing properties, which will be discussed at the end of this chapter.

The last section of the tunnel is the diffuser which is designed so that the kinetic energy of the flow is transferred to pressure energy with as little loss as possible. Also included in this section are fairings which support a streamlined cone, for the fan motor. The details of the fairings are shown in Fig. 7, and Fig. 8 is a diagram of the modified tunnel.

2.1.4. Reduction of Vibration

It was anticipated at the time of construction, that vibrations of any sort, would have a very serious effect on the vane. Since the vane itself was expected

to have only a small displacement due to the wind velocity fluctuations, then any external vibrations of the gear supporting the vane, would also give rise to a displacement of the vane, which could be considered as noise. In fact this noise level would probably constitute the limiting factor to the sensitivity of the vane.

Efforts were therefore made at the outset to reduce vibrations to a minimum. All the tunnel supports and motors were built into concrete blocks, which had a layer of felt isolating them from the floor. The floor, also being concrete, it was hoped that no vibrations would be transmitted through it. To prevent any mechanical vibrations, due to the drumming of the fan with the diffuser outlet, being transmitted to the working section, a flexible canvas coupling was inserted. The location of this coupling is seen in Fig. 7.

2.1.5. The Working Section and Flat Plate.

The working region of the tunnel is the section following the contraction cone. In this case the cross-section was octagonal with 18" between the faces. This shape is more economic in power than a square shaped section, and also the conversion to the circular shape of the diffuser is fairly simple. The walls are made of $\frac{1}{4}$" Perspex, and the section is 5 ft 6" long. Perspex windows, flush with the inside of

the tunnel were also fitted to the walls for easy access to the flat plate.

Positioned vertically, midway across the working section is the flat plate. It is also made of $\frac{1}{4}$" Perspex and the leading edge is sharpened to a smooth contour to ensure smooth flow around this region. It is bolted top and bottom between brass angle brackets which prevent any distortion. The plate is 6 ft. long and the leading edge is 1 ft. upstream from the start of the working section. The exact position is shown in Fig. 8.

2.1.6. Power Installations

For the power supply and speed control it was decided to use an A.C. Motor-Generator-D.C. Motor, arrangement. This was reputed to be cheaper and also to give more accurate speed control than a variable speed A.C. Motor. A photograph and circuit diagram of the power installations is shown in Fig. 9.

The 3-phase A.C. Motor and generator were mounted together on a cast concrete base and the shafts aligned as accurately as possible using clock gauges and an auto-collimator method. The D.C. motor, which carries the fan, is a specially trued 7.5 H.P. D.C. motor, with a maximum speed of 2800 RPM, mounted on a reinforced brick column. The field of the D.C. motor is excited at a constant voltage of 200V DC. and the field of the generator is controlled by the

resistance box. Since the armature of the generator is connected to the armature of the D.C. motor, then accurate control is obtained over the speed of the fan. The fan is a four-bladed type and designed for a maximum speed of 3000 RPM.

2.2.1. Windspeed and Noise Level Calibrations.

In this section the free stream velocity is calibrated against the fan revolutions, for a varying number of screens. As a wind tunnel, speed control balance had not been constructed at this stage, it was decided to use a Stroboscope to measure the fan speed and simply adjust the field of the generator until the desired wind speed was obtained. As Pitot-Static tubes and small Total Head tubes were used throughout for the calibrations, then an indication of the theory of this type of instrument is advisable.

2.2.2. Pitot-Static tubes and Chattock Manometer.

A tube, placed with its entrance normal to the wind stream and stem parallel with the flow, if connected to a manometer or other pressure measuring device will record the sum of the kinetic and static pressures inherent in the flow. The kinetic pressure corresponds to the velocity of the air stream and the static pressure being that at right angles to the main flow. From

Bernoulli's equation, $\frac{1}{2}\rho U_o^2 + P = \text{constant}$ (assuming incompressible flow), we see that the sum of these two pressures is a constant. To obtain the wind-speed from the pressure readings, i.e. U_o, the static pressure has therefore to be subtracted from the total head reading, leaving the component due to velocity. The Pitot-Static tube accomplishes this and when the outlets are connected to opposite ends of a differential manometer, the pressure reading obtained is due to the velocity. A typical Pitot-Static tube is shown in Fig. 10. In a well designed Pitot-Static tube, the position of the holes is such that the increase in pressure due to the stem is cancelled by the decrease in pressure due to the nose. This effect is shown in Fig. 11. A number of Pitot-Static tubes of various sizes were constructed and also a Chattock Manometer.

With this manometer the pressures to be compared are applied to opposite arms and the out of balance is shown by a bubble in the centre chamber. The bubble is observed through a telescope and is restored to its initial position by either raising or lowering the adjustable limb of the Chattock gauge, to compensate for the pressure variation. From a knowledge of the design of the instrument the wind speed can therefore be calculated from the 'Balancing Head'. For this instrument the relation is

$$V = 1.094\sqrt{H}$$

where H is the number of small divisions recorded on

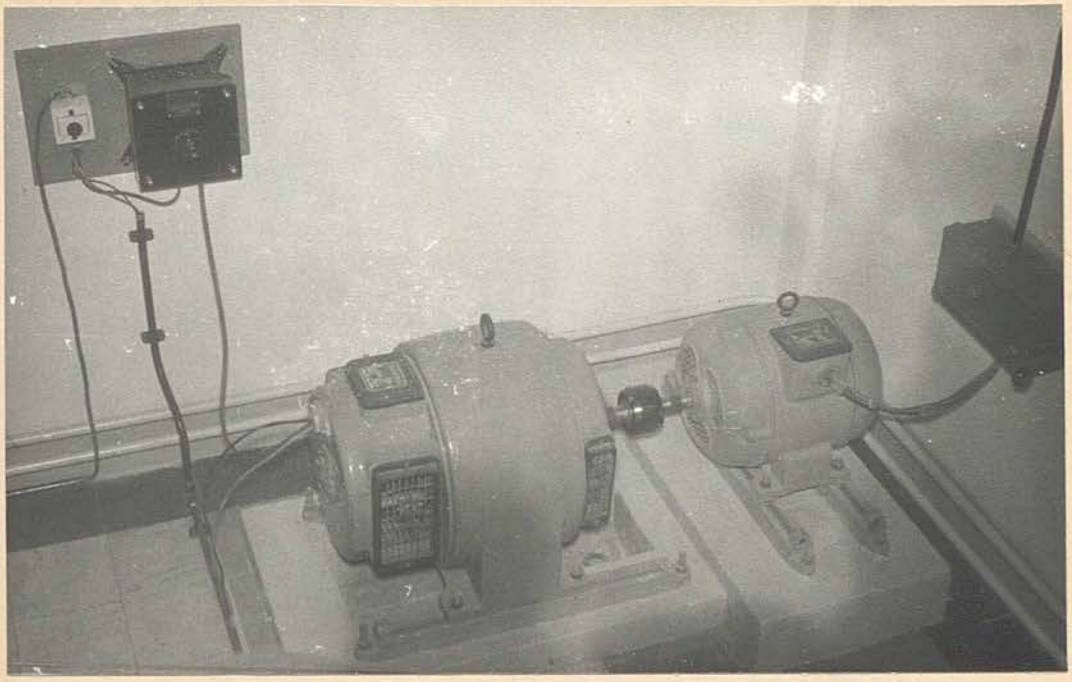

FIG.9 Circuit Diagram and Photograph of Power Installations.

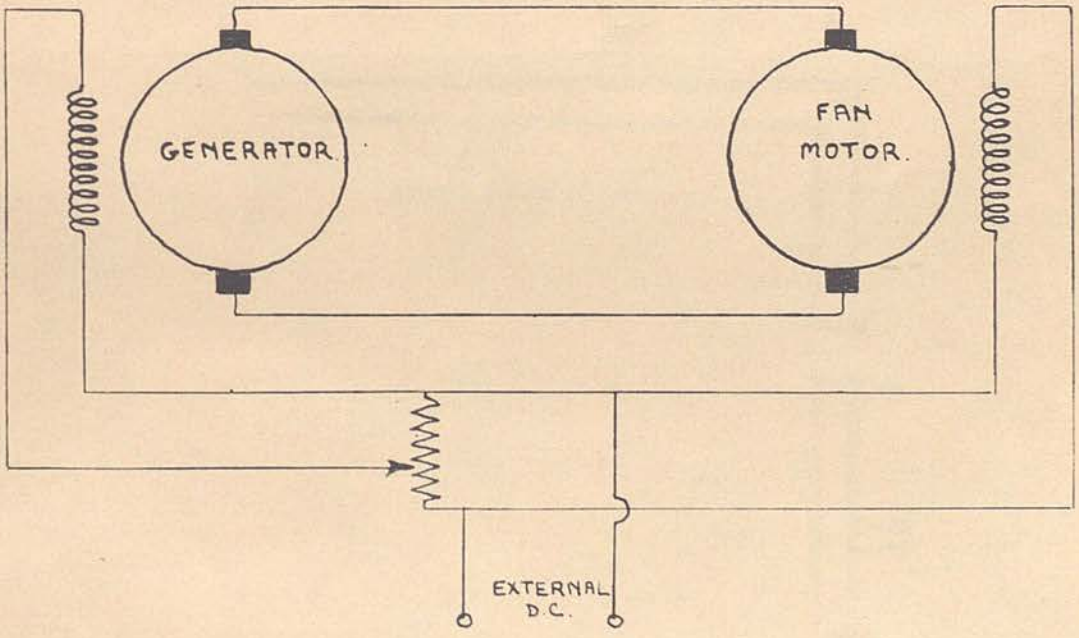

SPEED CONTROL CIRCUIT.

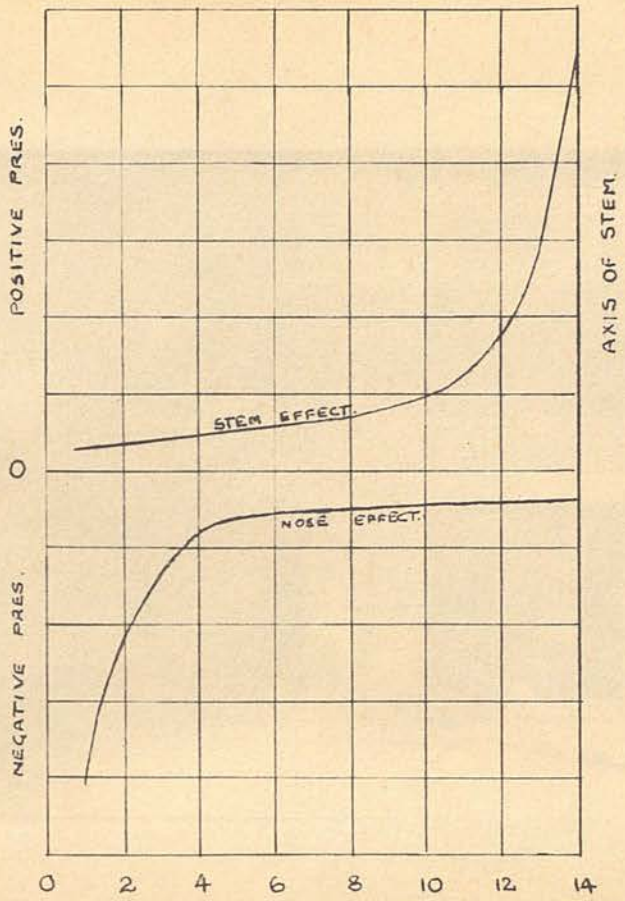

FIG.11 X DISTANCE FROM NOSE (TUBE DIAMETERS)

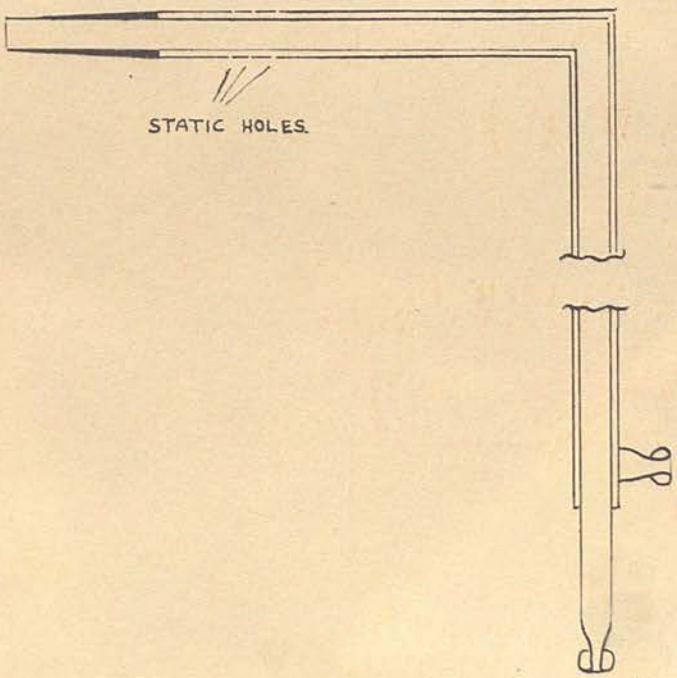

FIG.10 NPL. STANDARD PITOT-STATIC TUBE.

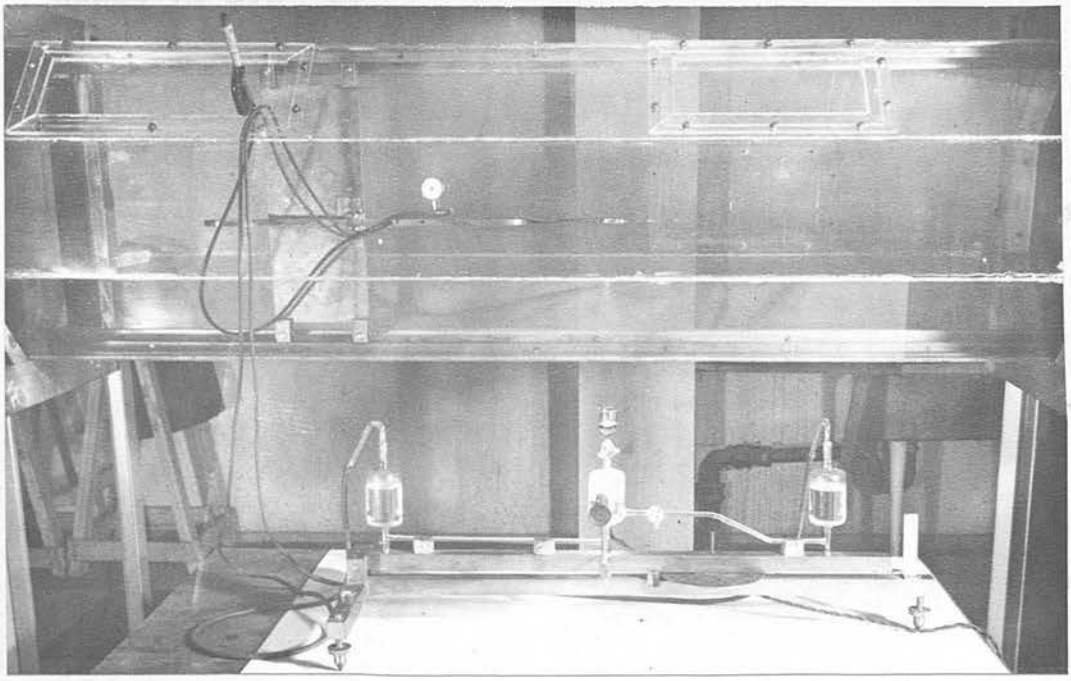

FIG.12 View of Working Section with the Chattock Manometer in the Foreground.

FIG.15 View Inside the Working Section showing the Carriage and Flat Plate.

the balancing disc = $\frac{1}{180}$ m.m. The Chattock manometer used is shown in Fig. 12.

2.2.3. Wind speed Calibration

The first calibration to be attempted was necessarily the relation between the free stream velocity, and fan revolutions or field current, for different numbers of screens. This was done, by simply arranging a large standard Pitot-Static tube centrally in the flow, slightly upstream of the working section, and measuring the wind speed for different field currents and fan revolutions. The results are shown in Fig. 13. This was repeated for up to three screens and as can be seen, a slight loss of about $\frac{1}{2}$ HP occurs for each additional screen. at windspeeds around 75 ft/sec.

2.2.4. Carriage for Total Head tubes

For all future calibrations and measurements on the working section an instrument carriage had to be built. For this purpose brass runners were attached to the top and bottom of the working section of the tunnel, along which ran a rectangular brass carriage 14" x 6" x $\frac{1}{8}$". Ball races were fitted, top and bottom, to ensure smooth movement. This ran parallel to the flat plate at a distance of $1\frac{1}{2}$" away from it and presented very little impedance to the flow, due

to the very small cross sectional area. A certain amount of blockage was desired here, to direct the flow at a slight angle to the leading edge of the plate, so that the stagnation point was displaced slightly from the sharp edge, to the working side of the plate. Mounted on the carriage was a brass 'boom', 18" x $\frac{3}{4}$" x $\frac{3}{4}$", and a diagram of the arrangement is shown in Fig. 14 and a photograph of the carriage and flat plate is shown in Fig. 15. The instruments were then mounted on the upstream end of the boom so that they were unaffected by local pressure fluctuations caused by the carriage. For Boundary Layer Profile work accurate control of movement in the y direction was necessary. For this, the boom was pivoted about a point near the centre and a piece of flexible cable was attached to the rear end. This could then be controlled from outside the tunnel by the micrometer (see Fig. 14) and therefore relative y distances could be measured accurately, by simply reading the clock gauge. Special methods for determining the zero position will be mentioned later. Since the majority of the measurements were carried out on the centre line of the flat plate this arrangement was quite satisfactory, but for a chart of the flow over the plate, the z coordinate had to be altered. This was effected by adjusting the height

of the boom on the carriage, for each separate z height.

2.2.5. Static Pressure Gradient on Flat Plate.

The first investigation was to determine the extent of the pressure gradient along the flat plate. A pressure gradient was to be expected due to the thickening of the boundary layers, on both the plate and the walls of the tunnel, with increasing Reynolds number. It was hoped, however, that it would be small, i.e. $\frac{\Delta p}{\frac{1}{2}\rho U_o^2}$ less than 1 % and not require compensation. Since the pressure gradient is one of the critical factors affecting boundary layer stability, then it was necessary that it should be as near zero as possible.

For the calibration, a small Static tube was used, which was attached to the boom and positioned in mid-stream. It was traversed in the x direction and balanced against a fixed wall static tube. When a graph of Static-Pressure against x distance was drawn, Fig. 16, it was seen that the pressure gradient was much larger than anticipated and could by no means be neglected. The overall Pressure gradient was about 20 % , and false walls had therefore to be built into the tunnel which reduced the area at the upstream end by 10% , and which tapered into the

tunnel walls further down the working section. They were made of $\frac{1}{16}$" perspex, shaped to fit with the octagonal cross section and were built on to the two outside walls of the tunnel. The upstream end had to be fitted in to the contraction, to ensure that a smooth contour was obtained at the join, and the downstream end merged with the outside walls, 3 ft. from the front of the working section. Over the working section a certain amount of flexibility was present and could be used to compensate for local pressure fluctuations.

The new pressure gradient was then measured, see Fig. 16, and found to be less than 1% negative over the first 4 ft. of the plate. This was considered small enough to be neglected for the purpose of this investigation.

2.3.1. Investigation of Flow over Flat Plate.

Obviously it was of great interest to examine the flow over the flat plate and determine the locations of the laminar, transition and turbulent regions. Also, since the plate was fairly narrow, i.e. the effective width was 17", wedges of transverse contamination were expected. These wedges of turbulence originate at the intersection of the leading

edge of the plate, with the tunnel walls, and the angle of formation was of interest.

2.3.2. Boundary Layer Profiles.

The classical and most illustrative method of determining the various regions of the plate, is to observe the change of the Boundary Layer Profiles with increasing Reynolds number. This is done by using a very small total head tube and plotting wind velocity against y distance. The total head tube was made of hypodermic tube 0.040" outside diameter, with the nose flattened to enable the measurement of pressures to within 0.005" from the surface. The walls of the tube at the flattened end were 0.004" thick and the gap was 0.005" . A diagram of the total head tube is shown in Fig. 14.

To determine a boundary layer profile, a small static tube was mounted just outside the boundary layer at the same x distance as the total head tube. This particular static tube was of 0.040" outside diameter, hypodermic and had 0.007" diameter static holes drilled at equal intervals round the circumference. The total head and static tubes were then connected to opposite arms of the Chattock gauge, and the total head moved outwards from the plate until no

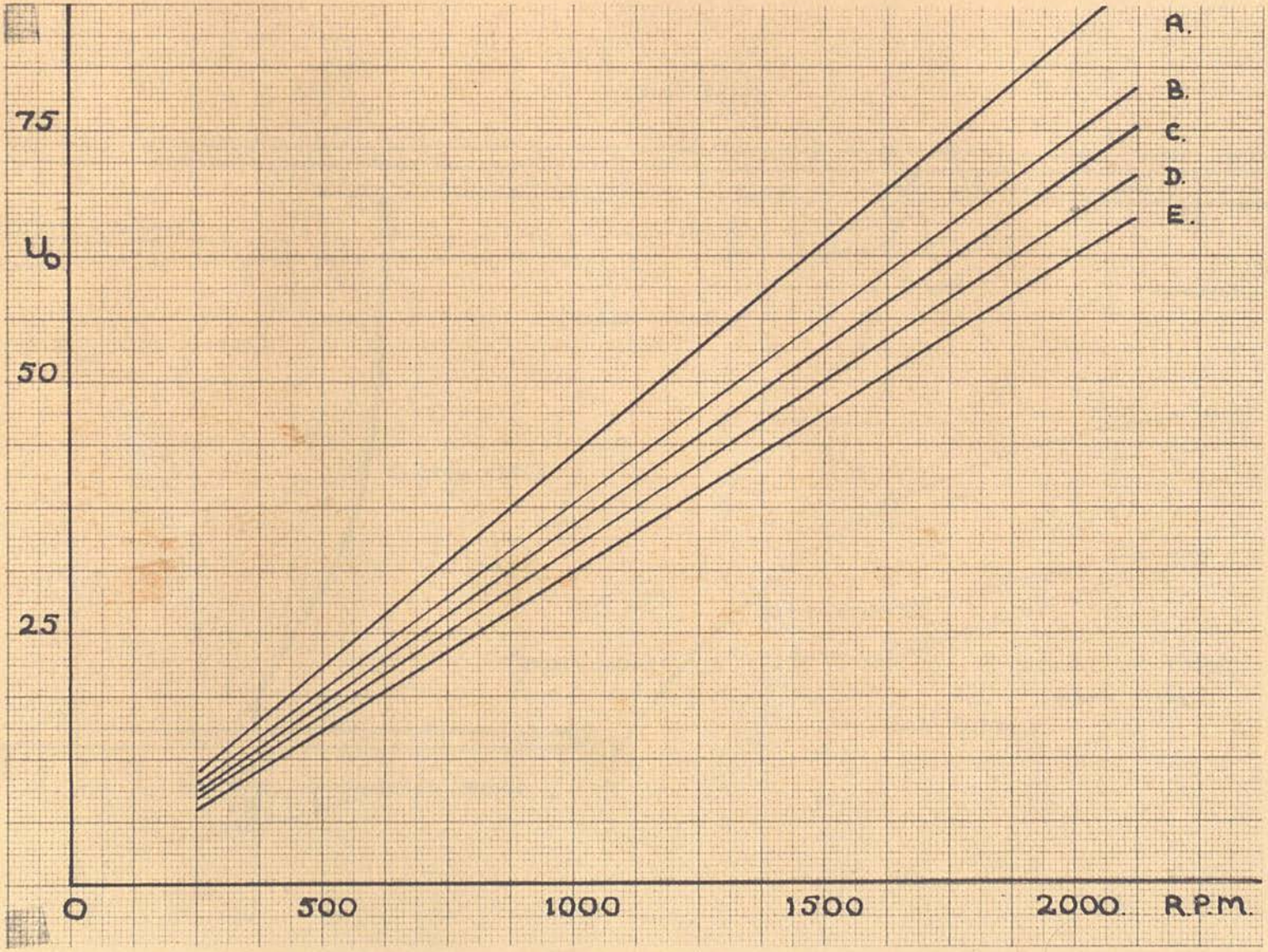

FIG.13 Wind Speed Calibration Curves :- windspeed U_0 ft/sec. against fan revs. for variation of Screens. A-no screens, B- 1 screen, D-2 screens, E- 3 screens C-2 screens and false walls.

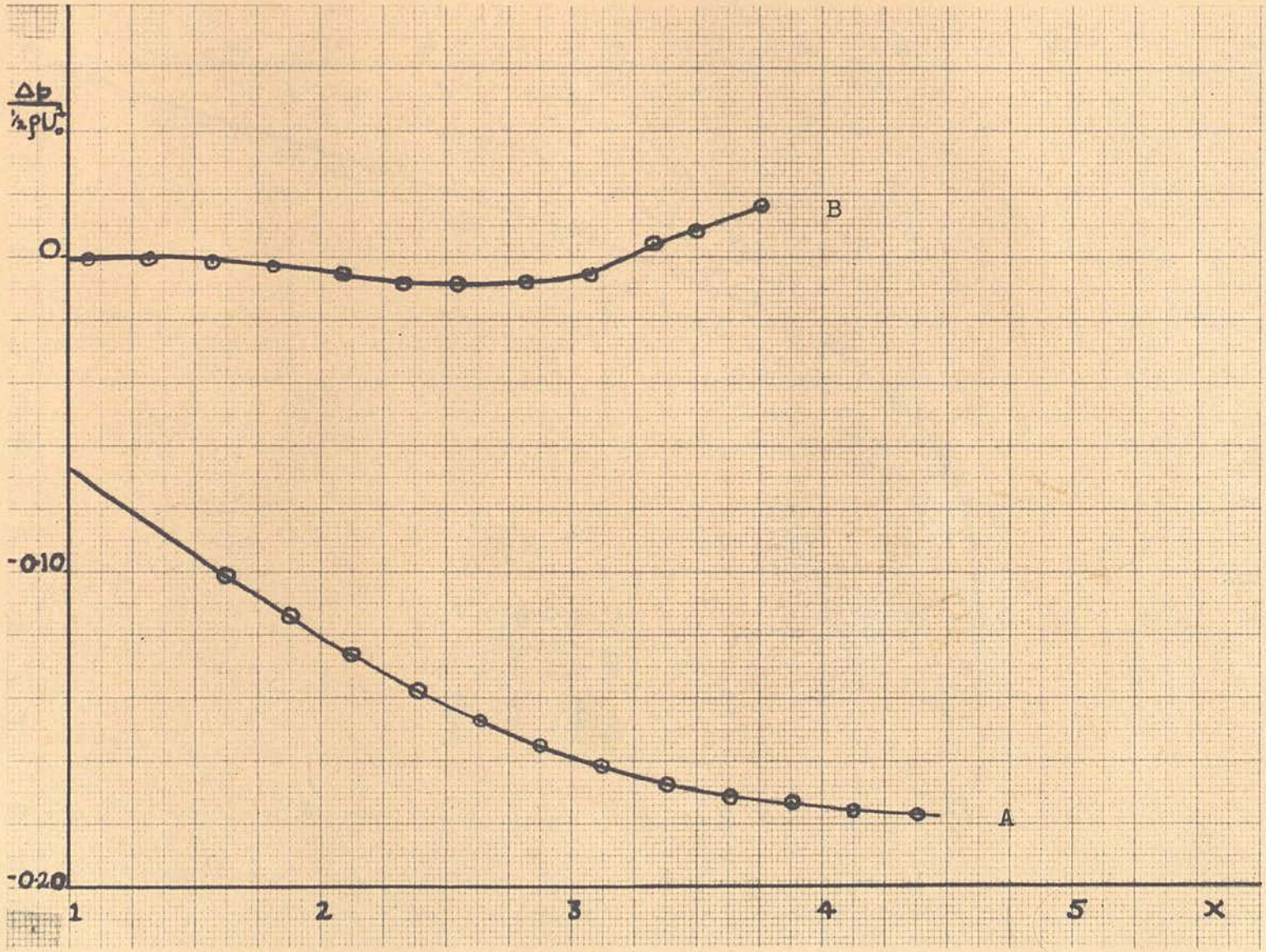

FIG.16 Variation of Pressure Gradient with x distance in ft. Leading Edge of Plate at x = 0. A-Original Pressure Gradient. B-Modified Pressure Grad.

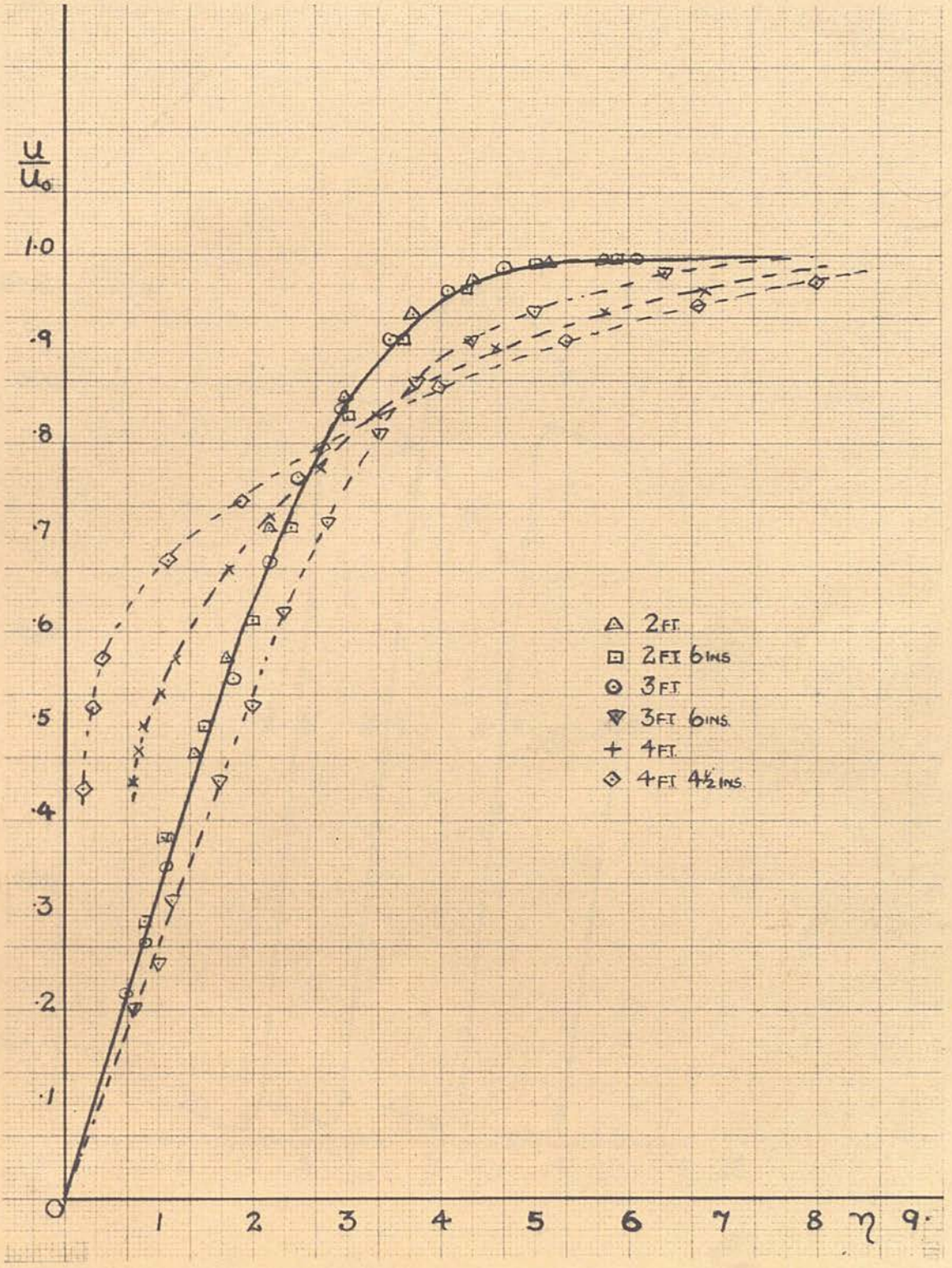

FIG.17 Variation of Boundary Layer Profiles with x-distance

Axes are non-dimensionalized and $\eta = y\sqrt{\frac{U_0}{\nu x}}$

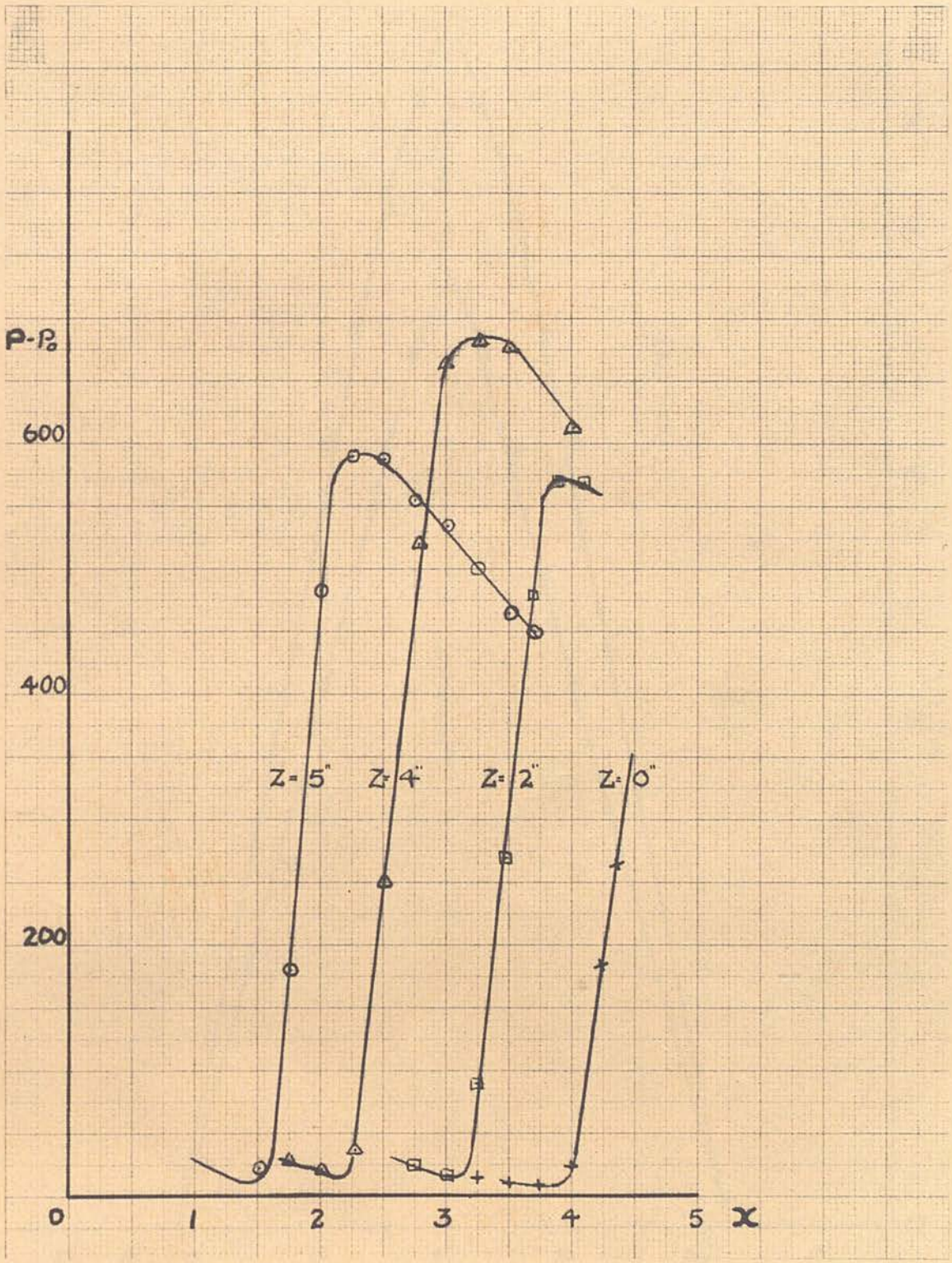

FIG.18 Surface Traverse showing Variation of Total Head

with x-distance in ft. for different z values.

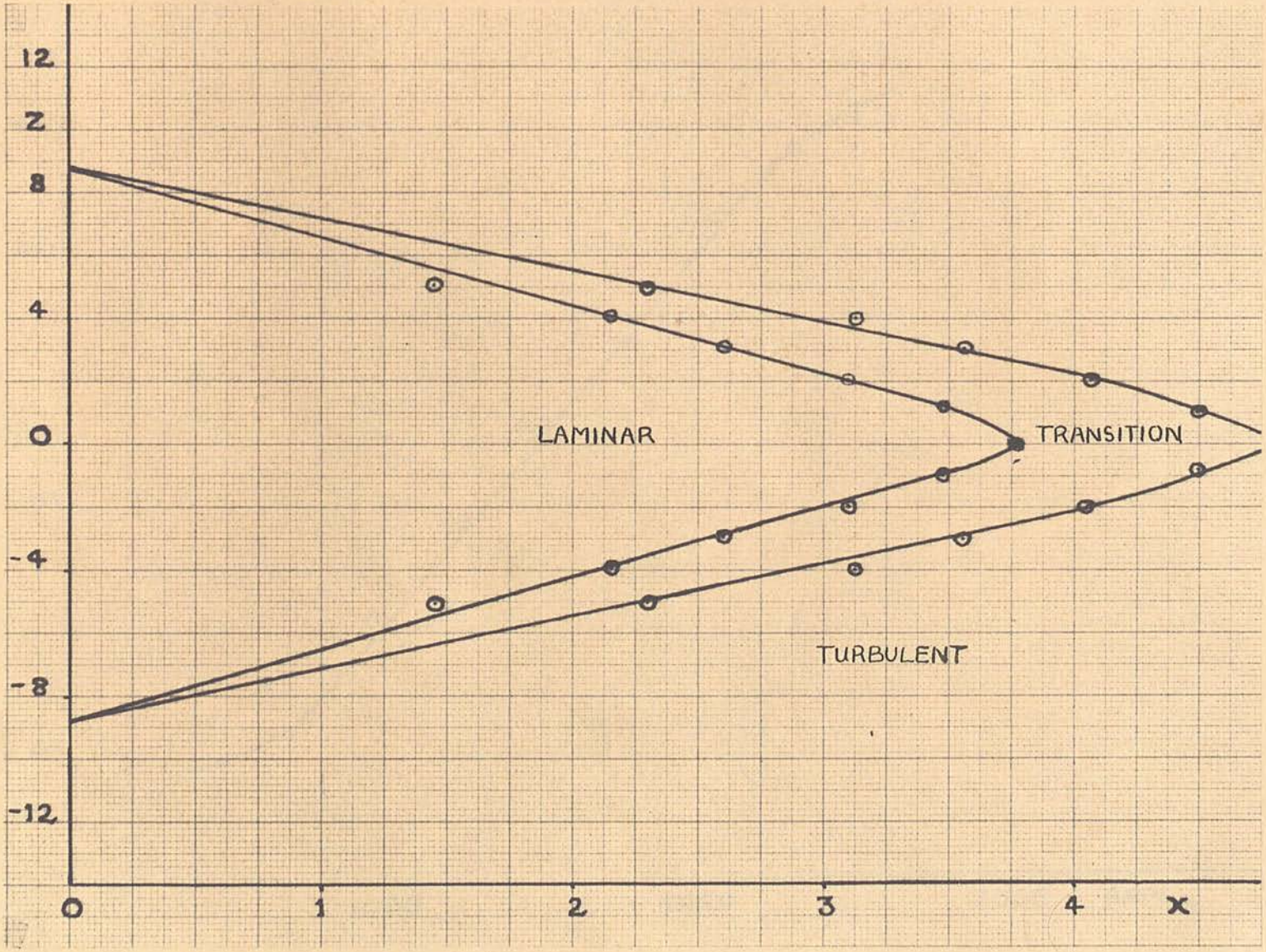

FIG.19 Chart of Flow over Plate showing Formation of Transverse Contamination Wedges. x in ft., z in inches.

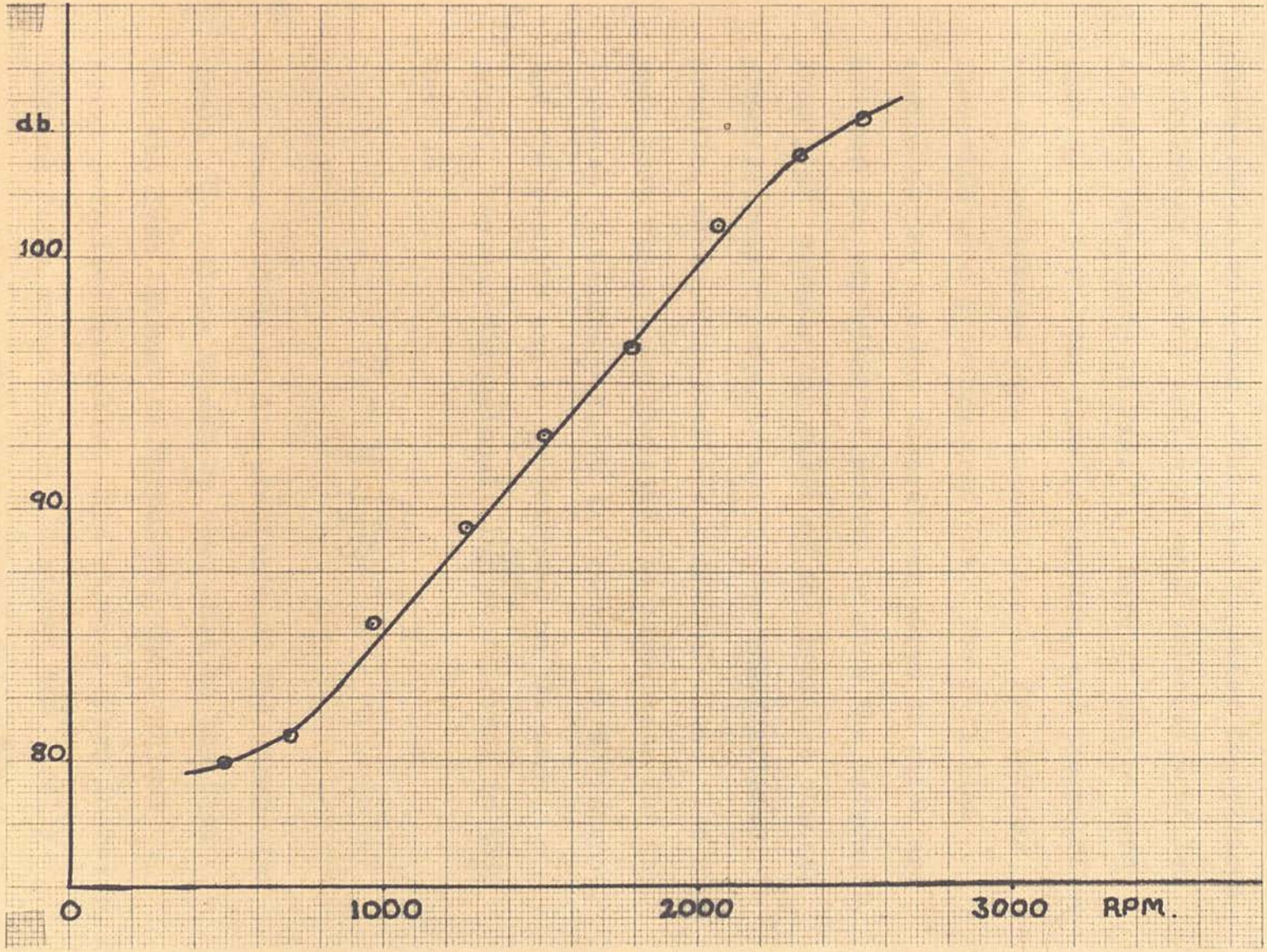

FIG.20 Variation of Noise Level (d.b.) with Fan Speed (r.p.m.).

further difference in pressure with increase of y distance was recorded. This was repeated for various x distances and the series of mean velocity profiles obtained are shown in Fig. 17. Here it can be seen that up to 3'3" the flow is laminar, and the profiles are of the Blasius type characteristic for laminar flow with zero pressure gradient. The full line indicates the Blasius theoretical curve on which are plotted the experimental points to show the agreement. From 3'6" onwards the shape of the profiles changes progressively through transition to the flattened profile, which characterises turbulent flow. The axes have been non-dimensionalized, to compensate for the increase in boundary layer thickness with x distance, and the results can be represented on the same graph. The non-dimensionalizing coefficient in this case is

$$\eta = y \sqrt{\frac{U_o}{x\nu}}$$

From a study of the gradients of the curves for small η values it can be seen that as the flow changes from laminar to turbulent, the gradient first decreases slightly, then shows a sharp increase, lasting for a considerable x distance and finally decreases again as the flow becomes fully turbulent.

This is illustrated by running a small total head tube along the surface of the flat plate. The pressure drops at first, is followed by a sudden rise and finally falls away again. The beginning of transition corresponds to the sudden rise in pressure and the end of transition is reached when the pressure falls again. Typical curves are shown in Fig. 18.

2.3.3. Chart of Flow over Flat Plate.

This quick method of determining the beginning and end of transition was used to obtain a chart of the flow over the plate, and hence to determine the extent of the transverse contamination wedges. The results are shown in Fig. 19 and it can be seen that transition due to the transverse contamination wedges begins at $x = 3'9''$. The boundary layer profiles previously measured were therefore due to this effect and not to natural transition along the flat plate. The angle of wedge turbulence formation was measured and agrees well with $10^{\circ} - 11^{\circ}$ obtained by Charters, 1943, and previous investigators.

2.3.4. Free Stream Turbulence.

Finally it was hoped that an indication of the free stream turbulence in the tunnel might be obtained from the Reynolds number which just caused the point of transition to be brought forward. The principle of this method is based on the result of Schubauer & Skramstad, 1947, which is shown in Fig. 3. It can be seen that for free stream turbulence above 0.10% a definite relationship exists between the turbulence level and the transition Reynolds number. Therefore by increasing the Reynolds number, in this case the wind speed, it was hoped to move the point of natural transition just forward of that due to the transverse contamination wedges. The free stream turbulence could then be obtained from the graph. Unfortunately this proved impossible, due to the effective top speed of the tunnel being limited to 80 ft./sec., and it was only possible to conclude that the free stream turbulence was under 0.5%. Other methods of measuring the free stream turbulence had therefore to be devised.

Since the particle velocity of the noise in the tunnel set the ultimate limit to Schubauer and Skramstad's turbulence level, then it was of interest to see how the noise levels compared. The sound intensity was therefore measured for different fan speeds and the results shown in Fig. 20. Calculations

based on the noise level at 80 ft./sec., i.e. 105 d.b. above a base level of 10^{-9} ergs/cm^2 gives a root mean square (r.m.s.) particle velocity of 0.028 ft./sec. This corresponds to a value of $\frac{u'}{U_o} = 0.035\%$ turbulence. This extremely low level of turbulence was not expected to be obtained but was nonetheless of interest.

2.4.1. Measurement of Free Stream Turbulence.

It was necessary that the tunnel turbulence level be known, not only for reference purposes but because it is probably the main factor controlling the capability of the tunnel for the research project. Previous results suggest that the upper limit of free stream turbulence permissible for the observations of laminar oscillations is about 0.4% . If the tunnel turbulence is greater than this, then the energy of the free stream alone is sufficient to precipitate turbulence. Various methods of measurement were considered and as the hot-wire anemometer is the recognized instrument for such work, its possibilities were thoroughly investigated. However, due to the expense and also the time involved in constructing a good instrument this possibility was ruled out.

Another method was investigated due to G.I. Taylor, 1935, and although this one has certain limitations

it seemed very suitable for the turbulence level anticipated. Only the v' and w' components of turbulence can be measured by this method and the sensitivity of the instrument has a lower limit of 0.1% turbulence. Due to the fact that the contraction ratio is 3.16 : 1, the free stream turbulence was not expected to be lower than 0.1% . An assumption that has to be made is that the turbulence is isotropic i.e. $u' = v' = w'$. This is probably not quite the case, but is a permissible assumption, because, if anything, the u' component will be smaller than those of the v' and w', since at the contraction it is the longitudinal component of turbulence that undergoes the greater reduction. It has been found however that isotropic conditions may return if a long enough settling length is present. The measured value of turbulence will therefore be slightly greater than the actual value.

2.4.2. Thermal Diffusion Method.

G.I. Taylor, 1935, and Schubauer, 1935, found that the spread of heat in the wake of a heated wire could be attributed to two effects. (1) Diffusion by true conductivity from each of the heated particles,

and (2) movements of the heated particles to distance $Y = \frac{U_o}{v} x$ from the source, Y being distributed according to the error law. Taylor found that the heat distribution due to each of these effects individually obeyed an error law distribution, and therefore the spread of the wake due to the collective effect would also be Gaussian. This can be expressed by the equation

$$\alpha_{obs}^2 = \alpha_{turb.}^2 + \alpha_o^2$$

where α is the angle subtended by the source and the two positions where the temperature rise was half that in the centre of the wake. α_{turb} is the angle corresponding to the degree of turbulence, α_o is the angle due to thermal diffusion and α_{obs} is the angle subtended due to the collective effects. Hence if α_{obs} can be measured and α_o calculated, then α_{turb} can be found. From this value is calculated $\sqrt{\overline{Y}^2}$, i.e. r.m.s. value, and the free stream turbulence is then obtained from the relation $\frac{v'}{U_o} = \frac{\sqrt{\overline{Y}^2}}{x}$ where x is the distance downstream at which the measurements are made.

The problem resolved itself into designing a suitable instrument for measuring the temperature distribution across the wake of a heated wire. The requirements were therefore a heated wire and a

and a sensitive thermocouple that could traverse the wake at suitable x distances. This instrument is shown in Fig. 21 and a circuit diagram in Fig. 22. The heater wire is 0.001" diameter Nichrome, and a Pallador thermocouple was specially made of 0.001" diameter wires, with the ends butt welded. The calibration curve for this thermocouple is shown in Fig. 23. The thermocouple was attached to a micrometer screw gauge which enabled it to traverse the wake, and give accurate y distance readings. The leads were insulated from the hypodermic supports by thin glass tubes 0.015" outside diameter and 0.005" inside diameter.

The heater wire was connected to a constant current source which was adjusted to give a temperature easily recorded on the thermocouple, the output of which was connected to a galvanometer. Normally the wire was heated to red heat and therefore an initial tension of about 20 dynes, was put on the wire to prevent sagging.

Since the curves obtained were Gaussian, these could be represented by

$$\Theta = \Theta_o \, e^{-\frac{Y^2}{2\bar{Y}^2}}$$

where Θ_o is the temperature in the middle of the distribution and at half width $\Theta = \frac{1}{2}\Theta_o$.

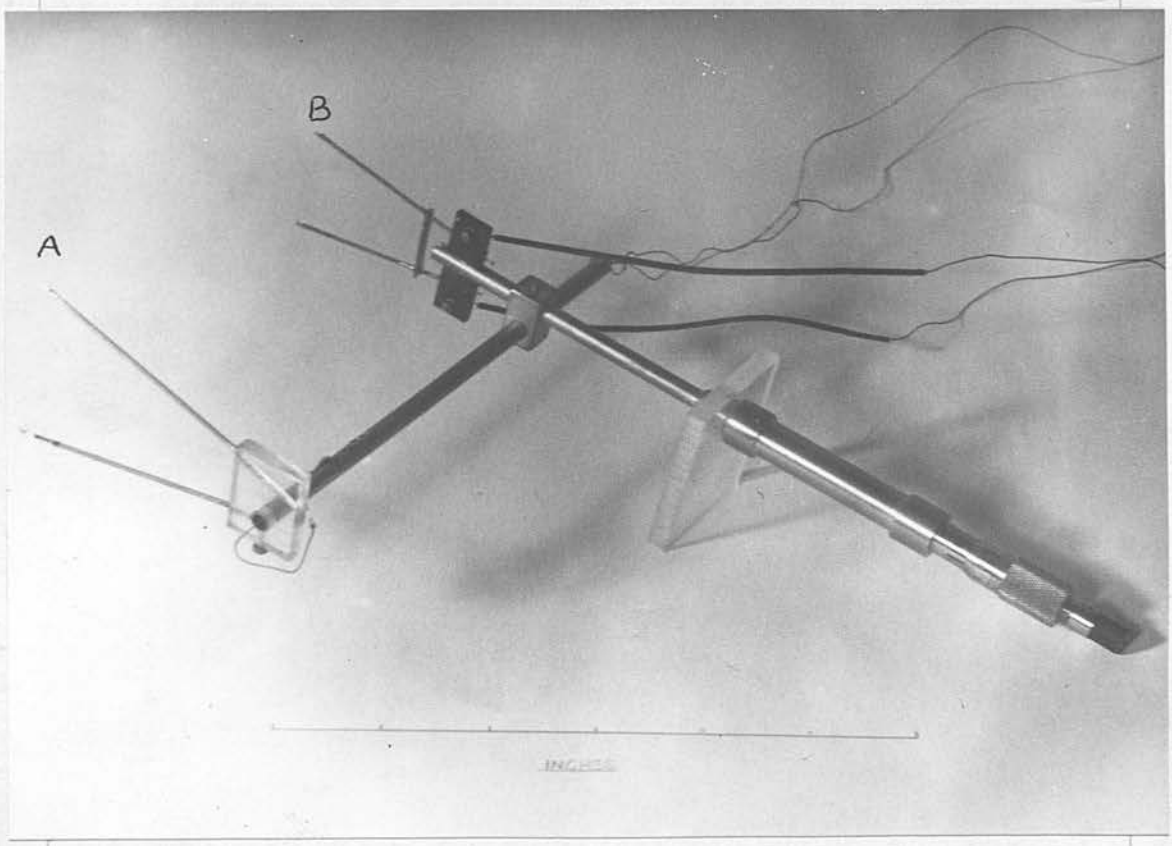

FIG.21 Instrument for Turbulence Measurements

A - Heated Wire. B - Thermocouple.

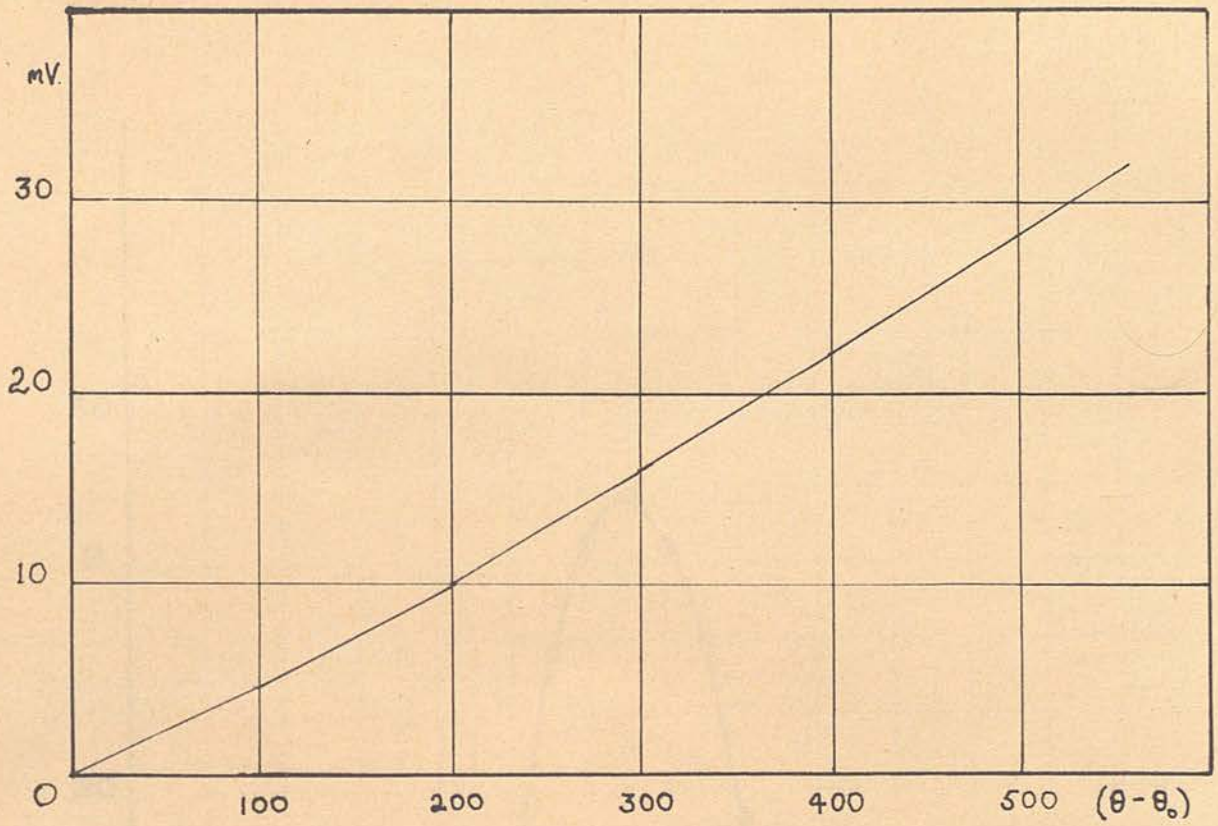

FIG.23 Calibration Curve for Pallador Thermocouple.

Output in m.V. for $(\theta-\theta_0)^{\circ}C$.

FIG.22 Circuit diagram of Turbulence Measuring Instrument.

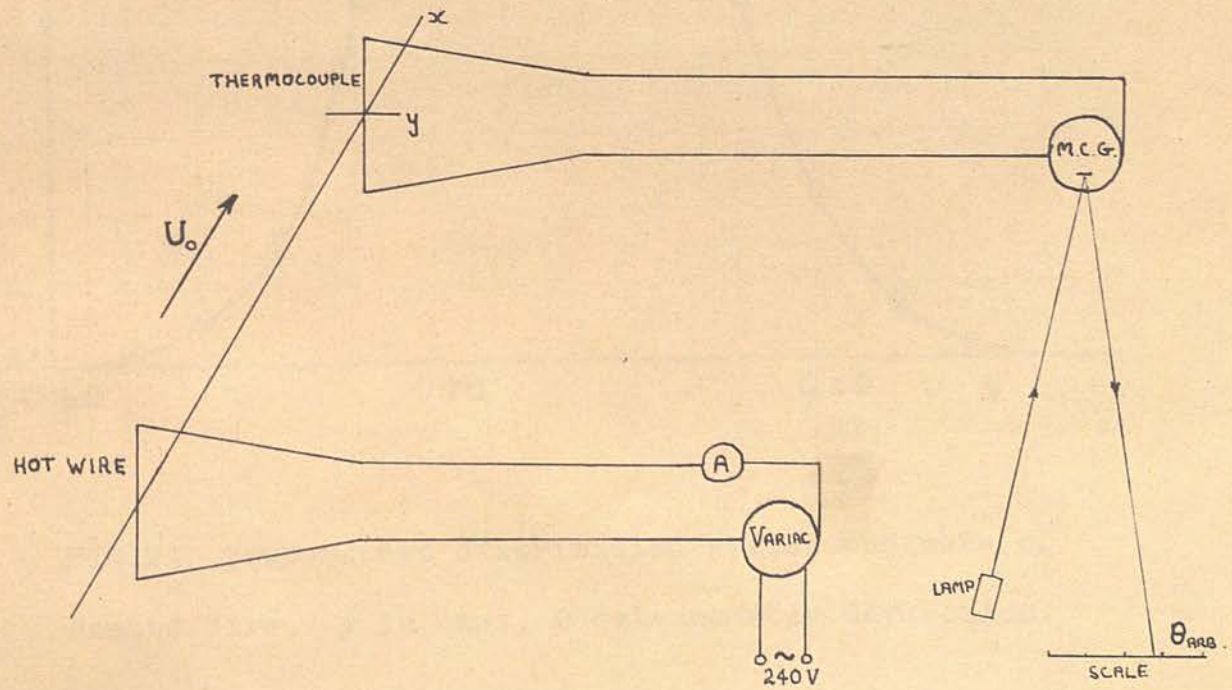

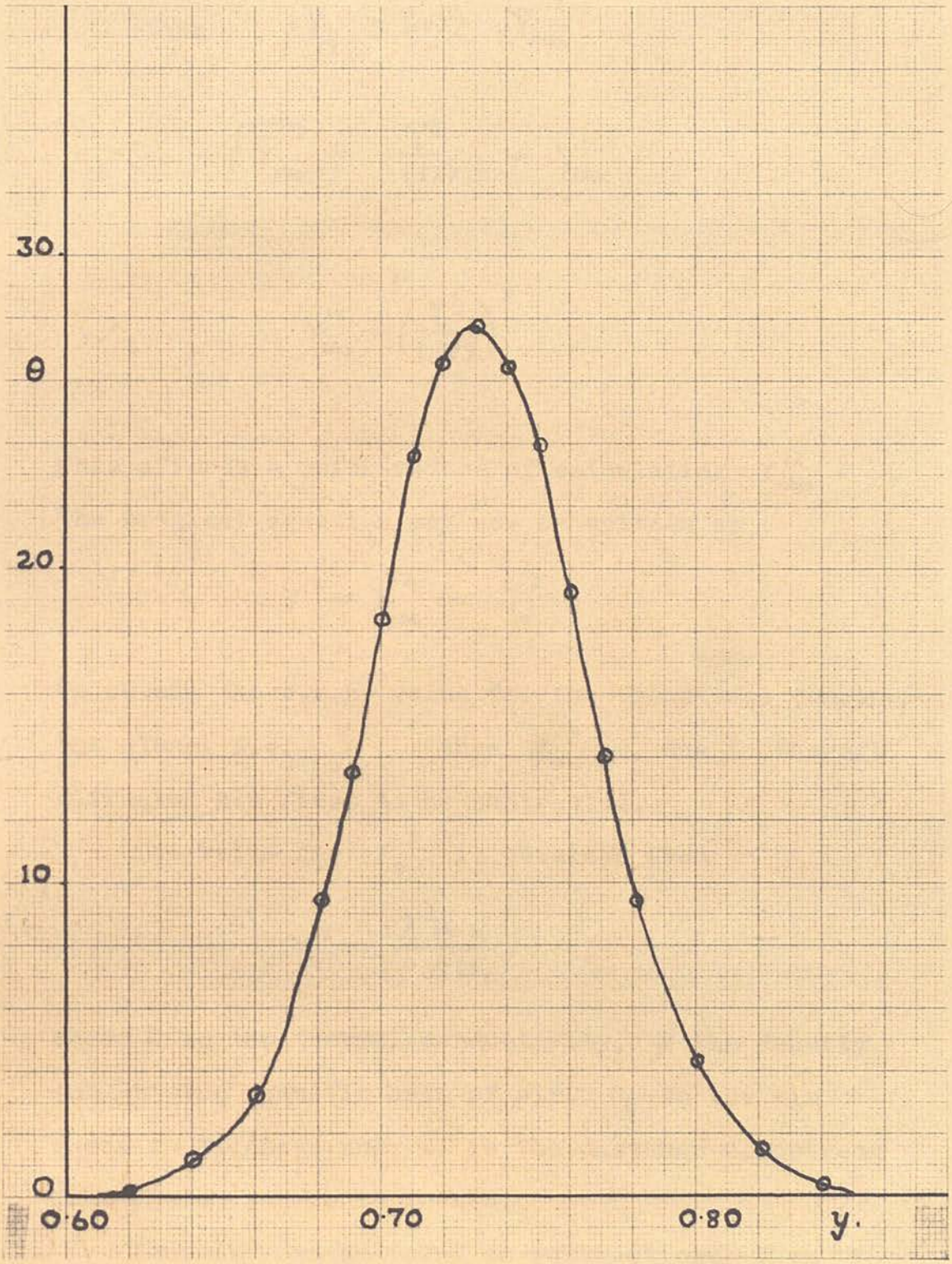

FIG.24 Temperature distribution across the wake of Heated Wire. y in cms., θ Galvanometer deflection.

then $$Y_{\frac{1}{2}} = 1.177 \sqrt{\overline{Y}^2_{obs.}}$$

$$\therefore \quad \sqrt{\overline{Y}^2_{obs}} = \frac{Y^{\frac{1}{2}}}{1.177} = Y'_{obs.}$$

$$\therefore \quad Y'^2_{obs} = \left(\frac{Y^{\frac{1}{2}}}{1.177}\right)^2$$

This affords a quick method of calculating Y'^2_{obs}.
The original equation may now be written as

$$Y'^2 = Y'^2_{obs} - Y_o^2$$

To obtain the r.m.s. value for the turbulence component alone, i.e. Y' then Y_o^2, due to thermal diffusion has first to be subtracted.

The value for Y_o^2 is obtained from

$$Y_o^2 = \frac{2Kx}{\rho \sigma U_o}$$

where K is the thermal conductivity, ρ the density and σ the specific heat of air, U_o is the air speed in ft./sec. and x is the distance downstream from heated source in inches.

Thus Y' can be found on subtraction. When Y' has been obtained then $\frac{Y'}{x} = \frac{v'}{U_o}$

i.e. % Turbulence $= \frac{Y'}{x} \times 100.$

A typical curve is shown in Fig. 24, and throughout this section 50 or 60 such curves were drawn and analysed.

Before any reliable results could be obtained from the instrument its own performance had to be investigated. The correlation between the turbulence values for different x settings was first examined. From the curve in Fig. 25, it can be seen that the turbulence indicated by the instrument rises sharply as x decreases below 2". This is due to the fact that the wake from the heater wire has not quite decayed and is probably contributing to the value of turbulence measured. However for x settings greater than 3" the correlation is good and it was decided to take all future measurements at x = 3.5". Perhaps if a thinner wire had been used, then measurements much closer to the wire would have been possible.

2.4.3. Variation of Turbulence with Wind Speed.

The first investigations with this instrument concerned the variation of % Turbulence with wind speed. It was thought that the increasing vibration and noise from the fan at the higher wind speeds might lead to an optimum operating speed, as regards turbulence, but this was not the case. The curve obtained

is shown in Fig. 26, and as the wind speed increased the % turbulence decreased, suggesting that the vibration had no serious effect. The honeycomb straightener becomes more efficient at the higher speeds. Above about 55 ft./sec. the turbulence remains effectively constant.

2.4.4. Effect of Screens on Turbulence Level.

The effect of screens on the turbulence level was examined next, and this of course was the most important item of the turbulence measurements. The results are shown in Fig. 27. It is seen that for no screens the turbulence is 0.44% and for 1 screen the turbulence is reduced to 0.31%. The anomalous result for two screens placed 6" apart can possibly be explained by the principle on which a screen functions, i.e. that the large eddies are broken up at the expense of smaller ones being shed from the screen, which gradually decay. However when the screens were placed only 6" apart the wake from the upstream one had not had time to decay sufficiently before impinging on the second, and an interaction took place, nullifying the effect of the screens. It must be remembered that in expressions such as

$$\frac{\overline{v_2}^{12}}{\overline{v_1}^{12}} = \left[1 - \frac{K}{10\left(1+\frac{2}{5}K\right)}\right]^2 = \frac{\overline{w_2}^{12}}{\overline{w_1}^{12}}$$

due to Batchelor, 1945, where K is the blockage coefficient of the screens, v_2' and v_1' are measured far upstream and far downstream of the screens and the turbulence introduced by the screen itself is neglected. In the first few inches after the screen there is probably an increase in turbulence and it is probably due to this that the odd result can be attributed. However, when the separation between the screens was increased to 1 ft., this difficulty was overcome and an improvement in turbulence was obtained for addition of screens.

Another effect observed when there were no screens and also when two were placed 6" apart, was that the distributions were not strictly Gaussian, i.e. a discrepancy existed between the values obtained from the half-width formula and by obtaining Y'^2, the r.m.s. value from the numerical integration of $\frac{\int y^2 \Theta \, dy}{\int y \Theta \, dy}$. They differed by a considerable amount which could not be attributed to errors in observation. In an attempt to explain this discrepancy a probability plot of a typical curve was drawn and examined but no significant deviation could be observed. This curve is shown in Fig. 28. However when one screen was inserted the curves regained their Gaussian character and the two values once more agreed. This would appear to indicate that the air flow was not completely random but had some localised disturbances present in it. The effect of a screen would then be

to distribute the turbulence more evenly over the cross-section of the tunnel, and a Gaussian distribution was recorded.

On examination of Fig. 27 it can be seen that little improvement is gained by adding a third screen, and so for power considerations it was decided to limit the number of screens to two. The turbulence level of the tunnel was therefore taken to be $\frac{v'}{U_o} = 0.3\ \%$.

Finally an estimation of the theoretically obtainable level of turbulence, calculated from the dimensions of the honeycomb, screen and contraction is given.

2.4.5. Theoretical Turbulence Level.

Many expressions are available for the decay of turbulence behind honeycombs and screens but not all have been verified experimentally. Those used in this section are among the most reliable and certain assumptions have to be made at the outset.

Taylor, 1935, showed that the wake from a honeycomb decayed according to the relationship

$$\frac{u'}{U_o} = \frac{1}{K + \frac{5}{A^2} \cdot \frac{x}{M}}$$

where M is the honeycomb mesh size, x is the distance downstream of the honeycomb at which u' is measured and K is a constant which is negligible far downstream. For values of $\frac{x}{M}$ up to about 500, A may be assumed constant and equal to 2.1, so that

$$\frac{u'}{U_o} = 0.9 \frac{M}{x}$$

This expression gives the intensity of the wake for different x distances and, an assumption that has to be made is that the v' component is of similar magnitude as the u' component, i.e. the turbulence is isotropic, and u' = v' = w'. Since the instrument measured v' and w', only these components will be treated in detail in this discussion.

From the curve shown in Fig. 29 it can be seen that when the contraction is reached, in the case for no screens, the v' component of turbulence is 0.36%. At the contraction no definite reduction of the v' and w' components has been shown, and indeed these components may actually rise to quite high values at some early part of the contraction, before falling again to approximately their original value at the end of the contraction. The magnitude of the u' component is much the same as the v' and w' ones at the end of the contraction but due to the increase in U_o $\frac{u'}{U_o}$ is decreased.

For the no screens case then, the v' component can be taken as $\frac{v'}{U_o} = 0.36\%$ in the working section

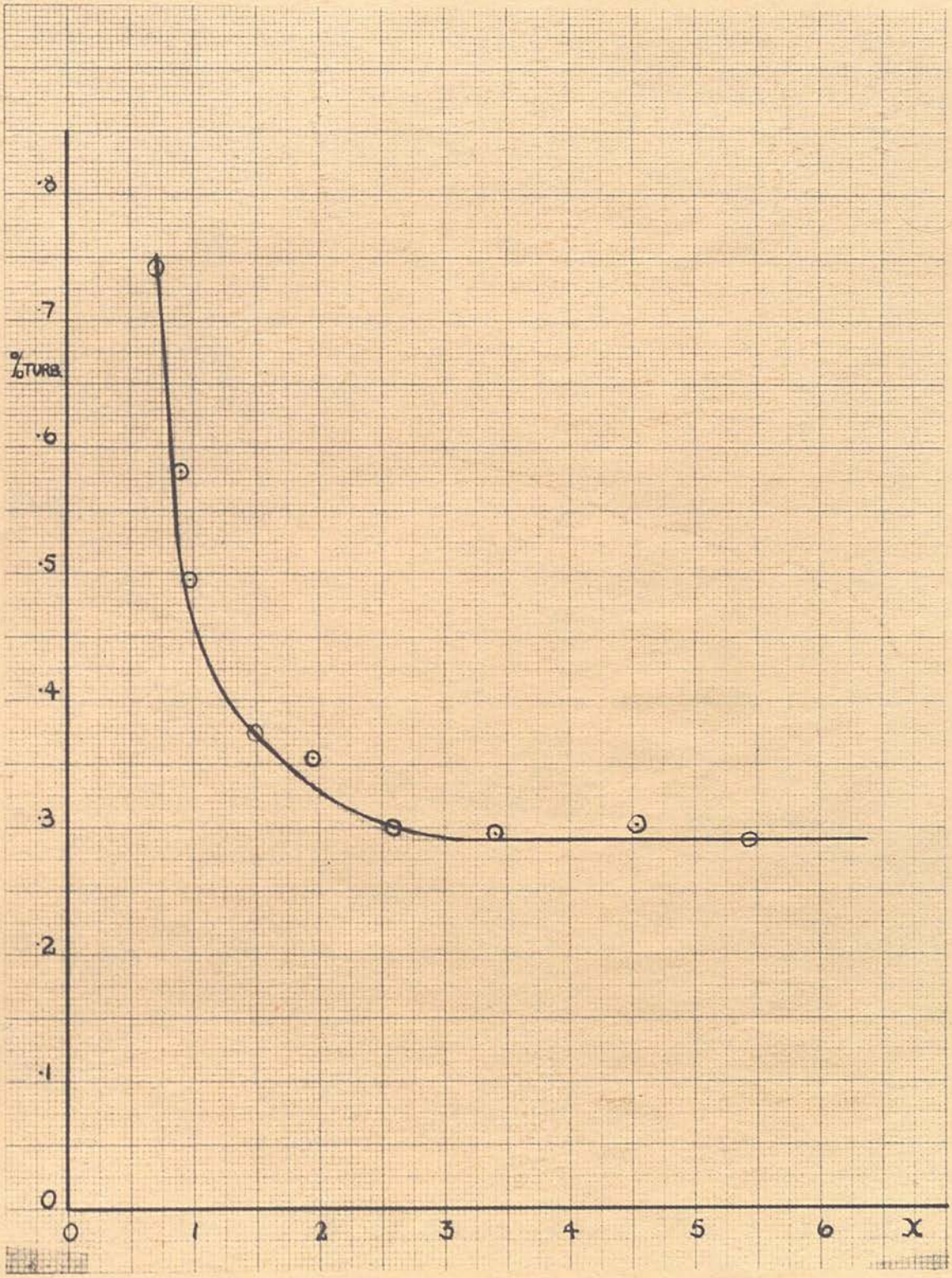

FIG.25 Decay of Turbulence in the wake of the Heated Wire.

x measured in inches behind wire.

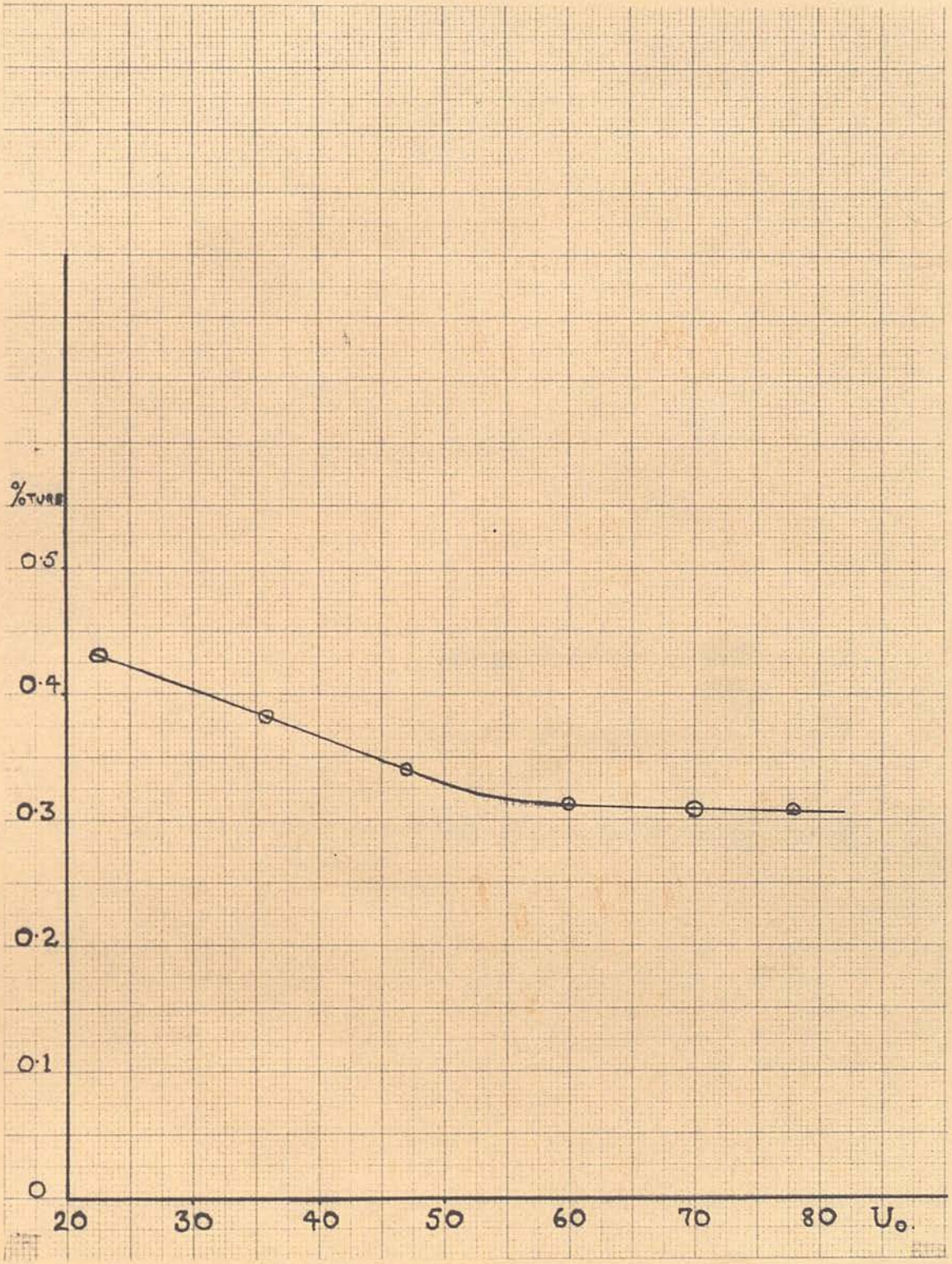

FIG.26 Variation of Turbulence with wind speed U_o ft./sec.

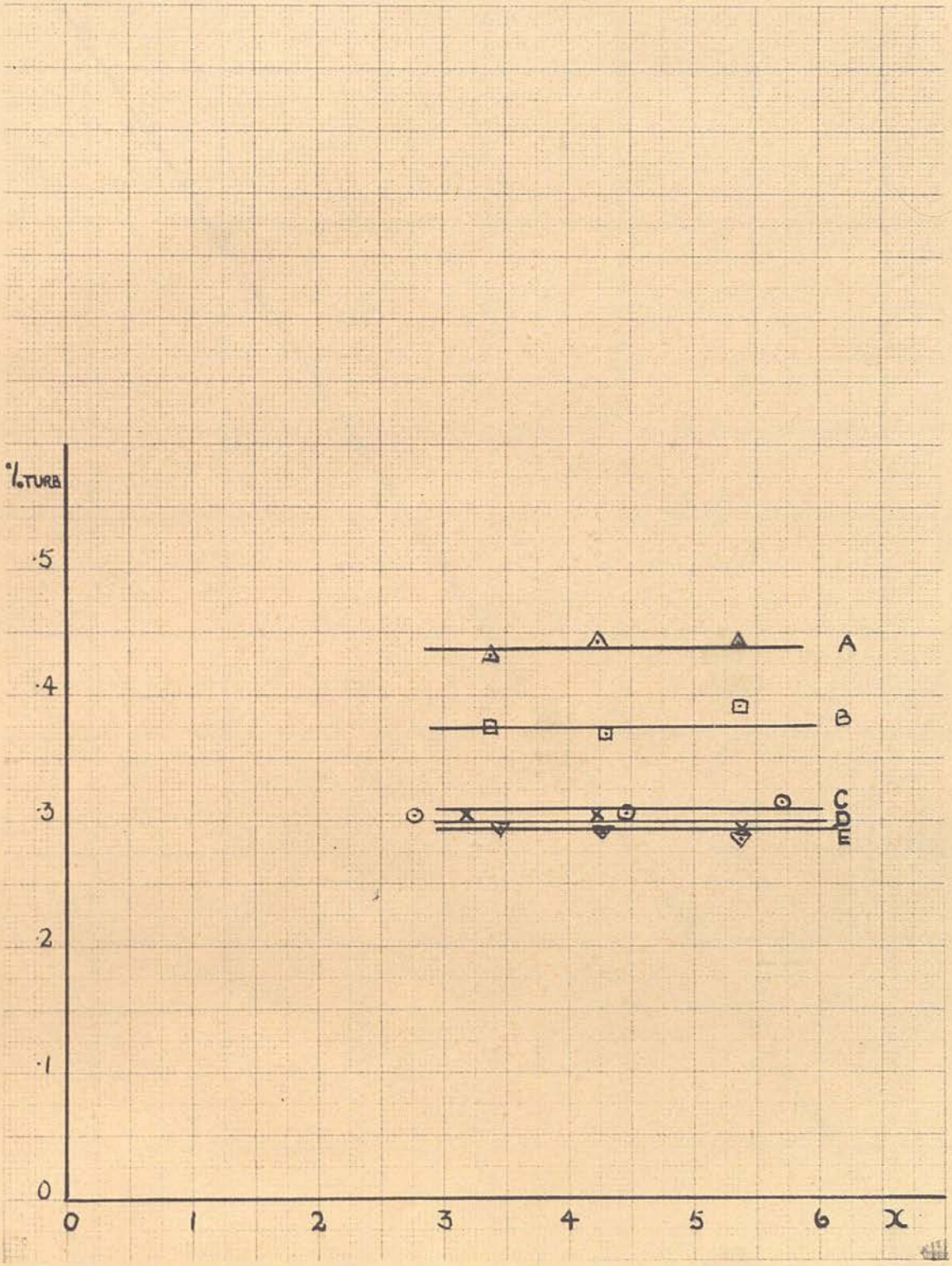

FIG.27 Effect of Screens on Turbulence Level. x in inches downstream of Heated Wire. A-no Screens, B-2 Screens 6" apart, C-1 Screen, D-2 Screens 1' apart, E-3 Screens 1' apart.

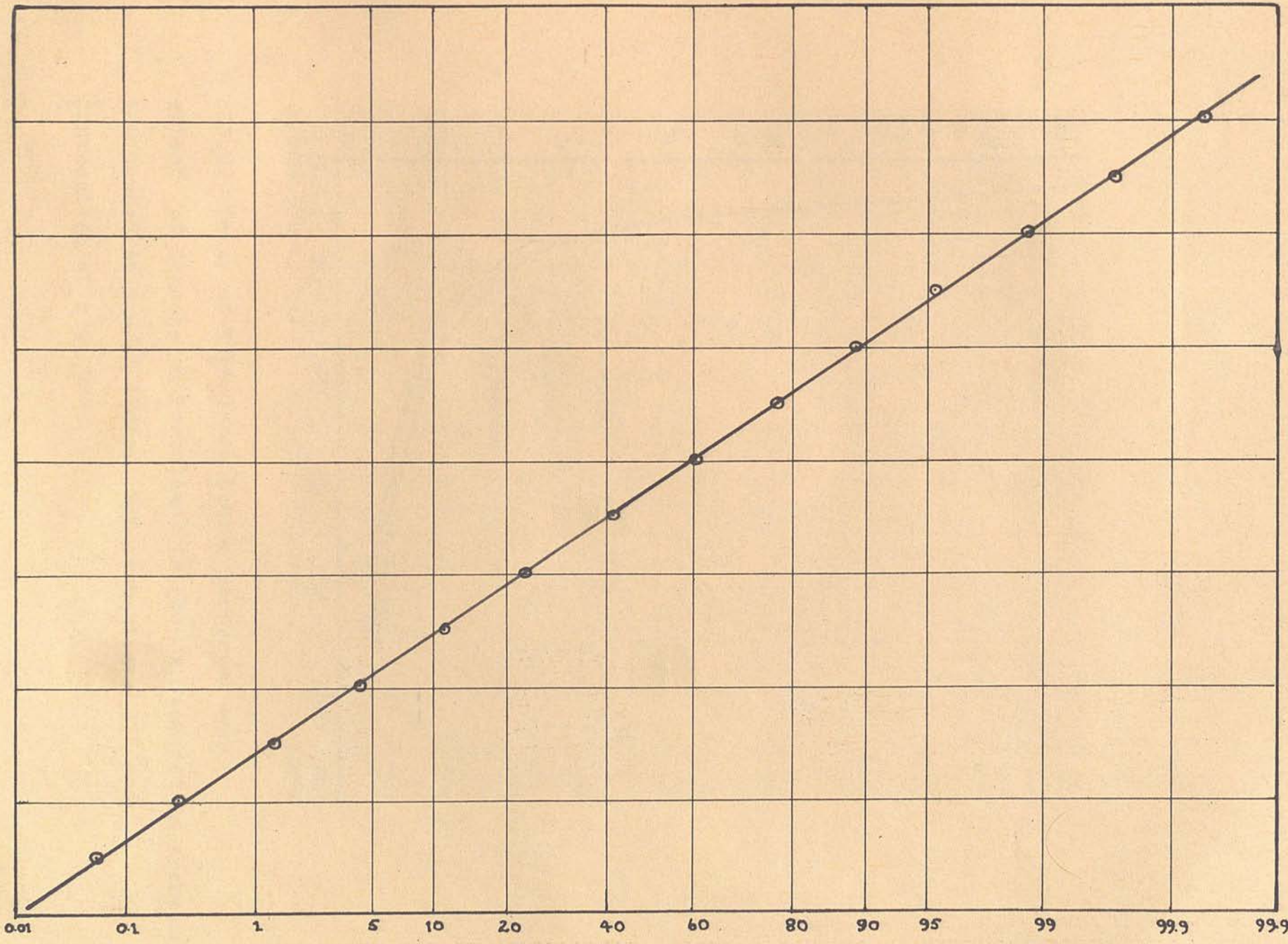

FIG.28 Probability Plot of Temperature Distribution across wake of Heated Wire.

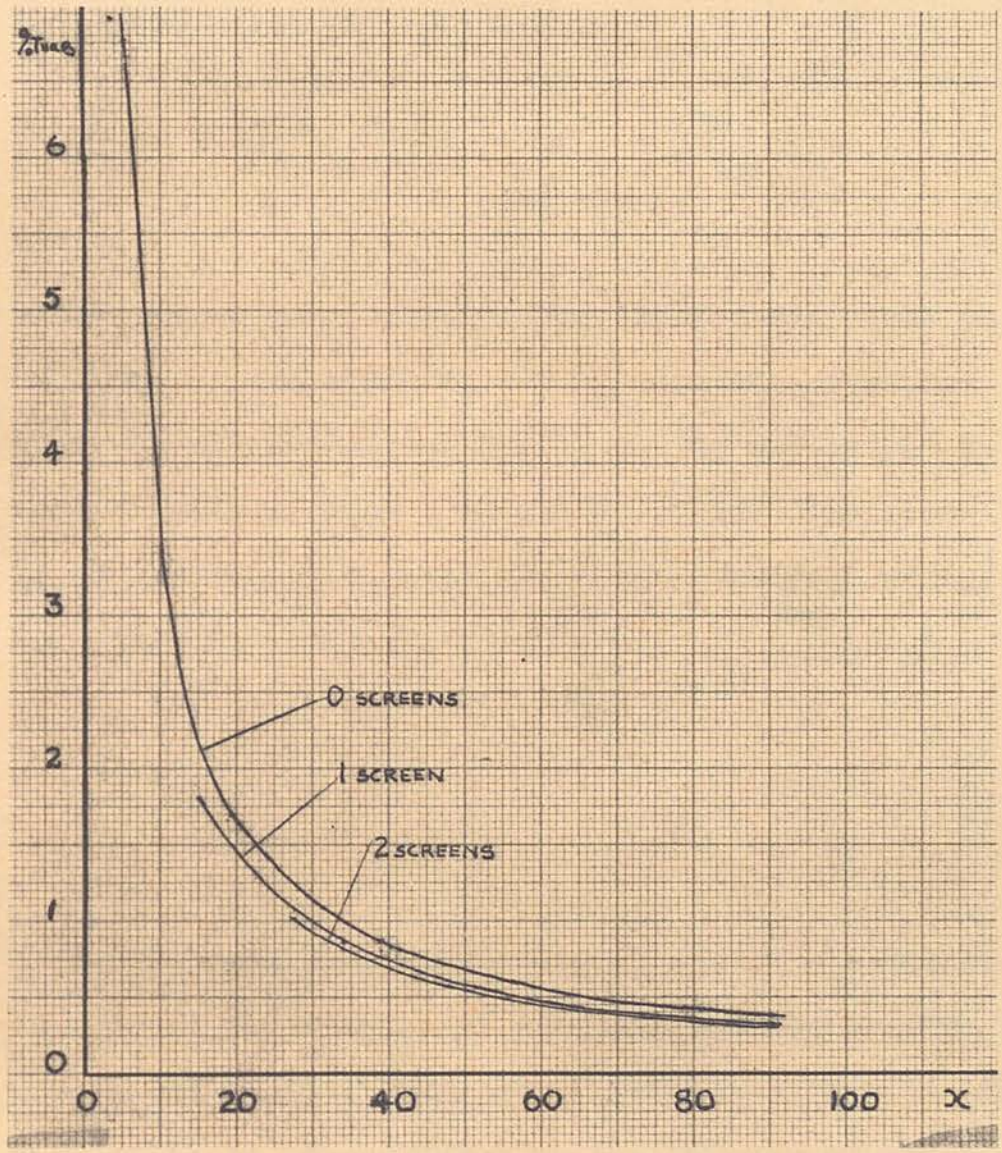

FIG.29 Decay of Turbulence behind Honeycomb and effect of Screens on Turbulence Level. x measured in inches 1st Screen at x = 15 inches, 2 Screen at x = 27" and Contraction at x = 92".

since no improvement can be expected after the contraction or during it. This is slightly lower than the value of 0.44% obtained from experiment.

For the reduction of turbulence by screens Batchelor gives the expression

$$\frac{\overline{v_2'^2}}{\overline{v_1'^2}} = \left[1 - \frac{K}{10\left(1+\frac{2}{5}K\right)} \right]^2 = \frac{\overline{w_2'^2}}{\overline{w_1'^2}}$$

where K is the pressure drop coefficient equal to $\frac{p_1 - p_0}{\frac{1}{2}\rho U_0^2}$ and where p_1 and p_0 are the pressures upstream and downstream and U_0 is the velocity. K can be obtained from a knowledge of the dimensions of the screen, i.e. wire gauge and number of wires/inch. K in this case was equal to 3.25.

Using this value of K then,

$$\frac{v_2'}{v_1'} = 0.86$$

The turbulence components v' and w' are reduced to 0.86 of their original value on passing through the screen and it is a reasonable assumption that the decay will still be proportional to the inverse of the distance as is the case of decay from the honeycomb. MacPhail, 1944, has in fact shown this to be the case. The second curve on Fig. 29 corresponds to the one screen case and allowing no change during or after the

contraction, this gives a value in the working section of 0.31%, which agrees well with the 0.31% found by experiment.

For the introduction of a second screen the expression has to be corrected, since the pressure drop coefficient will now be 2K for the two screens. The reduction will therefore be

$$\frac{\overline{v_2}^{12}}{\overline{v_1}^{12}} = \left[1 - \frac{2K}{10(1+\frac{4}{5}K)} \right]^2$$

$$\therefore \quad \frac{v_2'}{v_1'} = 0.82$$

The new value of turbulence obtained with two screens will now be 0.295%, and which once again agrees well with the experimental value. Similarly, assuming that for three screens the pressure drop coefficient is 3K, then the value of $\frac{u'}{U_o}$ in the working section is 0.285% Justification is therefore obtained for not increasing the number of screens beyond two.

It was mentioned in connection with the turbulence measuring instrument, that the sharp fall in the turbulence component measured, with increasing x distance might be due to the decay of the wake of the heated wire. The similarity between Fig. 25 and Fig. 29 is quite distinct and in fact the higher turbulence recorded at small x distances was due to the turbulence

generated by the wire itself.

2.5. Conclusions

After fully calibrating the tunnel, it was obvious that conditions were slightly worse than had been hoped for and far from ideal. It had to be decided then, whether the tunnel was suitable for the project. This is best answered by studying the effects caused by the two most serious limitations, i.e. the high turbulence level and premature transition caused by the transverse contamination wedges.

First consider the effect of the turbulence wedges. This can best be assimilated by studying the neutral stability curve with a cut off line drawn at 3'6", representing the beginning of transition on the centre line caused by the wedges. In Fig. 30 branch 2 of the neutral stability curve has been redrawn, with new axes of frequency and x distance along the flat plate for different wind speeds. As can be seen, the band of frequencies which have received the most amplification up to 3'6" is limited to 150-200 c/s. and the really low frequencies which receive the greatest amplification cannot be expected to contribute much to the frequency spectrum at transition. Schubauer and Skramstad, due to the extremely low turbulence level in their tunnel detected natural oscillations of around 60 c/s., which would of course have received

a much greater amplification as they crossed the loop. If any laminar oscillations are to be found at transition then, the most likely frequencies will be in the range 150 c/s. - 200 c/s. depending on the wind speed.

Due to the high turbulence level however it is to be expected that the percentage of total energy concentrated at this frequency will not be as great as it would have been with a lower turbulence level, and this will make pure natural oscillations difficult to detect.

Another drawback caused by transition occurring unnaturally is that the vane would not have a chance of following a particular occurrence from the laminar to the turbulent region. However, useful data might still be obtained from the turbulent region present on the plate.

It was decided that the turbulence level would be just low enough to permit the laminar oscillations to play some part in transition, and that the only way to obviate the effect of the wedges, would be to increase the wind speed above 80 ft./sec. From Fig. 3 a wind speed of 80 ft./sec. is necessary to bring natural transition forward to 3 ft. 1 in., i.e. just in front of that caused by the wedges. With this speed the fringe of the transition region might possibly be examined but the noise from the fan was unbearable, and it was also approaching the upper limit of the tunnel.

CHAPTER 3

THE ELECTRONICS

3.1 Introduction

As an introduction to this chapter a little has to be said about the form of the vane, to justify the choice of an electronic method of detection.

The dimensions of the vane were governed by the frequencies to which it was expected to respond. The smallest wavelengths anticipated were of the order of 0.5" and therefore the dimensions of the vane had to be less than this, so a standard vane size of 0.4" x 0.4" was chosen. The vane was kept as thin as possible and the average thickness was about 0.0003" . A theoretical solution for the effect of forced oscillations on the vane was never attempted and it was thought that the deflection of the vane might be proportional to either a linear or square ratio of the two velocities imposed on it. It was anticipated that the ratio of the velocity of the fluctuations to the velocity of the free stream, would be of the order of 1.0%. If it did in fact respond to a square law therefore the angular deflection would be $10^{-4^{\circ}}$. If a linear law defined the conditions more accurately, then the deflection would still be small, but much more easily detected. Since the worst possible case had to be allowed for,

the most sensitive method of detection had therefore to be employed, and this finally proved to be an electronic one.

It will be seen in Chapter 4 however, that conditions were much better than had been anticipated. The velocity fluctuations were larger than expected and also, by using the vane as a resonant detector, its amplitude response was greatly improved.

3.2. Optical Method of Detection

The first and most obvious possibility was an optical method. A well collimated beam of light could be directed on the vane and the reflected beam focussed on to a moving film. This method was in fact used to determine the natural frequencies of vibration of larger vanes. However, when the vanes became extremely light, the material of which they were made, normally mica, tended to warp, and when silvered it was impossible to focus the reflected beam, due to the high degree of scattering.

Another drawback of the optical method, was that for the very small deflections anticipated, the path length of the reflected beam would have to be very long, before any significant directional variation of the beam could be observed. Assuming $\frac{v'}{U_o} = 1\%$,

then the total angular deflection of the vane would be 2×10^{-4}°. The angular change of the light beam would be 4×10^{-4}°, and therefore for a path length of 5 metres a deflection of 2 mm. would be observed. Since the size of the spot on the recording film produced by even a well focussed beam would be comparable with this, then the resolution of such a system was considered unsatisfactory, and other methods of detection were investigated.

3.3.1. Electronic method of detection

The potentialities of an electrical method were next examined. The vane surface could be silvered and when used at small distances from the surface of the flat plate, could be made to form an air dielectric capacitor with it. The surface of the plate would also be coated with some conducting substance. The problem would therefore be to detect the changes in capacitance induced by the velocity fluctuations. A reasonable spacing between the vane and flat plate, estimated from considerations of boundary layer thickness, on which to base calculations would be 0.040" . With a plate area of 0.4" x 0.4" this gives a total capacitance of 1.1μμF. With a vane length of 0.4" and assuming the same angular deflection as before, then it would be required to measure changes of the order

of 0.1% in a total capacitance of 1.1μμF.

Various methods for measuring small changes in capacitance were investigated, but most were discarded, mainly due to insensitivity.

3.3.2. One attractive possibility was the circuit of Whiddington, 1929, shown in Fig. 31. This consisted of two similar oscillators tuned to the same frequency N. The vane could then be inserted in the tuned part of one of them and the changes of capacitance would cause a heterodyne effect, which could either be detected audibly as a beating effect or observed on a cathode ray oscilloscope. Although this circuit could be made very sensitive it was of a fairly basic type and instability, such as frequency drift, was expected. This would give rise to spurious signals and also a certain amount of noise, and for these reasons this type of oscillator was discarded.

For stability considerations, the use of quartz crystals was investigated. The presence of a quartz crystal as a tuned circuit, leads to very good frequency stability, due to the inherent mechanical properties of the crystal, which govern its mode of vibration. When mounted in a vacuum tube, a crystal is also insensitive to temperature, to which other circuit elements such as inductors and capacitors are

subject. Future circuits have therefore been designed with a crystal forming an integral part.

It was also decided that the circuit should be of the form,

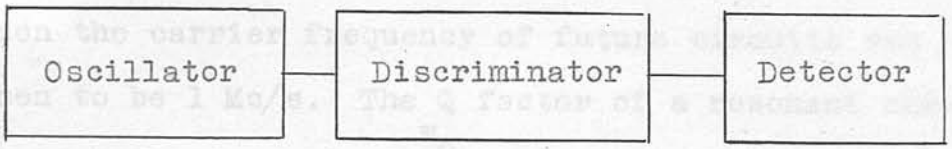

The vane would be inserted in the tuned part of either the oscillator or the discriminator, and the fluctuations of capacitance would modulate the carrier wave.

3.3.3. Resonance of tuned circuits

Since the resonant properties of tuned circuits are referred to regularly throughout this chapter a brief explanatory note is advisable at this stage.

The relation $f = \frac{1}{2\pi\sqrt{LC}}$, where f is the frequency, L the inductance element and C the capacitance element, gives the resonant frequency of a parallel tuned circuit in terms of the circuit elements. Furthermore $\delta f = -f\,\frac{\delta C}{2C}$ and it is obvious that to obtain a maximum amount of frequency modulation for δC, then C must be as small as possible. Allowing for the self-capacitance of the

inductance, and also for stray capacitance a practical value for C is 12.5μμF. From $\delta f = -f \frac{\delta C}{2C}$ it can also be seen that the greater the carrier frequency is made, the greater becomes the frequency change, δf, which is consequently easier to detect. For this reason the carrier frequency of future circuits was chosen to be 1 Mc/s. The Q factor of a resonant circuit is defined as $Q = \frac{w_o}{w_1 - w_2}$ where w_o is the resonant frequency, and w_1 and w_2 are the frequencies on either side of the resonance curve, measured at points where the response is 3 d.b. down from the peak. The Q of a resonant circuit can be regarded as either the magnification, selectivity or quality.

3.3.4. Vane in Discriminator Section

At first it was thought best to build a highly stable oscillator (10^6 c/s. $\pm$ 3 or 4 c/s.) and have the vane in the discriminator section. The circuit would be as in Fig. 32. The requirements of the discriminator or filter would have to be (1) that the change in capacitance of the vane would have an appreciable effect, and (2) that it should have an exceptionally high Q, in order that a detectable degree of modulation would be given to the carrier frequency.

Condition (1) could be met by using either a parallel or a series tuned LC circuit. When put in

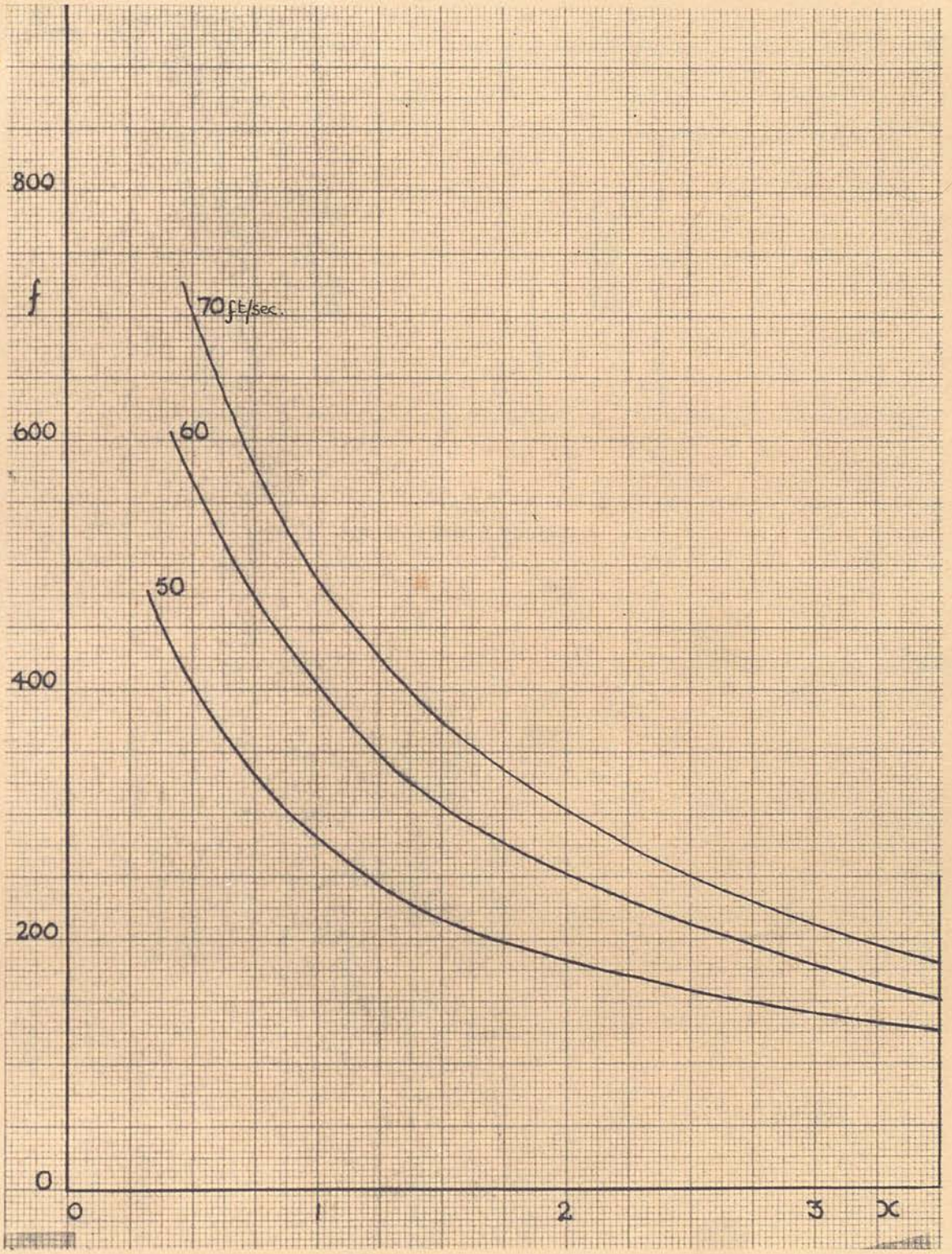

FIG.30 Effect of Windspeed on Branch 2 of Neutral Stability Curve. Axes are frequency f c/s and x in ft.

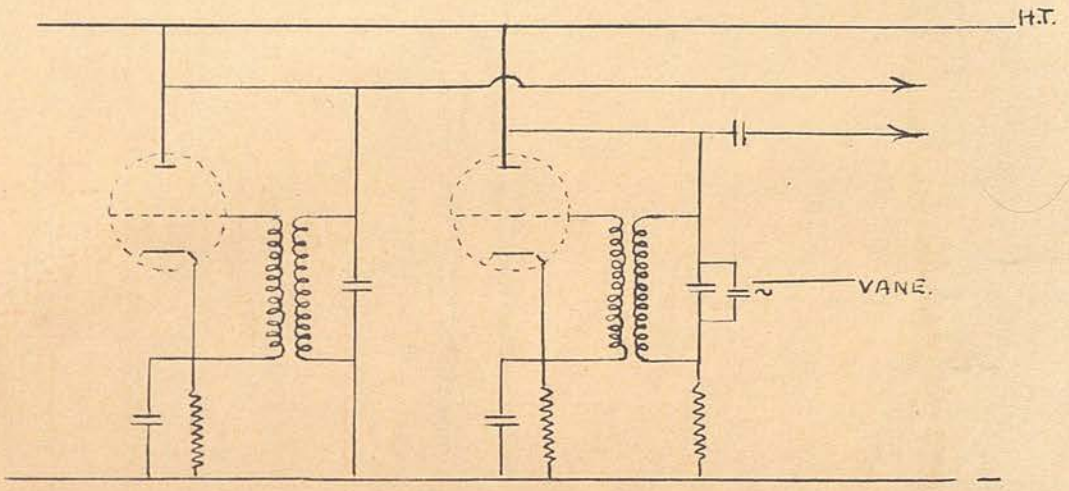

FIG.31 Circuit of Whiddington.

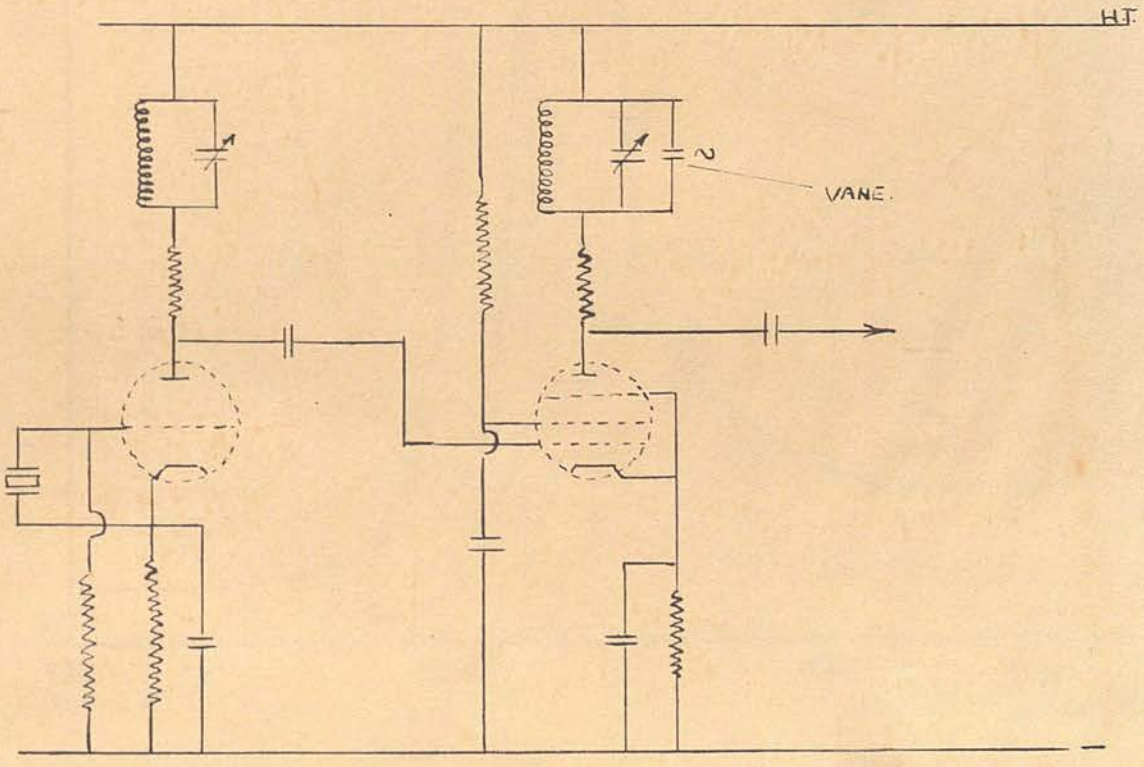

FIG.32 Crystal Oscillator with Vane in Discriminator.

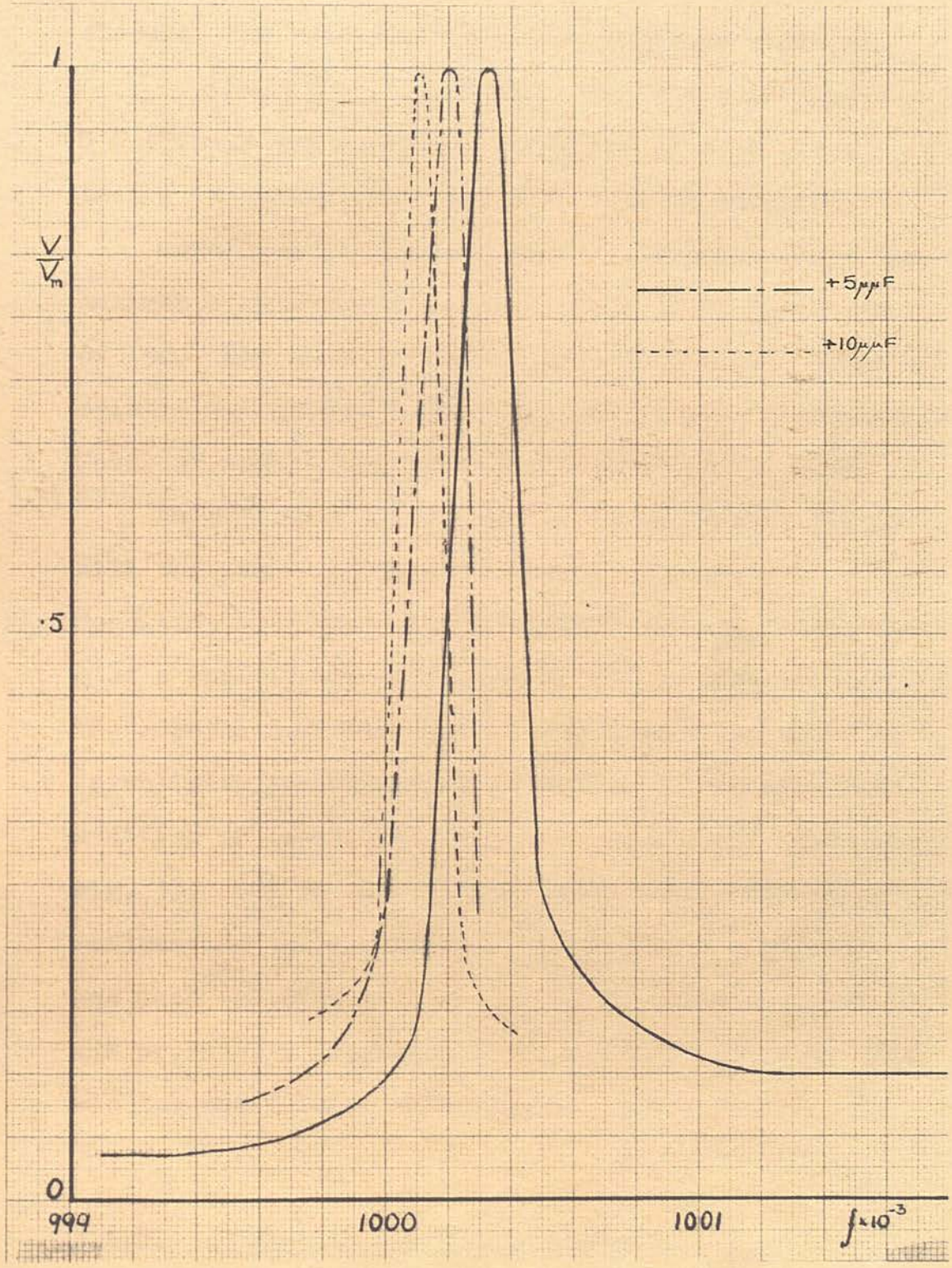

FIG.33 Effect of Capacitance on Crystal Filter Response.

parallel with the capacitance element of the tuned circuit, the vane would cause a frequency shift of $\delta f = -f\frac{\delta C}{2C}$. Assuming $\delta C = 5 \times 10^{-4}$ μμF, C = 12.5μμF and a carrier frequency $f = 10^6$ c/s., then a frequency shift $\delta f = 20$ c/s. is obtained.

Condition (2) however was unattainable since the maximum possible Q of an LC circuit is of the order of 150. The slope of the impedance-frequency characteristic was therefore much too low to give a detectable level of amplitude modulation to the carrier wave.

Another possibility was to use a crystal filter with the vane connected in parallel across it. Condition (2) could then be adequately met, since the Q of a crystal can be very high and in fact the Q of the crystal used was 6,000. Tests were performed to investigate the variation of resonant frequency with addition of capacitance and the results are shown in Fig. 33. Due to the inherent mechanical properties influencing the frequency of vibration the crystal was much too stable and a change of capacitance of 10^{-3} μμF produced a frequency shift of only 0.02 c/s. This was too small to be detected.

3.3.5. Vane in oscillator circuit

The alternative was to have the vane in the oscillator circuit and use a crystal filter. A

suitable circuit was found which was a modification of the 'Clapp' (1948) oscillator and which was claimed to be stable to within 4 or 5 c/s. in 10^6 c/s. The circuit is shown in Fig. 34 and is similar to that of the Colpitts oscillator except that an LC circuit has replaced an inductor, giving increased stability. The criterion for oscillation of this circuit is $\frac{wL}{Q} = gm\, X_1 X_2$, where g_m is the mutual conductance of the tube, X_1 and X_2 are the reactances of C_1 and C_2 and w, L and Q have their usual meanings. For high stability performance Q was required large and therefore X_1, X_2 were small. The feed back capacitors C_1 and C_2 were made as large as possible, and were in fact tuned to almost cut off. Other considerations taken into account were the rigidity and placing of components as this affected the eventual stability of the oscillator.

The vane could be inserted in parallel with C and would have the effect $\delta f = -f \frac{\delta C}{2C}$ as before. An oscillator of this type was constructed and operated successfully at a frequency of 1 Mc/s. This frequency could be adjusted by the variable capacitor C, for tuning purposes. The stability of the oscillator, once time had been allowed for the components to reach a stable working temperature, proved very satisfactory, and the frequency drift could be considered non-existent after 30 mins.

3.3.6. The Crystal Filter

The purpose of the filter is to convert the incoming frequency modulated wave to an outgoing one, amplitude modulated. It is in performing this function that the very high Q is most useful. The circuit is as shown in Fig. 35.

The operation of this stage is as follows. When the carrier wave frequency is other than the resonant frequency of the crystal, the Radio frequency is developed across the 100KΩ resistor and no output signal is obtained. However, as the resonant frequency of the crystal is approached, the crystal impedance becomes very large compared to that of the 100 KΩ resistor and almost the full RF voltage is developed across the crystal. The voltage frequency characteristic is as shown in Fig. 36. The curve represents the voltage developed across the crystal as resonance is reached and the voltage scale is non-dimensionalized for convenience.

The oscillator is tuned to operate at a frequency corresponding to the mid-point of the straight part, on the low frequency side of the curve. This will be the frequency of the carrier wave, which will be frequency modulated due to the fluctuations of the vane. When this is injected across the filter, the envelope of the carrier wave will become amplitude

modulated, the envelope frequency being the frequency of the vibrations of the vane, and the amplitude of the modulation being related to the displacement of the vane.

The oscillator and filter circuits just described form the two most critical parts of the instrument. The sensitivity depends entirely on these two parts. The oscillator, although being very stable gives a large degree of frequency modulation for a small capacitance change, due to the series resonance of the components in the oscillator. The filter, due to the very steep slope of the voltage/frequency characteristic gives a detectable degree of amplitude modulation for very small values of frequency modulation.

3.3.7. Radio Frequency Amplifiers

To obviate any load effects on the oscillator, it was necessary to have a buffer amplifier inserted between the oscillator and filter sections. An R.F. Amplifier stage was also necessary to boost the voltage obtained from the oscillator. It was also much easier to build, and would cause less distortion at this stage, than an audio-amplifier placed after the detector.

3.3.8. Cathode Follower

A cathode follower was built in after the filter. This served to match the high impedance of the filter

with the low impedance of the detector. It also afforded an appropriate point at which to connect a valve voltmeter. This enables the voltage across the crystal to be measured accurately, and also allows the carrier frequency to be adjusted to the appropriate operating point on the response curve.

3.3.9. Detector

The next requirement was a detector, and for this a conventional circuit was adopted. The operation of this stage is as follows. The envelope is first rectified, and then by the appropriate choice of filters, the R.F. component is eliminated leaving only the wave form of the envelope. In this case the filter consisted of a 47KΩ resistor and a 220$\mu\mu$F capacitor. At a frequency of 1 Mc/s., the impedance of the capacitor is $10^3\Omega$, and therefore frequencies of this order will be developed across the 47KΩ resistor. But at frequencies of the order of 1 Kc/s. the impedance will become of the order of $10^7\Omega$, and therefore signals of this frequency will appear across the output. Thus the R.F. component is effectively eliminated from the output signal.

3.3.10. Audio-amplifier stage

To give the signal a final boost before observation on a Cathode Ray Oscilloscope, an audio-amplifier stage was added. By using electrolytic capacitors for coupling and cathode bias, an attempt was made to maintain a flat frequency response down to 50 c/s. This condition was necessitated by the fact that frequencies of below 100 c/s. were expected to be examined with the vane. The complete circuit diagram is shown in Fig. 37.

3.3.11. Noise Level

In an attempt to produce a very low noise level so that the highest possible signal/noise ratio would be obtained, the individual stages were separated from each other by metal screens. This reduced pick-up, as did the co-axial cable, used exclusively for outside connections to other instruments. To reduce main's hum the heaters of the instrument were supplied from accumulators and for the H.T., a very stable low noise power pack was bought. By earthing the chassis of all the units used, mains hum was largely eliminated.

Measurements at the output indicate a noise level of 40 mV. Assuming a least acceptable signal/noise ratio of $^{10}/_{1}$, then the capacitance change corresponding to 0.4 volts output, is considered as

the lower limit of the instrument. This information is obtained from the next section.

3.4.1. The Calibration of the instrument

For use the instrument had to be calibrated, i.e. the relation between capacitance change of the small vane and the resulting output voltage had to be determined. From this data it was hoped to calculate the absolute deflection of the vane. The calibration could be done in two possible ways. It could be calibrated by considering the performance of the instrument stage by stage, or a direct calibration could be made, if a small enough, known capacitance change could be fed in across C. Naturally it was desirable to try both methods, and use one as a check on the other.

3.4.2. Stage by Stage Calibration

For this method of calibration, the first relationship required is that between the frequency and the capacitance C of the oscillator. This was obtained by first calibrating the tuning capacitor, which had a range of about 15 $\mu\mu$F, on a capacitance bridge, and then measuring frequency changes of the

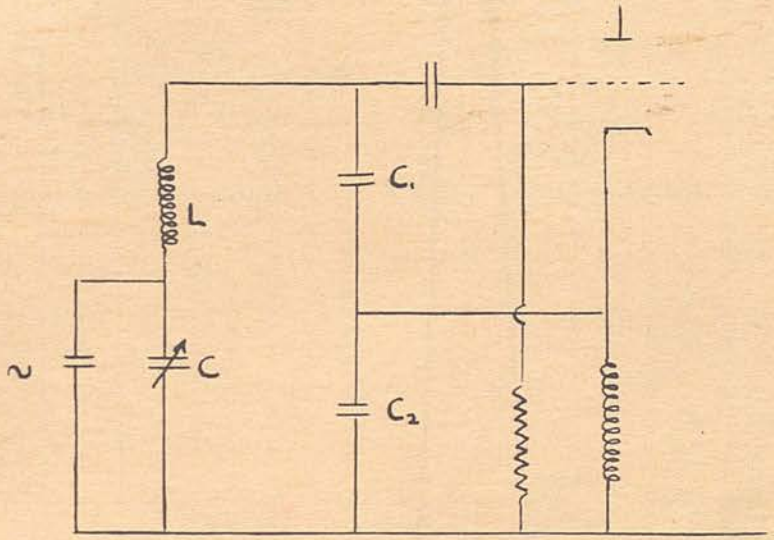

FIG.34 Circuit Diagram of Oscillator.

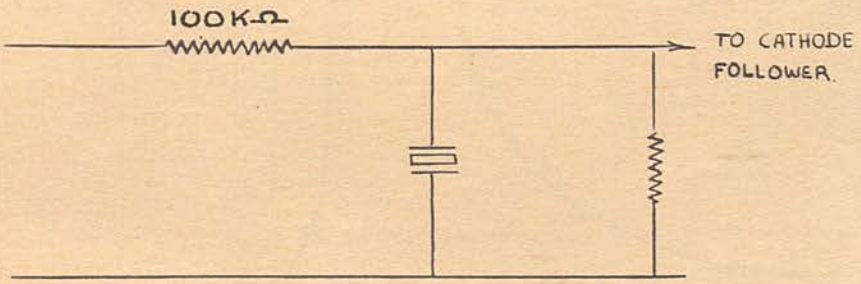

FIG.35 Circuit Diagram of Filter.

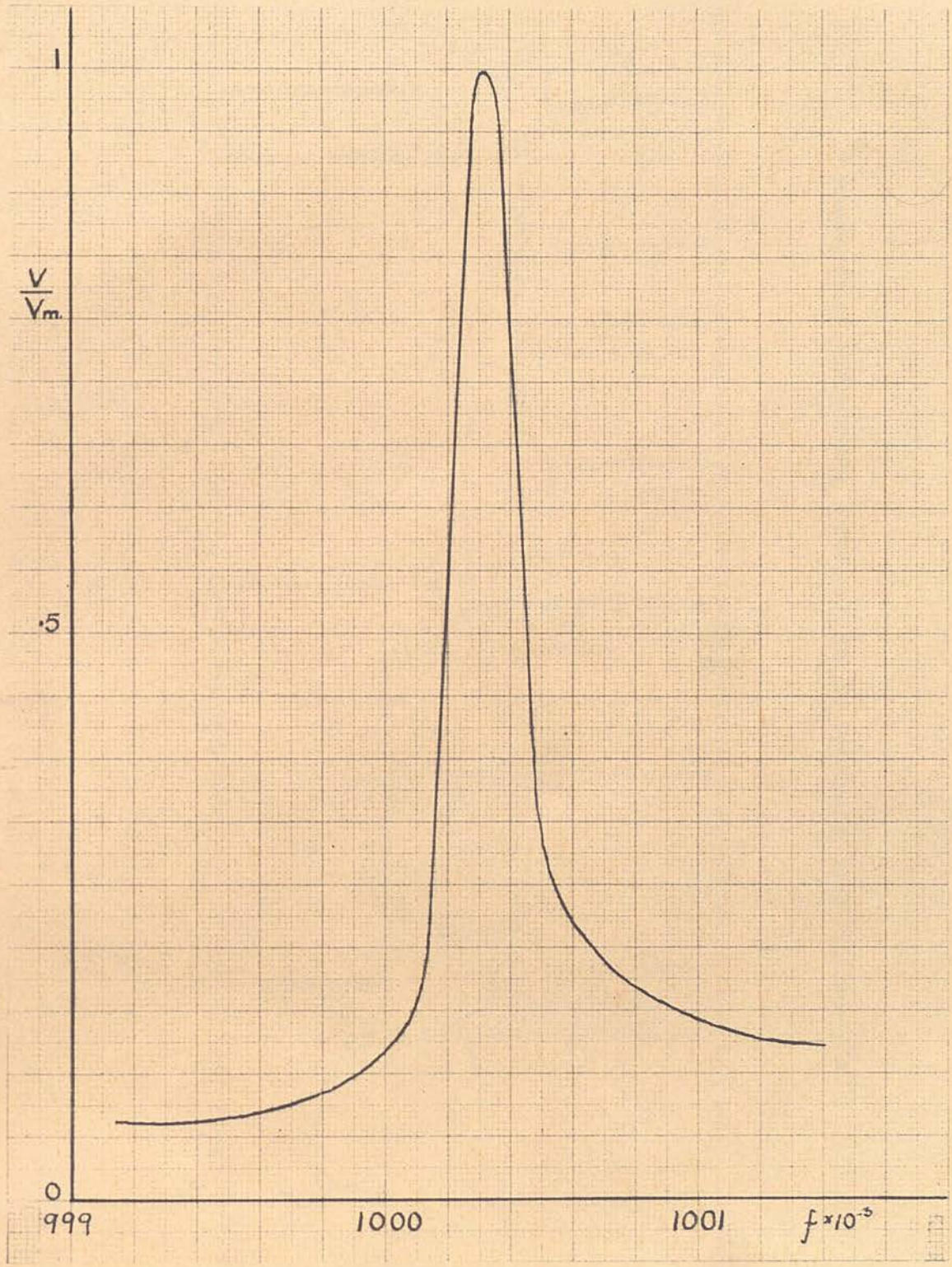

FIG.36 Response Curve of Crystal Filter, Voltage Scale non-dimensionalized to allow for variation of Crystal Voltage.

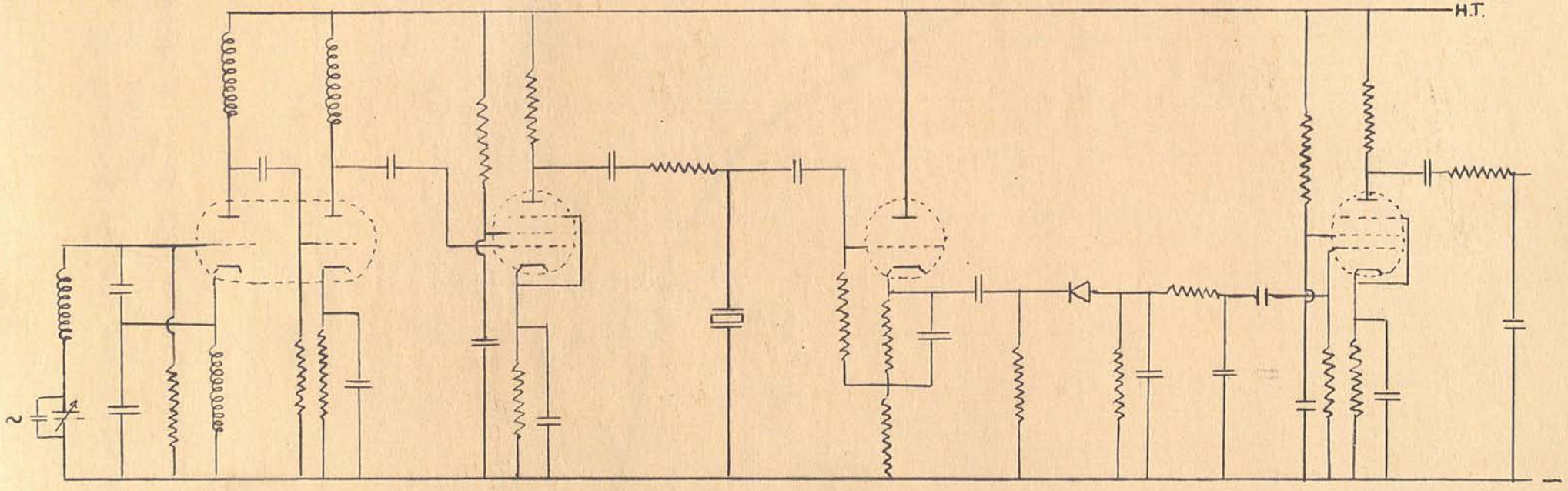

FIG.37 Complete Circuit Diagram of Electronic Recording Instrument.

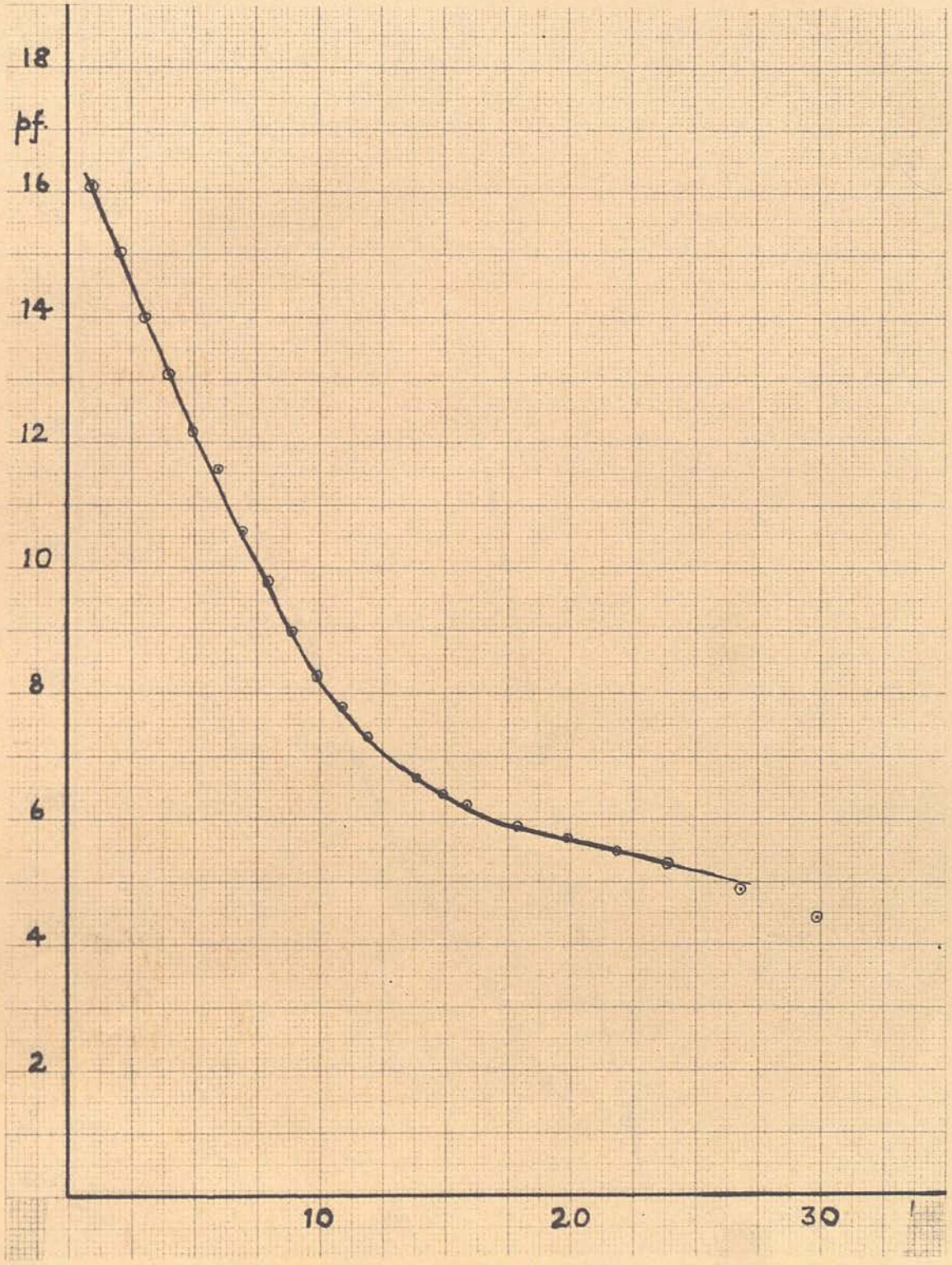

FIG.38 Calibration Curve of Tuning Capacitor. Capacitance in pf = $\mu\mu$ F against scale divisions.

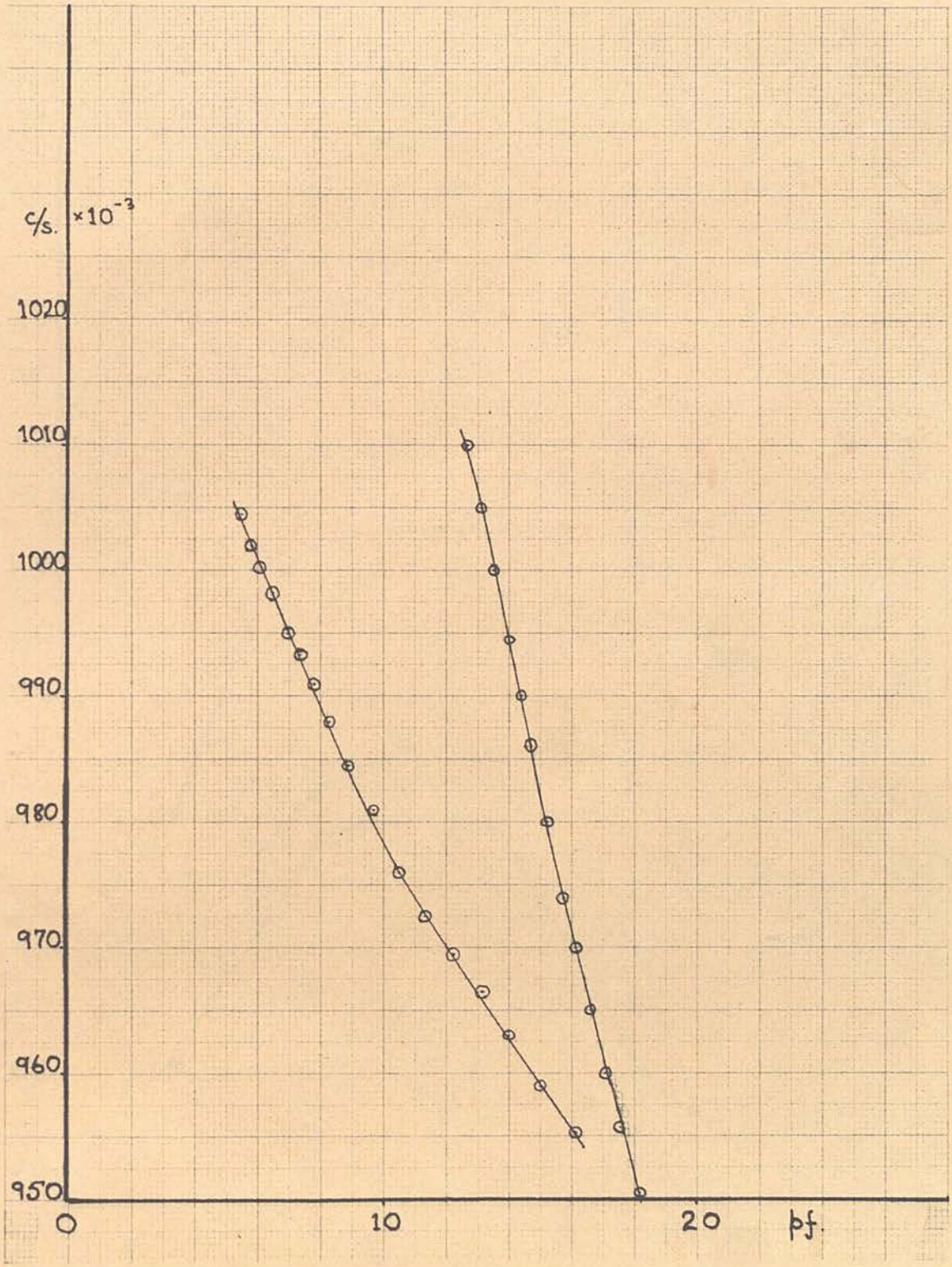

FIG.39 Variation of Oscillator Frequency (c/s) with tuning Capacitor C.

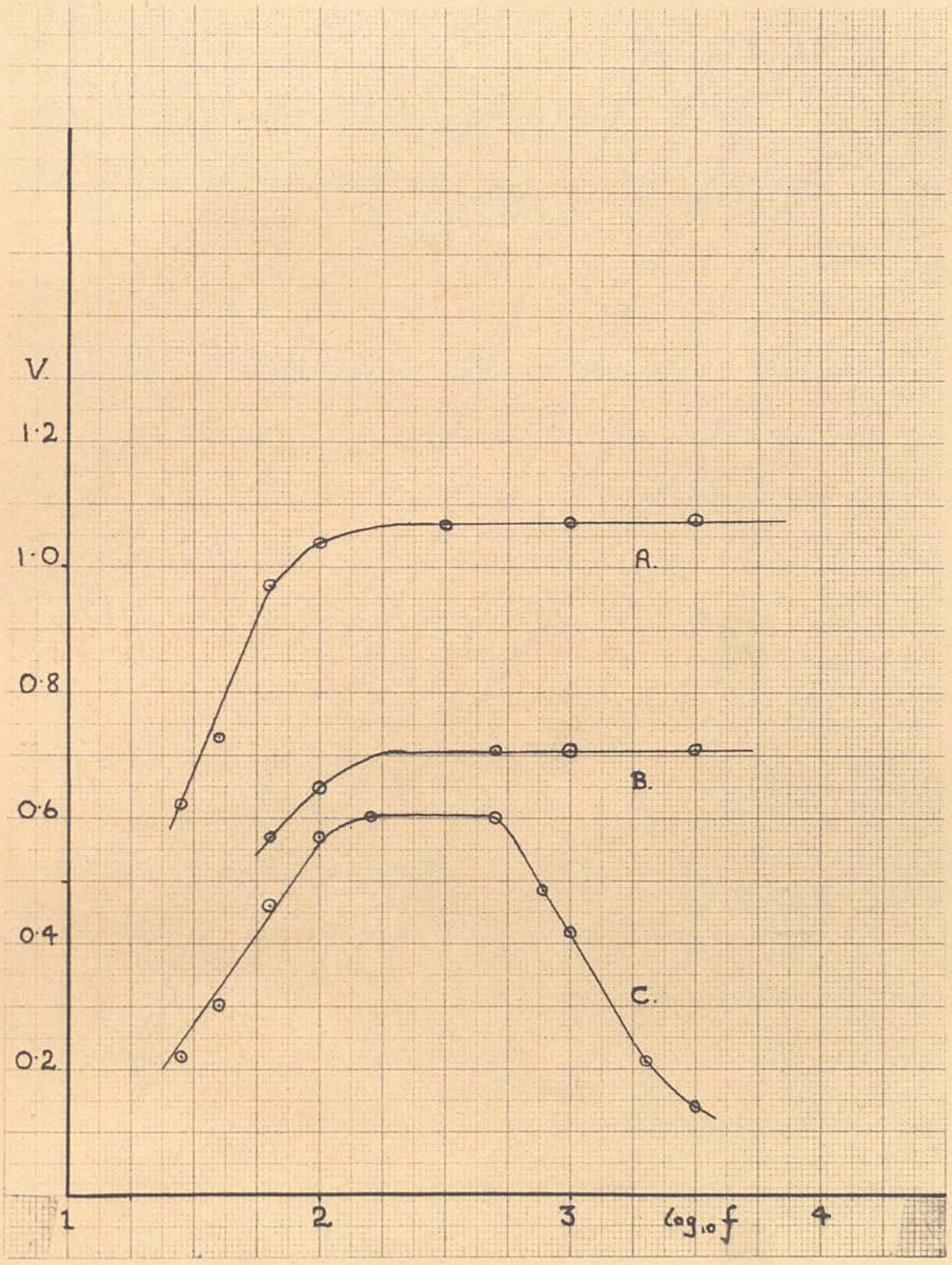

FIG.40 Frequency Response Curves of Audio Stages of Instrument

A-Amplifier, B-Amplifier Detector, C-Amplifier Detector

Filter. V arbitrary voltage scale.

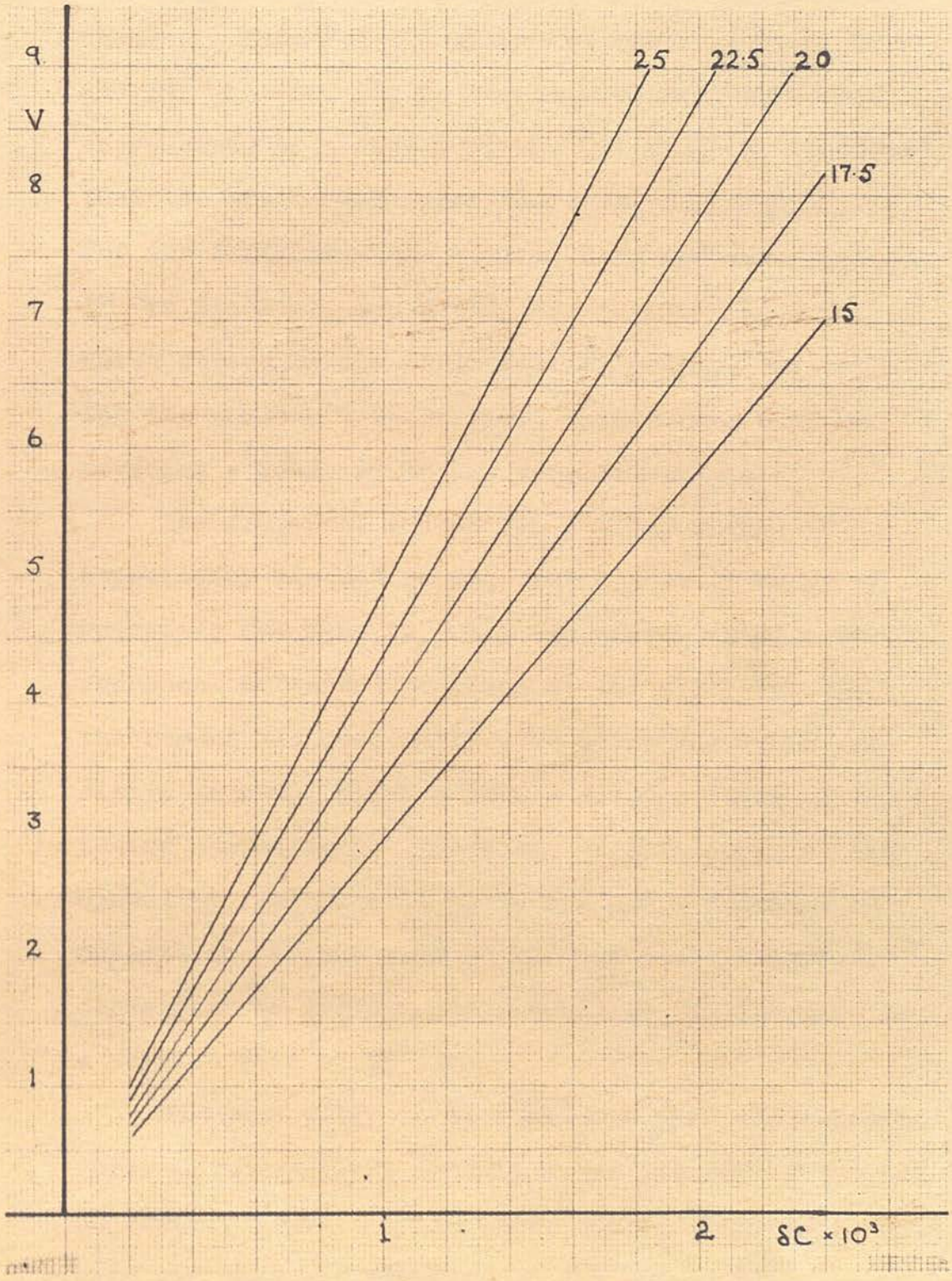

FIG.41 Theoretical Calibration Curves of Instrument for different peak voltages across Crystal. Output in volts for variation of input Capacitance in μμF.

oscillator corresponding to the now known capacitance changes. These relationships are shown in Figs. 38 and 39. In Fig. 38 d is in arbitrary units and corresponds to a dial reading. It might be mentioned that the tuning capacitor was constructed specially for the instrument and consisted of two brass plates, 1" in diameter, one fixed and the other adjustable, which formed an air dielectric capacitor. By varying the spacing between them, capacitance changes covering a range of 15 $\mu\mu$F were obtainable.

The frequency change for a given change in capacitance was now known, over a certain range of operating frequencies. The two curves in Fig. 39 represent different tappings of the coil, and the instrument has been calibrated using the least sensitive tapping, which allows a greater range of tuning capacitance. The slope of this curve at the operating frequency is 4,440 c/s/$\mu\mu$F. A change in capacitance of the vane of 10^{-3} $\mu\mu$F would therefore correspond to a frequency modulation of 4.44 c/s. on a carrier wave of 10^{6} c/s.

The next stage to be considered was the response curve of the crystal filter, since the amplifiers had no effect, other than to boost the R.F. voltage. This gain was measured directly on the valve voltmeter and therefore individual gains need not be taken into account. The impedance-frequency characteristic of the filter was obtained as accurately as possible

using an R.F. signal generator, frequency meter and valve voltmeter. The curve obtained is effectively the same as that shown in Fig. 36. From Fig. 36 the slope of the low frequency side is $6V_{max}^{mv}/c$ where V_{max} is the peak response voltage in volts. This voltage was slightly dependent on the length of coaxial cable from the instrument to the vane inside the tunnel, which of course formed part of the oscillator circuit. It was also dependent to a certain extent on the heater voltage, which varied with the degree of discharge of the batteries, and varied between 15 and 25 volts. From the relation $6V_{max}^{mv}/c$ therefore the amount of amplitude modulation corresponding to a given frequency modulation can be calculated.

All that was required now was the gain of the final stages. This was found using a signal generator and valve voltmeter. A slight amount of attenuation had to be expected from the cathode follower and also some was present in the detector. The response curves for the final stages taken individually and collectively are shown in Fig. 40. Curve A is the amplifier response alone, B is the response of the amplifier + detector, and C the response of the amplifier + detector + filter. The overall mid-frequency gain of the last three stages was 7, and this information enabled a final set of calibration curves to be drawn, and these are shown in Fig. 41. Allowance has been

made for the peak voltage across the crystal and it can be seen that for the 20 V case, a $10^{-3}\mu\mu F$ change in capacitance gives an output signal of 3.9 volts.

Only the amplitude response at mid-frequencies is obtained from the curves of Fig. 41 and a final mention about the frequency response of the instrument is necessary before the calibration is complete. Since the initial capacitance change is very small, then the extent of the frequency modulation will also be very small, and for R.F. amplification purposes the carrier wave could be considered mono-frequent. Therefore no distortion will occur in the early stages up to the crystal filter, and it will only be after the signal has been detected, that the frequency response of the audio-amplifier and filters will have to be considered. From the response curves shown in Fig. 40 it can be seen that the low frequency 3 db. point is about 60 c/s. This lower limit is determined solely by the response of the amplifier, and it was attempted to make this as low as possible, by using electrolytic capacitors for coupling the stages. This low frequency response could be improved by employing more than one stage of audio-amplification and a more refined amplifier circuit, but the response of the instrument was adequate for the present requirements. The upper frequency 3 db. point depends on the response of the various filters

used. By choosing suitable components this can be varied to cut off at any desired frequency, and in this case was about 1000 c/s.

3.4.3. Direct Calibration

For this method of calibration a known, minute change of capacitance of the order of 10^{-3} $\mu\mu$F had to be produced. The basis of the method devised for this, is that when a comparatively large change of capacitance is put in series with a small fixed capacitor, the resulting capacitance change of the combination can be made to be very small, depending on the values of the circuit components.

The circuit diagram of the arrangement was as follows:

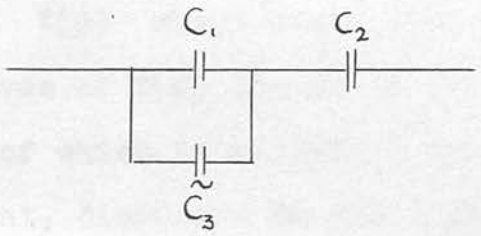

C_1 and C_3 can be considered as one capacitor, with a static and variable part, and C_2 is the small capacitor necessary for reducing the change of capacitance. The total capacitance C of such an arrangement is

$$\frac{1}{C} = \frac{1}{C_2} + \frac{1}{C_1 + C_3 f(\theta)}$$

where C is the total capacity and $C_3 f(\theta)$ varies in a sinusoidal manner. Therefore

$$C = \frac{C_1\left(C_2 + C_3 f(\theta)\right)}{C_1 + C_2 + C_3 f(\theta)}$$

It was also stipulated that C should be of the form,

$$C = C_4 + C_5 \sin\theta$$

i.e. a fixed part with a small sinusoidal change impressed upon it. Therefore,

$$C_4 + C_5 \sin\theta = \frac{C_1\left(C_2 + C_3 f(\theta)\right)}{C_1 + C_2 + C_3 f(\theta)}$$

This equation was solved by inserting realistic values for the components C_1, C_2 and C_3, and obtaining the value of $f(\theta)$ which would give a sinusoidal output. Curves of $f(\theta)$ against θ are shown in Fig. 42, a knowledge of which is necessary for the design of the instrument, discussed in the next paragraph. Since the capacitance of the vane was about 1.0 μμF then this is a reasonable value to choose for C_2. C_1 and C_3 were varied according to the magnitude of the desired capacitance change.

The device for producing the capacitance changes is shown in Fig. 43, and consists of two concentric

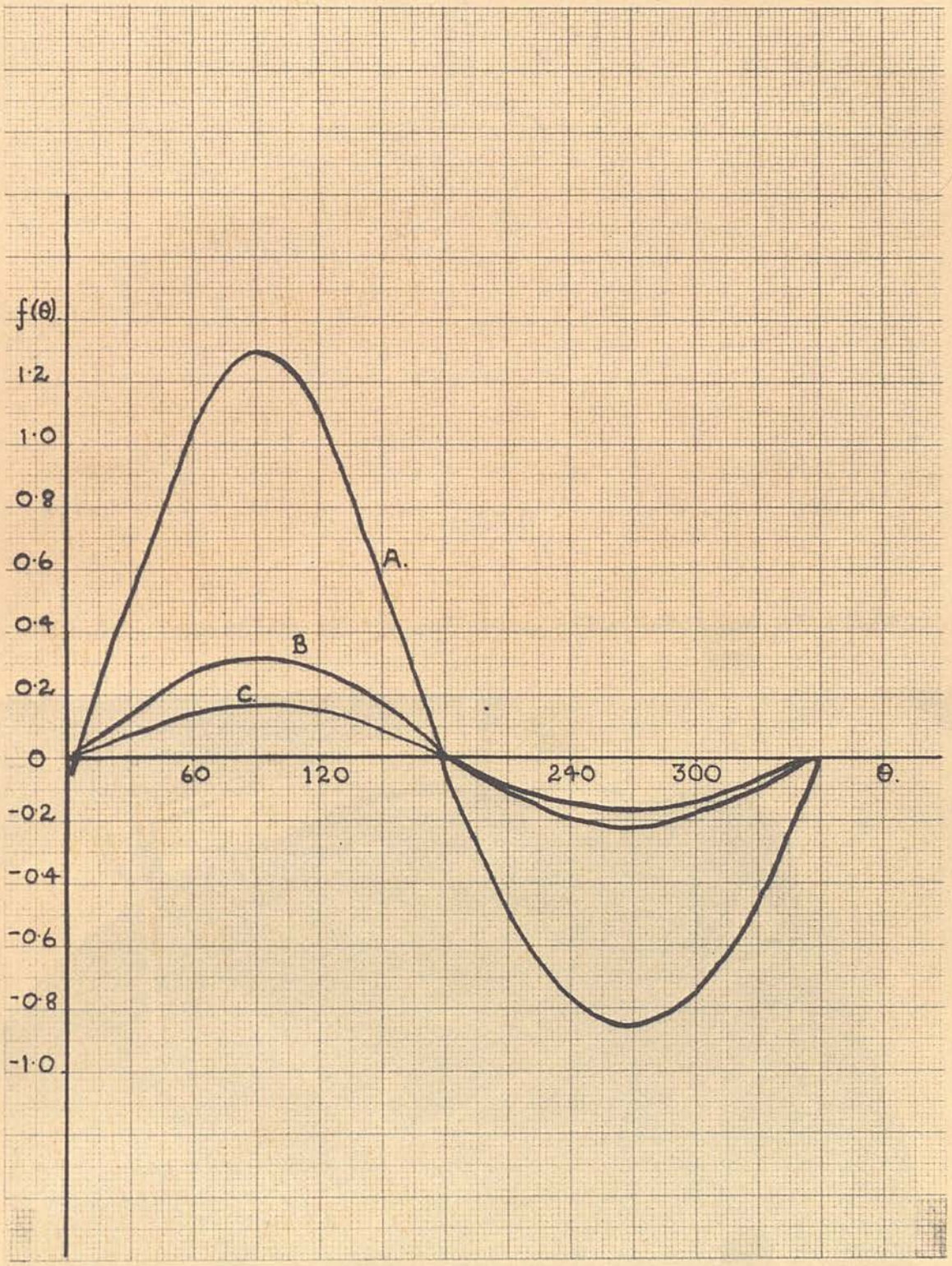

FIG.42 Curves of f(θ) against θ required to produce a sinusoidal variation in C. A-$C_1 = 20\mu\mu F$, $C_3 = 5\mu\mu F$, B-$C_1 = 10\mu\mu F$, $C_3 = 5\mu\mu F$, C-$C_1 = 5\mu\mu F$, $C_3 = 2\mu\mu F$.

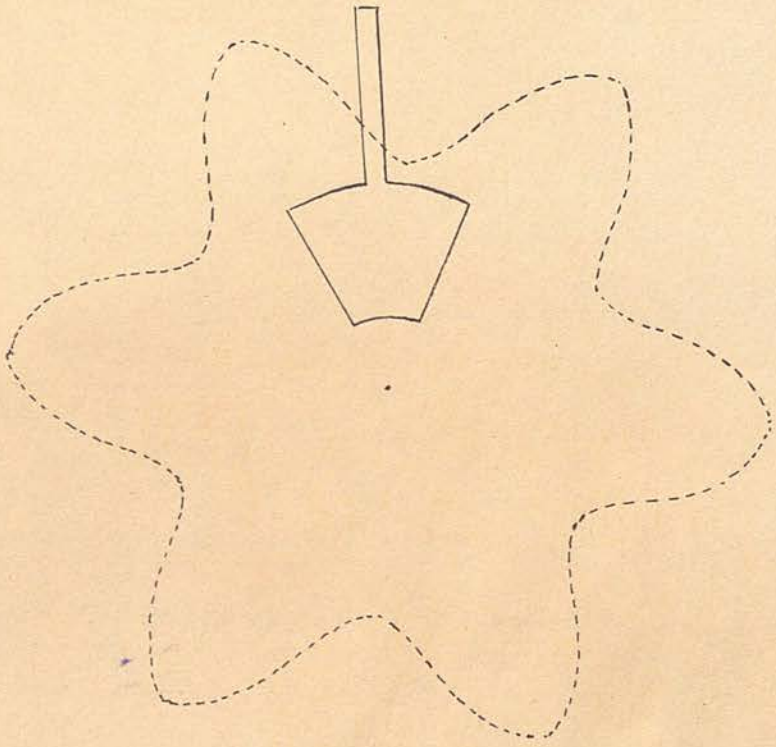

FIG.44 Variation of Capacitance with position of Scanner.

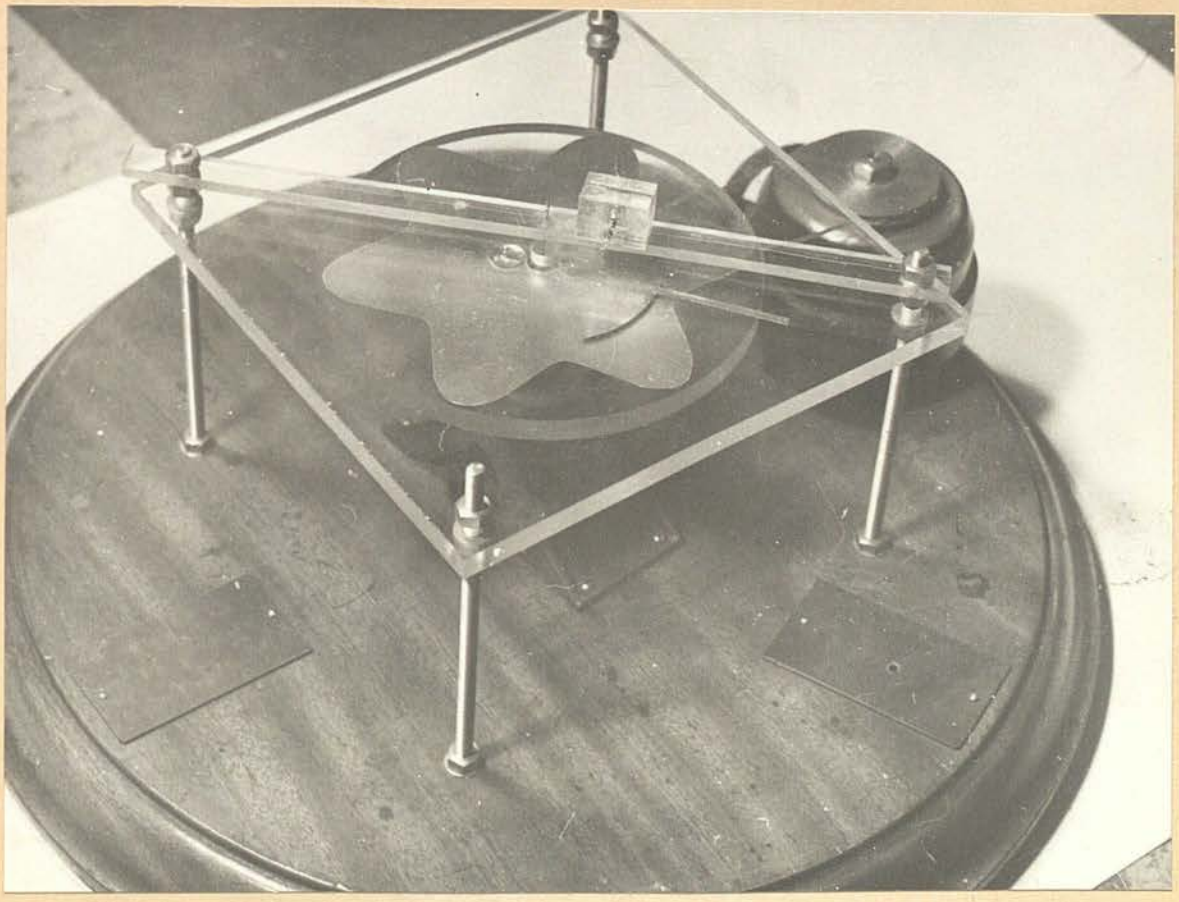

FIG.43 Apparatus for producing small changes of Capacitance.

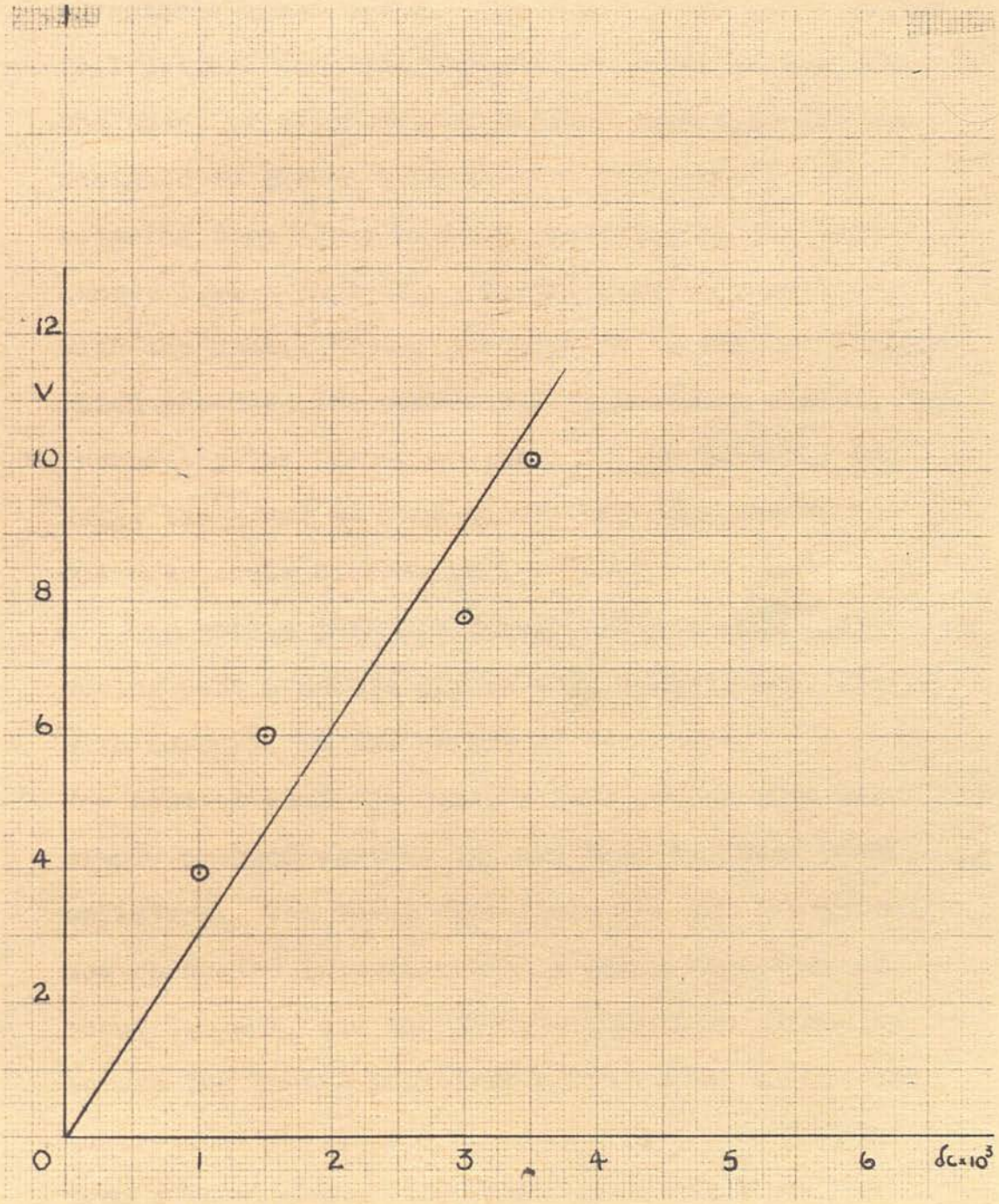

FIG.45 Calibration curve of instrument obtained from 2nd method. Output in volts and input Capacitance in μμF Maximum voltage across filter 20 volts.

perspex discs, d cms. apart. The upper disc was fixed, and the lower one able to rotate and driven by a variable speed motor. The fixed plate had a silver foil pattern covering the surface shown in Fig. 44, the shape of which was calculated from $f(\theta)$ and was designed to give a sine wave as the output. The rotating disc had a pattern indicated by the dotted lines, i.e. a part which formed a fixed capacitor with the static plate, and a small 'scanning' portion which produced the sinusoidal capacitance change. By increasing the number of peaks in the pattern, and using the motor at high speeds, frequencies up to 800 c/s. could be obtained.

To obtain good electrical contact with the moving part a needle dipped into a small cup, filled with mercury, in the centre of the shaft.
For contact with the foil, a thin copper wire was simply pressed against it, and held in place with sellotape. The total capacitance of the discs, was now connected in series with a small capacitor of about 1.0 $\mu\mu$F, and the whole arrangement connected across the tuning capacitor of the oscillator. The theoretical values for C_1 and C_3 were calculated from a knowledge of the shape of the foil and the separation distance d, of the plates. However it was soon obvious from the results that fringing affected the capacitance, and the calculated values could not

be relied upon. The idea of using the frequency capacitance characteristic of the oscillator was therefore conceived. Since the capacitances to be measured were of the order of (1 - 10)μμF, then the frequency shift of the oscillator, caused by the addition of capacitances of this order could be measured quite accurately. Using this method accurate values of C_1, C_2, C_{3max} and C_{3min}, could be determined and the value for the small change of capacitance δC, could be calculated. All that remained now was to measure the output voltage on the Cathode Ray Oscilloscope corresponding to known capacitance changes, and the results are as shown in Fig. 45. The voltage across the crystal filter in this case was 20 volts and it can be seen that the response is linear and the slope is 3.1 volts per 10^{-3}μμF. change in capacitance. This is fair agreement with the value of 3.9 volts/10^{-3}μμF obtained by the other method of calibration.

3.5. Range and Actual Use of Instrument.

Since the straight portion of the filter extends over 100 c/s. then a maximum capacitance change of 22.5 x 10^{-3}μμF can be detected without modification or distortion of the waveform. This figure forms

the upper limit of the instrument. The lower limit is calculated from a knowledge of the noise level, and this has already been stated as 40 m.v. at the output. Assuming a least acceptable signal/noise ratio of 10, then 0.4 volts is the output voltage corresponding to the minimum capacitance change. This gives a minimum capacitance change of 1×10^{-4} μμF, from Fig. 41. The range of capacitance change of which the instrument is capable of detecting, is therefore 1×10^{-4} μμF to 22.5×10^{-3} μμF.

For use, certain requirements limited the design of the instrument. Firstly, since the vane was mounted in the centre of the tunnel, the capacitance of at least 9" of co-axial cable had to be allowed for in the oscillator circuit. This amounted to about 12μμF. A tapping was therefore put on the coil which allowed for two ranges of sensitivity. The instrument was calibrated and used entirely on the low range, which corresponded to an increase in the capacitive element in the oscillator circuit.

Due to the intense noise and vibration in the tunnel room under operating conditions, a sound proof box had to be built to prevent spurious output signals, due to microphony in the valves, being obtained.

The instrument was located just outside the

tunnel wall, the co-axial cable passing through a small hole in it. After an initial warming up period the instrument was ready for use. The vane was then set in the particular part of the boundary layer which was to be investigated, the voltage adjusted by means of the valve voltmeter to the correct operating point, and the output observed on the Cathode Ray Oscilloscope.

CHAPTER 4

DEVELOPMENT OF THE VANE.

4.1.1. Reduction of Vibration

When the tunnel was in operation, it was evident that there was still a certain amount of vibration being transmitted from the diffuser to the working section, despite the canvas coupling between these two sections. Since the magnitude of the vibration was very small, the measurement of this would provide an excellent test for the newly calibrated electronics. The technique was similar to that used for the vane itself and was as follows. A piece of metal foil was attached to the surface undergoing examination, and this formed an air dielectric capacitor with a small static plate. This static plate was mounted on the electronic instrument, which itself was mounted independently, and was completely free from vibration. Any output signal obtained when the tunnel was in operation, could therefore be attributed to vibration of the tunnel wall.

The vibration of the wall of the working section was investigated using this technique. A small brass static plate 0.4" x 0.4" in area, was placed at a distance of 0.040" from the wall and Fig. 46 is a

record of the output signal with only the generator and the 3-phase motor running. The very low frequency was attributed to a panel vibration and the high frequency of 170 c/s. was discovered to be due to microphony of the electronics, which was removed by padding and sound proofing.

The vibration frequency of the tunnel walls with variation of fan revolutions was next investigated. The tunnel was run at different windspeeds and the vibration frequency measured on the C.R.O. From this emerged the interesting results shown in Table A.

Table A

Fan Speed (RPM)	Blade Frequency (c/s) = 4 x fan frequency	Recorded Frequency (c/s)
750	50	98
890	58.8	115
1017	68.0	129
1105	73.6	77
1220	81.2	160
1330	88.8	89
1560	104.0	106
1705	113.3	113

It can be seen that over a limited range of frequencies the walls of the tunnel vibrate in sympathy with the blade frequency. Where the fan blade frequency is lower than that covered by this range, the walls

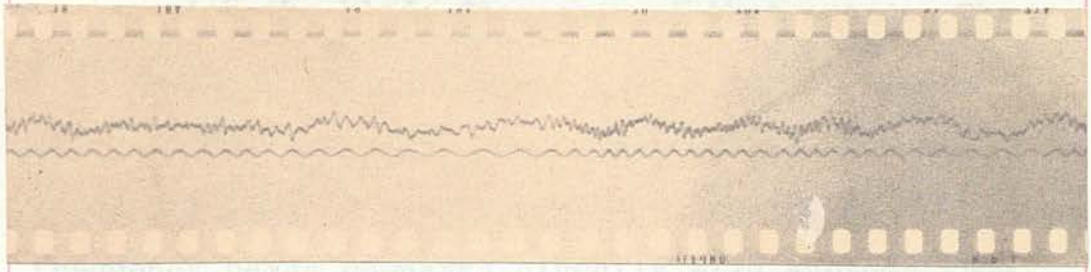

FIG.46 Vibration of Tunnel Wall caused by 3 phase Motor and Generator. High Frequency of 170 c/s due to Microphony of Electronic Instrument.

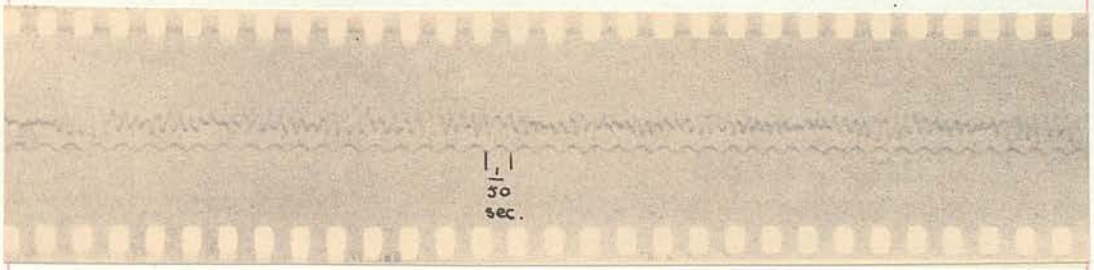

FIG.47 Vibration of Tunnel Wall under working conditions, showing Fan Blade frequency of 124 c/s.

Amplification of signal in FIGS.46 & 47 is 10 times that of all other photographic recordings.

vibrate at a frequency double that of the blade and which again lies in the range of frequencies from 75 c/s. - 160 c/s. Fig. 47 is a photographic record of the output signal corresponding to a fan speed of 1850 rpm, and shows a frequency of 124 c/s., which agrees with the blade frequency at that speed. The frequencies of the output signals obtained during these measurements were very well defined and a film recording was not always required, the vibration frequency being compared directly with another from a signal generator on the C.R.O.

The amplitude of the vibrations corresponded to a noise level of 80 m.V., i.e. twice the accepted noise level of the instrument itself, and the frequencies of the vibrations were in the range of the anticipated laminar oscillations. A separate framework, completely isolated from the rest of the tunnel, on which to mount the vane, had to be constructed. The movement of the vane could then be attributed solely to the velocity fluctuations. However since the flat plate formed the other plate of the small capacitor and since it was still subject to vibration, then the effective noise level of the system was 80 mV. It was hoped at this stage, that the true signal corresponding to the velocity fluctuations would be much greater than that due to the noise. If this were not

the case, then the output signal would have to be analysed and the frequencies known to be caused by vibration disregarded. As will be seen later in this chapter, this problem was solved by using a small static plate included in the vane head.

4.1.2. Framework for Vane Suspension

The framework was made of 2" angle iron, which formed a cage surrounding the working section of the tunnel. The legs were embedded in concrete blocks, which were insulated from the floor, by a layer of felt. To the uprights of this framework was attached the vane mount mechanism, which allowed for movement in both the x and y directions. A diagram of the framework is shown in Fig. 48, and it can also be seen in Fig. 60. The rail of the framework, on which the carriage carrying the vane ran, was positioned just inside the tunnel wall and the design had to be modified twice, before a satisfactory shape of the leading edge, which caused little or no variation in the local static pressure, was obtained. The carriage carrying the vane head had also to be streamlined. Originally a fairly robust carriage which ran on two rails was constructed, but the blockage caused by this arrangement, upset the flow

considerably and large, local static pressure variations resulted. Eventually, complete rigidity had in part to be sacrificed to obtain an aerodynamically sound carriage which did not upset the flow. The carriage spanned the flow, from the wall of the tunnel to $1\frac{1}{2}$" from the flat plate. The vane was mounted upstream of this on a boom of $\frac{1}{4}$" diameter brass rod, which slid through a collar on the end of the carriage. When the tunnel was run under working conditions, this arrangement was found to be free from any aerodynamic flutter or vibration. The natural frequency of the framework itself was about 10 c/s., but this was only observed when it received an accidental knock.

4.2.1. The Vane

In the Introduction, it was mentioned that almost all previous investigations of the boundary layer have been performed using hot-wire anemometers. A mention of the technique is given here, so that the respective merits of the vane and the hot-wire can be compared.

The simplest case of a hot-wire head is that of a single wire between two probes, mounted normal to the wind. This type of head can be used to gain very precise information on the u fluctuations and when

compensated for the effect of the time constant of the wire, the frequency response can be made flat to over 1 Kc/s. The time constant for a hot wire is

$$M = \frac{J m s (\bar{R} - R_A)}{i^2 R_o^2 \alpha}$$

where J is the mechanical equivalent of heat, m the mass of the wire, s the specific resistance, $\bar{R}$ the mean hot resistance, R_A the resistance at air stream temperature, R_o the resistance at $0^\circ C$, and α the temperature coefficient of resistance. For platinum wires 0.0001" to 0.0002" in diameter and about 0.15" long M varies from 0.001 to 0.002 secs. for U_o = 70 ft./sec. The amplitude response is given by $\frac{1}{\sqrt{1+M^2\omega^2}}$ and the phase by $\tan^{-1} M\omega$. From the amplitude relationship, it can be seen that as the frequency increases, the term $M^2\omega^2$ increases and therefore the amplitude decreases. Above about 300 c/s. the amplitude has fallen sufficiently to require compensation, and for this purpose complicated and costly electronics is required.

To measure the v and w components, two hot-wires have to be used and arranged in such a way that the output contains only the component required. An x arrangement of two wires each making the same angle to the wind, with voltage opposed produces a resultant voltage change only when the wires are differentially

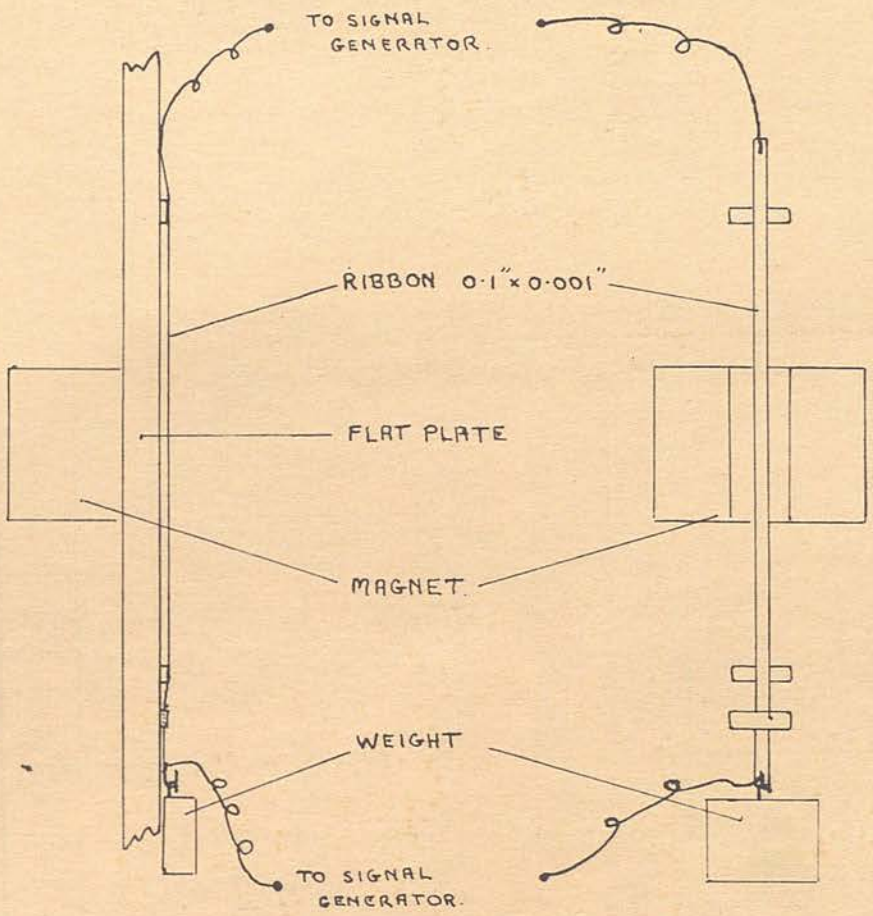

FIG.49 SKETCH of RIBBON LAYOUT

FIG.48 SKETCH of y-TRAVERSE EQUIPMENT.

SCALE: 1cm. = 1"

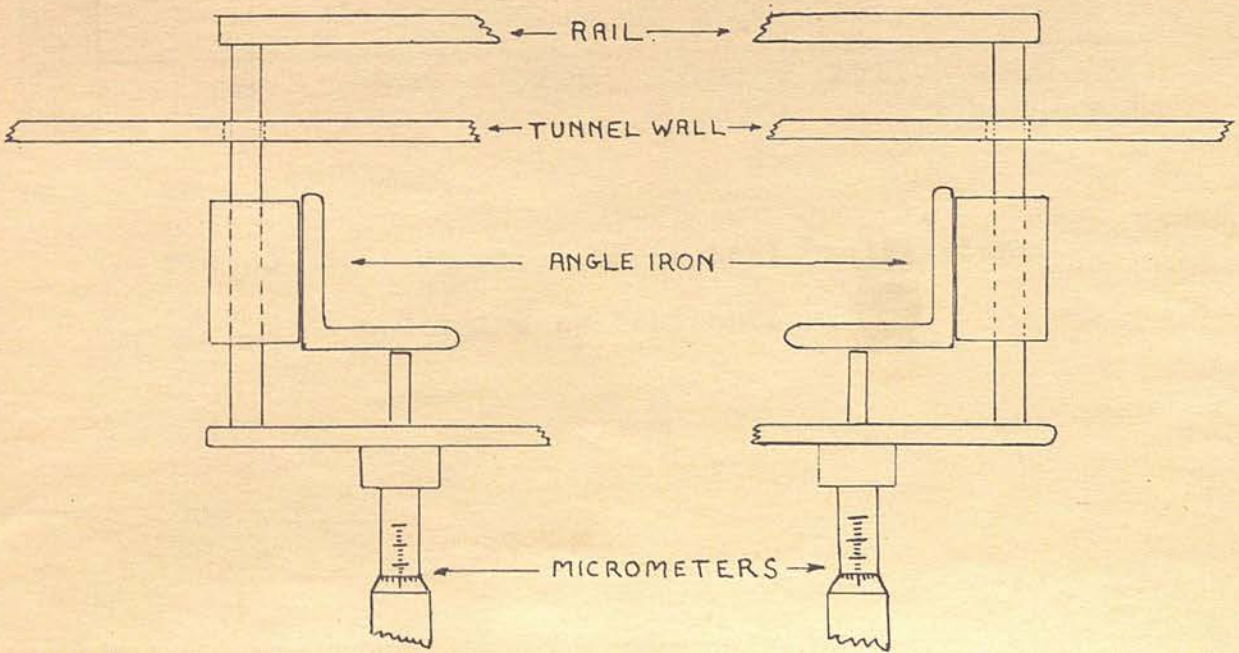

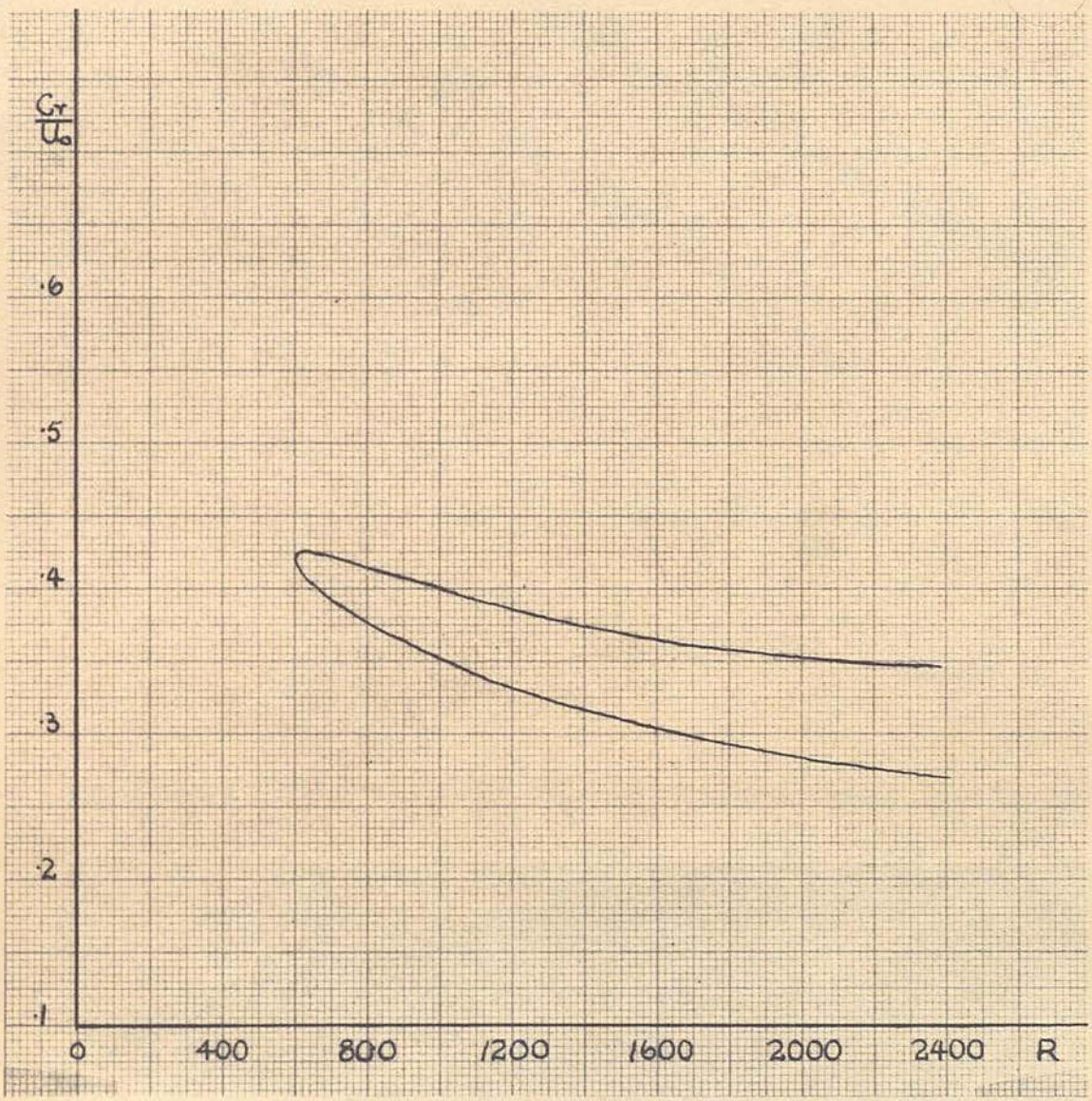

FIG.50 Wave Velocity of Neutral Oscillations according to Schlichting.

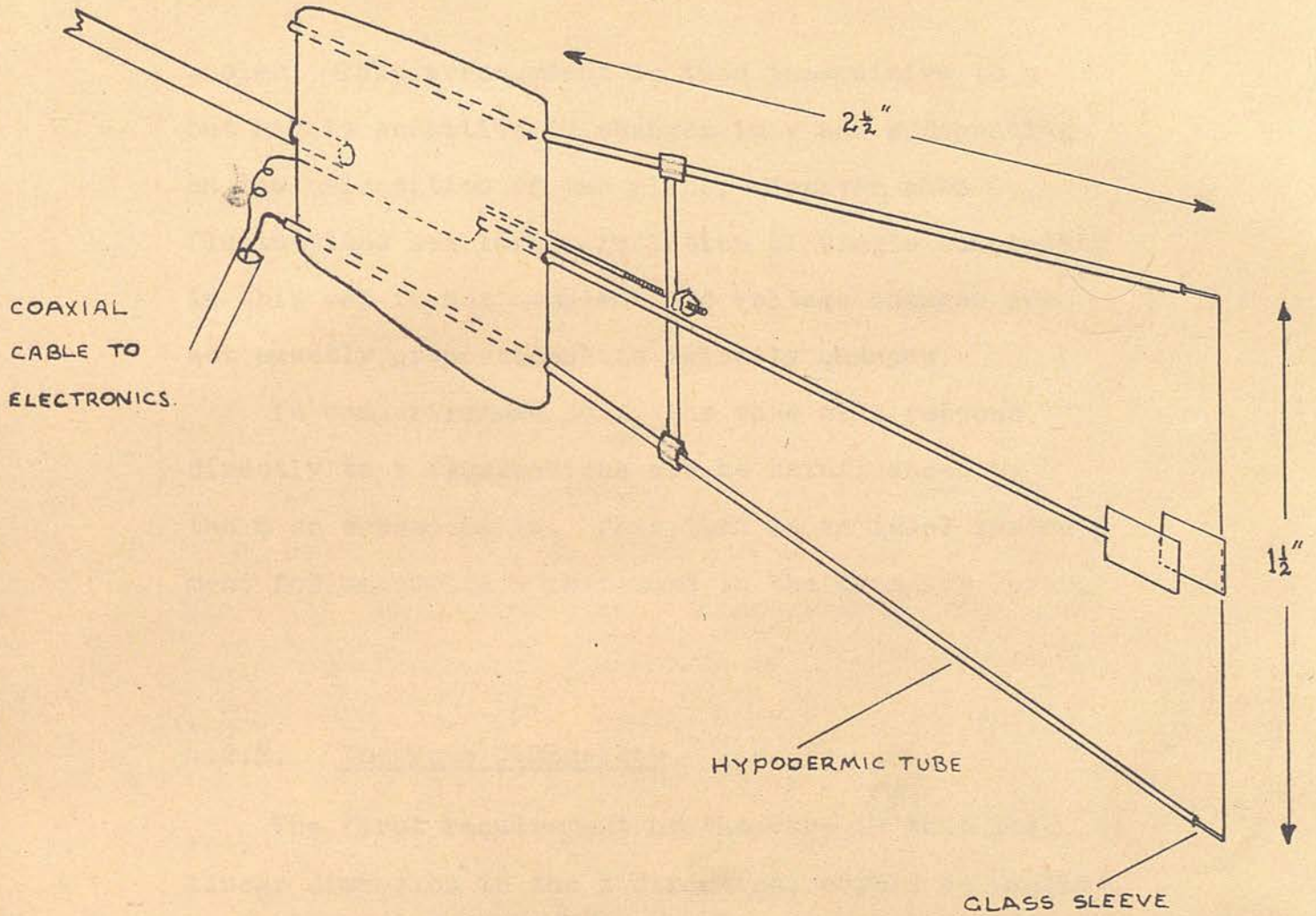

FIG.51 Illustrations of Vane Head showing Static Plate.

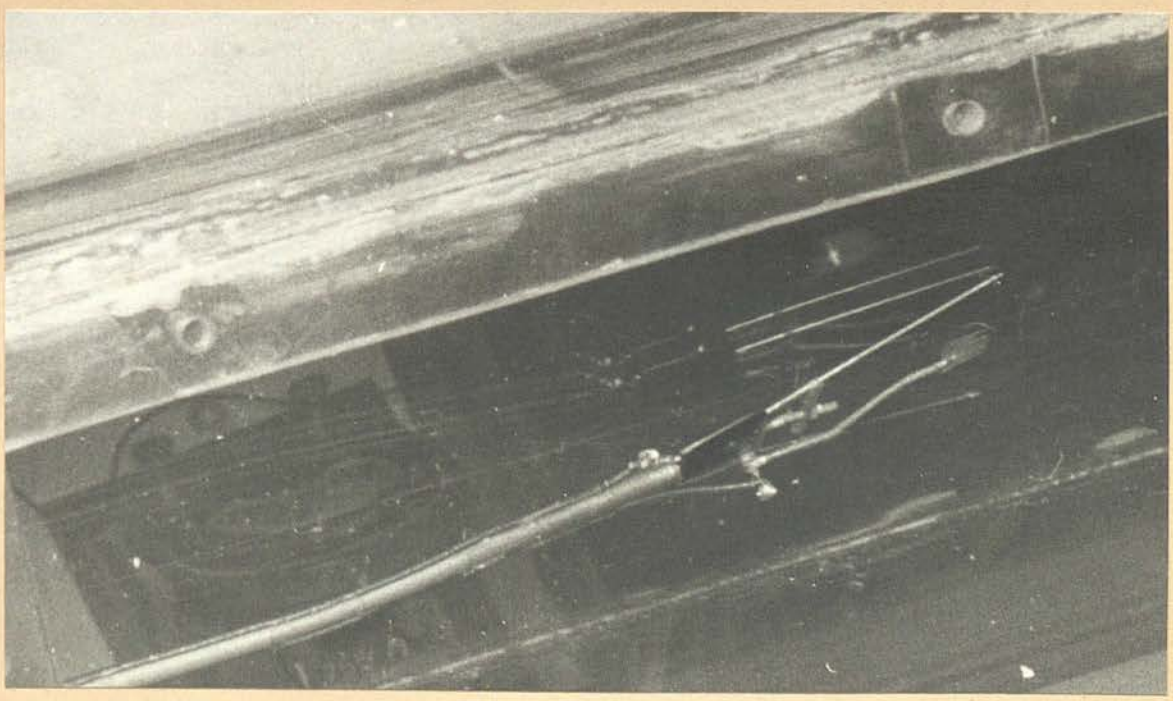

cooled. This arrangement is then insensitive to u but highly sensitive to changes in v and w depending on the orientation of the plane. However when fluctuations are large, isolation of single components in this way is not complete and voltage changes are not exactly proportional to velocity changes.

In comparison with this, the vane will respond directly to v fluctuations and be uninfluenced by the u or w components. This then is an ideal instrument for measuring v phenomena in the boundary layer.

4.2.2. The Vane Dimensions

The first requirement of the vane is that its linear dimension in the x direction, should be smaller, or at the most equal to half the smallest wavelength to which it is expected to respond. From the theoretical curve shown in Fig. 50, the wavelengths of the laminar oscillations can be calculated. The range of frequencies examined by the vane in this report is from 80 c/s. to 300 c/s. and for a windspeed of 60 ft./sec. this gives a wavelength variation from 2.4" to 0.9". The standard x dimension of the vane was chosen as 0.4", and the y dimension was generally about the same, although it was occasionally varied for fine adjustment of the natural frequency of the vane. It was desirable

to keep the vane thin, so that it should cause as little disturbance to the air stream as possible. The average thickness of vanes was therefore about 0.0003".

4.2.3. The Vane Structure

The vane consisted originally of a piece of mica, 0.4" x 0.4" x 0.0003", suspended and loosely hinged at its leading edge. Early vanes of this type had too small hinges, consisting of loops of 0.0007" diameter Nichrome wire, at the leading edge. Such vanes were extremely delicate and also the hinges tended to warp, restraining the movement of the vane. The main drawback, however, was that good electrical contact between the silvered surface of the vane and the suspension wire was not always obtained. A separate contact wire to the silvered vane surface was not permissible since this would constitute a constraint, and the movement would not be free. Hence the suspension wire had to be used, and contact had to be established between it and the vane surface, by means of the hinge. Various methods of attaching the hinge to the vane surface, and silvering both, were tried, but even if good continuity was obtained at this juncture, contact could not always be

guaranteed between the hinges and the suspension wire. A new type of vane was therefore designed. Very thin metal foil was used for this vane and, by folding the leading edge of the foil round the suspension wire, a free hinge and also good electrical contact was obtained. Either a double or single thickness vane could be made by simply continuing, or cutting off, the foil after the hinge had been formed. In this way the mass per unit area of the vane could be altered, and the natural frequency of the vane controlled over a range of frequencies from about 80 c/s. - 300 c/s. In the case of the high frequency vanes, i.e. single thickness foil, a mica stiffener was attached to the vane to maintain the same mode of vibration as the more rigid lower frequency vanes. The high frequency, single thickness vanes tended to 'flutter' about the centre of gravity, rather than oscillate about the leading edge, unless stiffened in this way.

The suspension wire was $1\frac{1}{2}$" long and made of 0.001" diameter Nichrome wire. It was threaded through two fine glass tubes, which insulated it from the hypodermic tube supports, and one end was connected to a terminal on the ebonite body of the vane head, to provide contact for the coaxial cable.

The tension in the wire was controlled by adjusting the position of the T piece, which was set between the hypodermic tubes. A diagram of the vane head is shown in Fig. 51.

At this stage of the investigation the flat plate with a piece of silver foil in the appropriate position, still formed the static plate of the instrument. However as the position of the vane was altered, it was very inconvenient to attach continually small pieces of foil to the surface. Also, when the y coordinate of the vane was adjusted, the electronics had to be retuned, due to the change in capacitance between the vane and the flat plate. Originally it had been intended that the y distance should remain fixed at 0.040", but as the research progressed this was an inconvenient limitation. To obviate these difficulties a small static plate was mounted on the same head as the vane.

4.2.4. Static Plate in Vane Head.

This static plate was mounted on a thin but rigid metal rod, and was positioned parallel to the vane, on the opposite side from the flat plate. The distance apart was normally about 0.1", and at this distance no interaction between the vane and the static plate was expected, i.e. any variation in the

local flow due to the static plate, would not be reflected on the vane. The vane head was now an independent instrument, which could be placed anywhere in the boundary layer without the oscillators having to be retuned. A diagram of the head showing the static plate is shown in Fig. 51.

Due to the thickness of the hypodermic tubes and the glass sleeves therein, the minimum y distance of the vane was 0.020" . This could have been improved on, but the boundary layer was much thicker than this over most of the plate, and it also afforded a means of making x traverses with the vane at a constant y distance of 0.020".

Fig. 51 shows a photograph of a typical vane head. The position of the flat plate is indicated by the reflection of the vane head.

4.3.1. The Deflection of the Vane.

To clarify certain points in previous chapters, approximate figures for the expected deflection of the vane have been quoted. It is proposed to go into more detail in this section. The theoretical curves of Schlichting, for the distribution of the u and v components of velocity fluctuation throughout the boundary layer, are discussed in the light of the verification by Schubauer and Skramstad for the

distribution of the u component. By analogy the expected magnitude and distribution of the v component is obtained.

Fig. 52 shows the theoretical distribution of the u and v components throughout the boundary layer. It can be seen that the ratio of the peak magnitude of the u component, to that of the v component is 3:1 in the branch 2 case, and 2:1 in the branch 1 case. The maximum value of $\frac{v}{U_o}$ at branch 2 is 3%. These curves however have been drawn for an arbitrary average value of $\frac{u}{U_o} = 0.05$, chosen by Schlichting, throughout the boundary layer from $y = 0$ to $y = \delta$. If this arbitrary level is a reasonable assumption then natural oscillations of the order of $\frac{v}{U_o} = 3\%$ may be present in the boundary layer. This value however is probably a function of the free stream turbulence, and in the very low free stream turbulence experiments of Schubauer and Skramstad, artificial oscillations of an order of magnitude of 10 smaller than that assumed by Schlichting, were introduced into the boundary layer, and verified the theoretical curve for the distribtion of the u component, Fig. 53. The dotted line represents the experimental curve and the solid line the theoretical curve. The areas under the curves have been made the same. Since the turbulence level of the tunnel used for this research is ten times greater than that of Schubauer and Skramstad

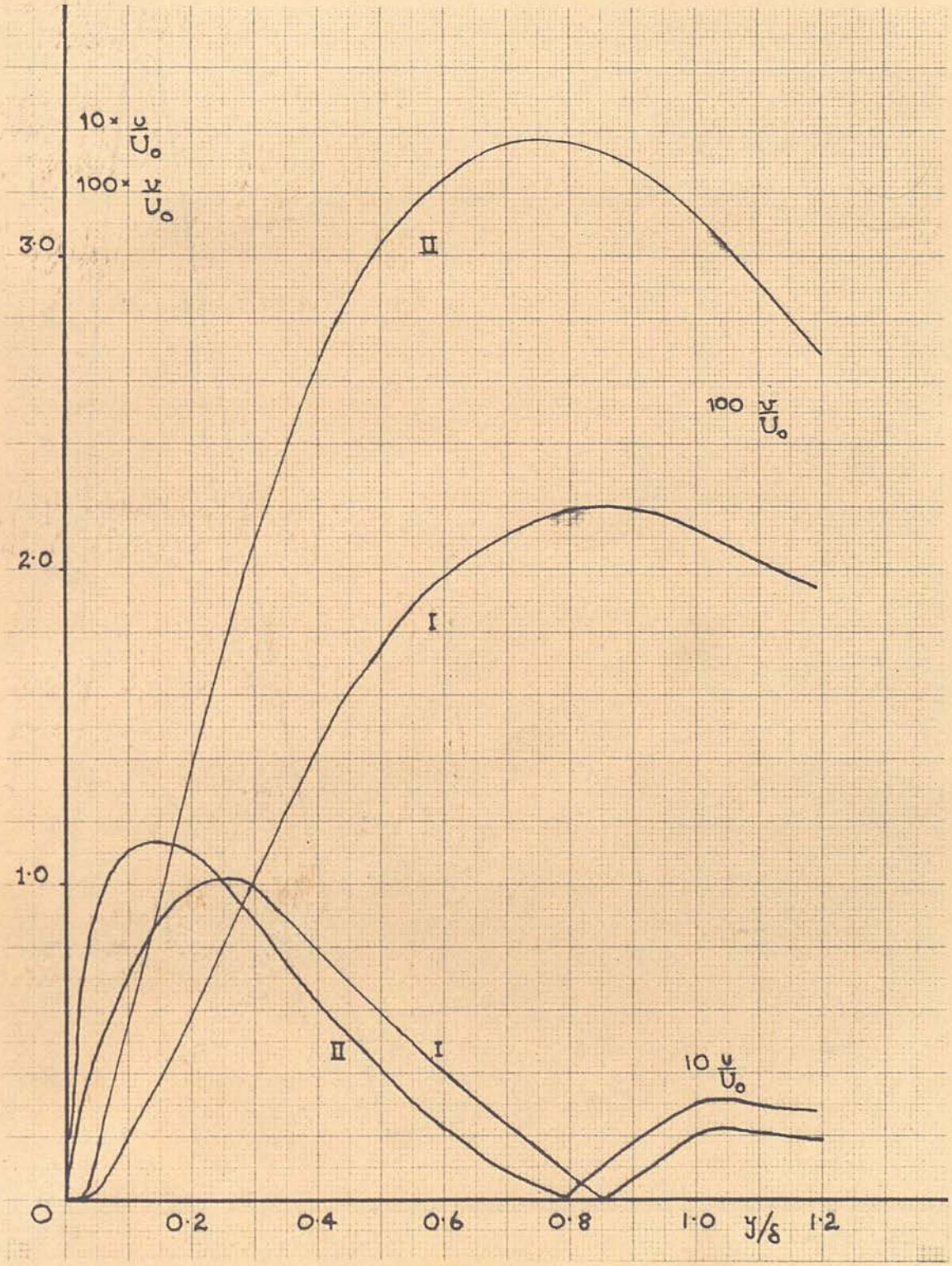

FIG.52 Theoretical distribution of u and v throughout the Boundary Layer according to Schlichting.

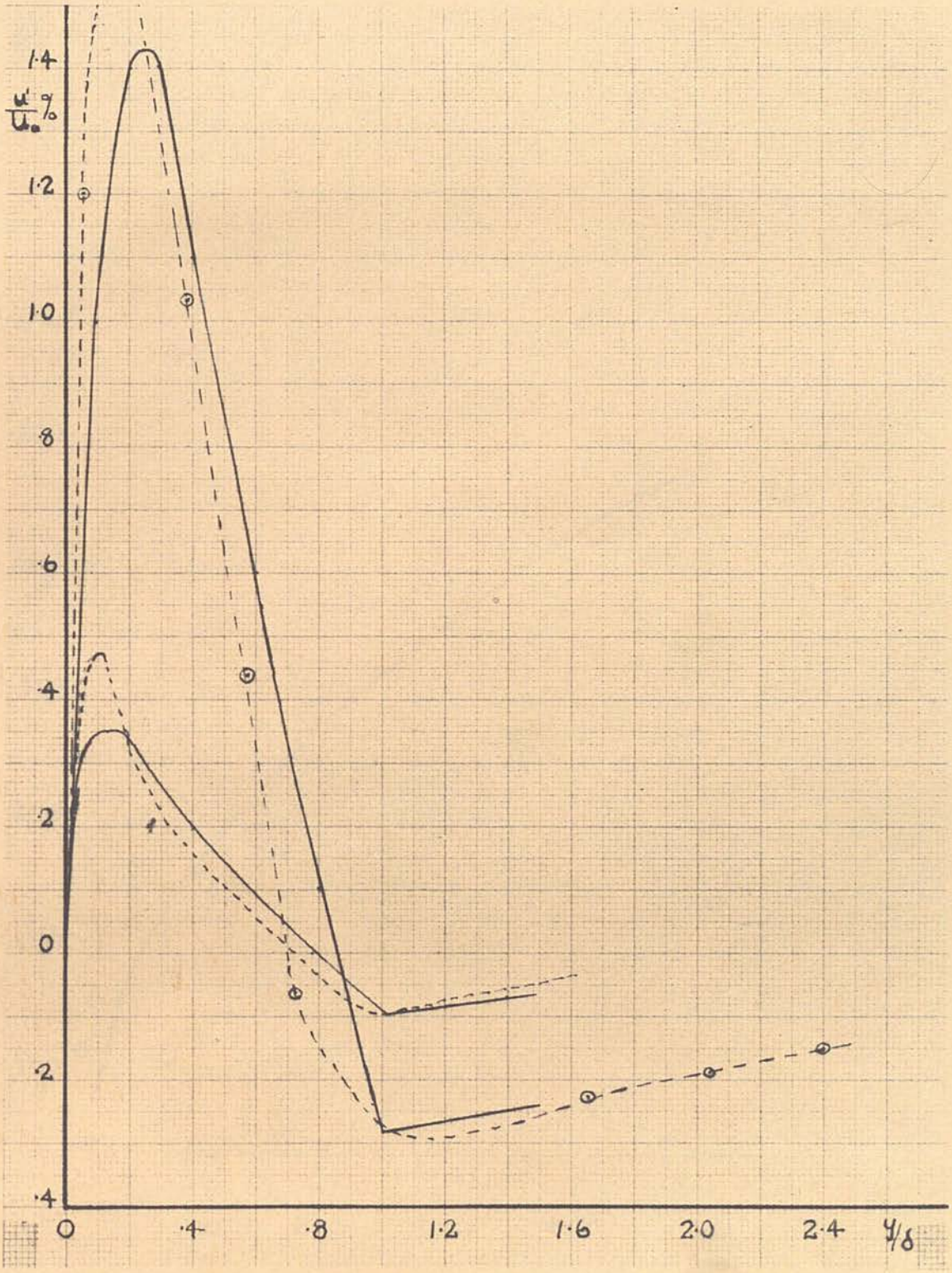

FIG.53 Agreement of results of Schubauer and Skramstad with theoretical distribution of Schlichting. Dotted line indicates experimental curve.

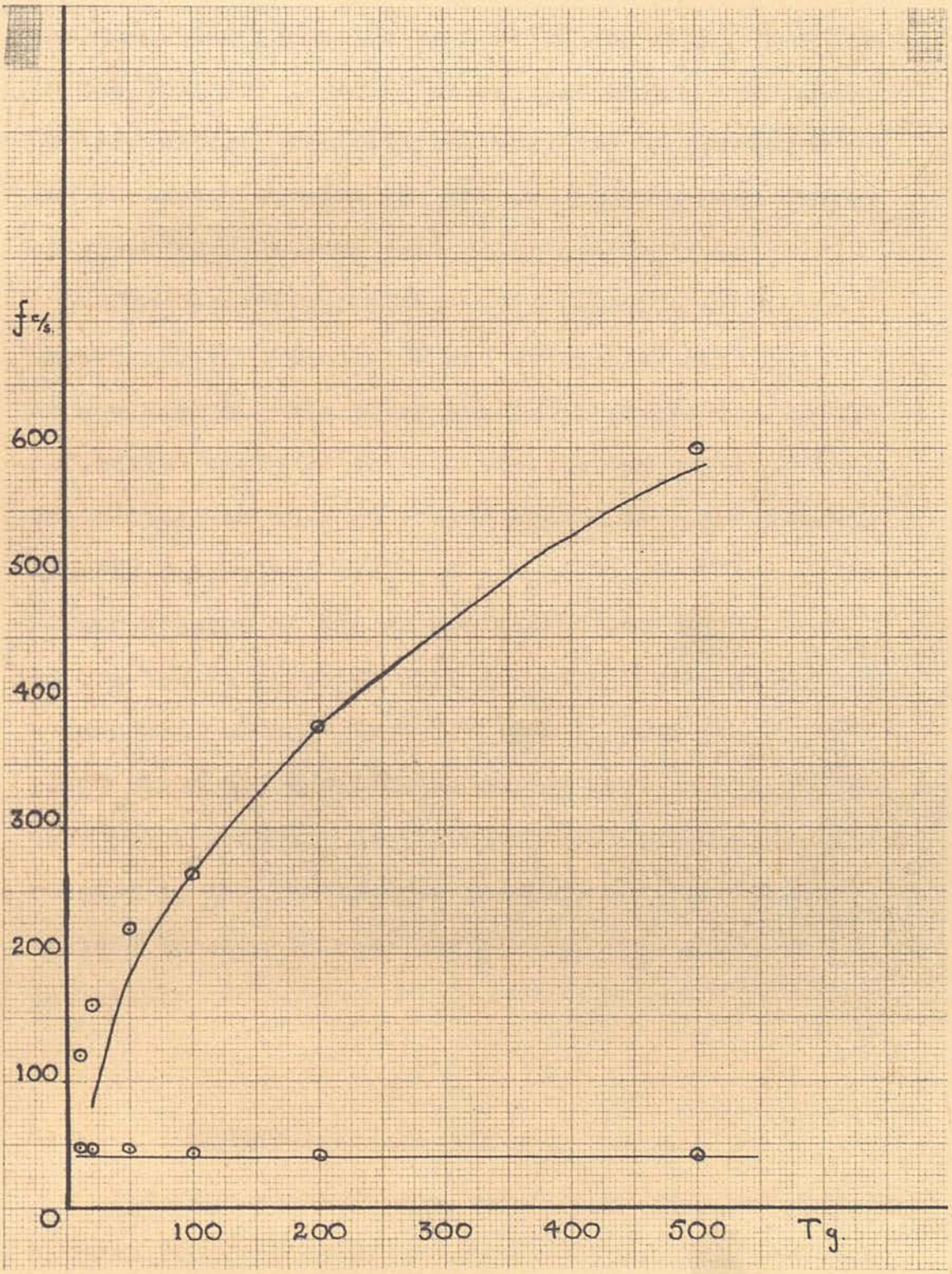

FIG.54 Variation of Natural Frequencies of vane and suspension with tension (gms.). Low frequency is that of vane.

then it is conceivable that natural oscillations of the magnitude predicted by Schlichting might be present in the boundary layer. But in view of the very much smaller natural oscillations observed by Schubauer and Skramstad a value of $\frac{v}{U_o} = 1\%$ has been chosen on which to base vane deflection calculations.

The theoretical effect of a disturbance on the vane was never calculated and it was thought that it would either lie along the local streamline, i.e. the deflection would be proportional to the ratio of the velocities, or else it would respond aerodynamically, and the deflection would be proportional to the ratio of the squares of the velocities. Considering the square law case, which will give the least deflection, a vane area of 0.4" x 0.4" , and a plate spacing of 0.10" then the capacitance change will be 2×10^{-4} μμF. This value although smaller than that originally calculated in the Electronics chapter, due to the increased spacing between the plates, will still be detectable.

4.3.2. Resonant Use of Vane.

J.G. Burns obtained a theoretical solution for the natural frequencies of the vane system. His solution gives two frequencies: a low one corresponding to the vane natural frequency and a higher one corresponding

to the natural frequency of the suspension wire. He obtained excellent experimental agreement, with slightly heavier vanes than those used for this research, using a small tunnel built for the purpose. His solution showed, that the coupling between the vane and the suspension was sufficiently loose so that the vane's natural frequency could be considered unaffected by the tension of the suspension wire. Fig. 54 shows the agreement between theory and experiment for the heavier vanes.

From the results of this theory it was predicted that the natural frequencies of vanes of the dimensions now used, would lie in the range of frequencies to be investigated. The possibility of making use of the natural frequency of the vane therefore arose. The vane could be tuned to respond to disturbances of one particular frequency and the progress of the disturbance followed down the plate. Much larger deflections of the vane would be obtained, using it in this fashion by virtue of the magnification occurring at the resonant frequency.

The frequency response of typical vanes was studied using a vibrating ribbon, which will be described in detail in the next chapter. The ribbon was placed in the boundary layer a few inches upstream of the vane, and in a region, where no

selective amplification of the frequency range to be covered was expected. The frequency of the oscillations injected into the boundary layer was varied over a range including the resonant frequency of the vane, and the voltage output against frequency plotted. Typical response curves for a low frequency vane are shown in Fig. 55, and a photographic record in Fig. 56. The variation of resonant frequency with windspeed is also shown, since the vane was positioned at the outside of the boundary layer. This was also predicted by the vane theory. For the low frequency response curves shown in Fig. 55, the Q factor is relatively small, only about 5, but for high frequency vanes of around 300 c/s., the response peak is very sharp and the bandwidth only 15 c/s. - 20 c/s., which corresponds to a Q of 30. Hence using the vane as a resonant detector increases its sensitivity by a factor which depends on its natural frequency. This will make possible the detection of even smaller velocity fluctuations than previously anticipated.

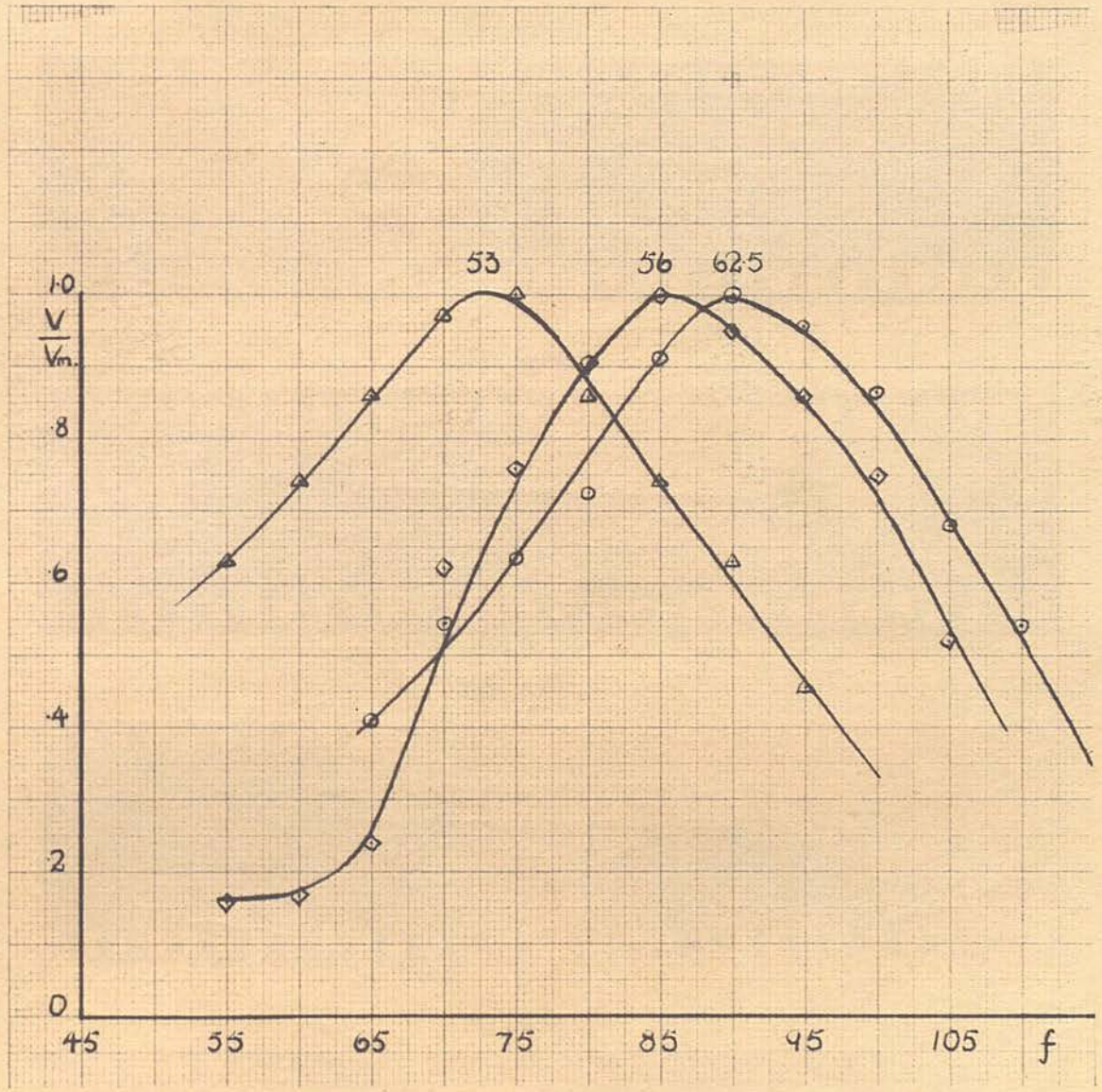

FIG.55 A typical Response Curve of a low frequency vane showing variation of natural frequency with windspeed.

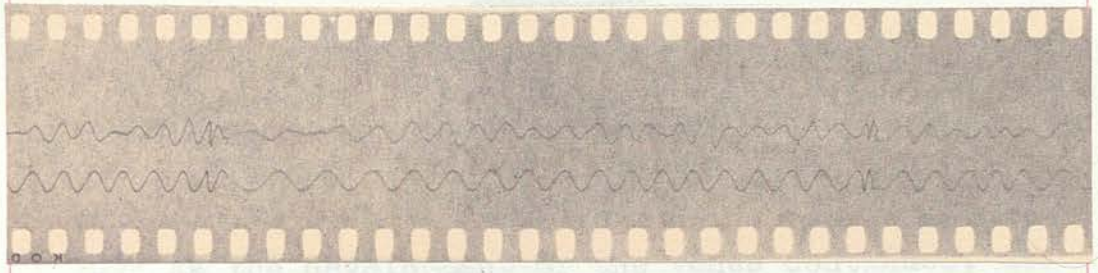

60 c/s.

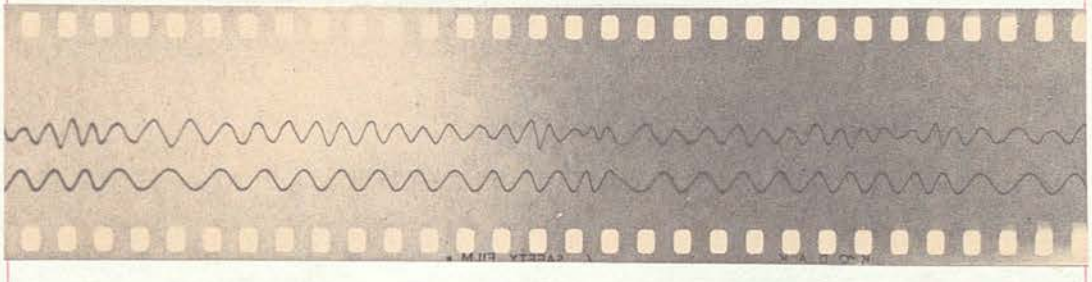

70 c/s.

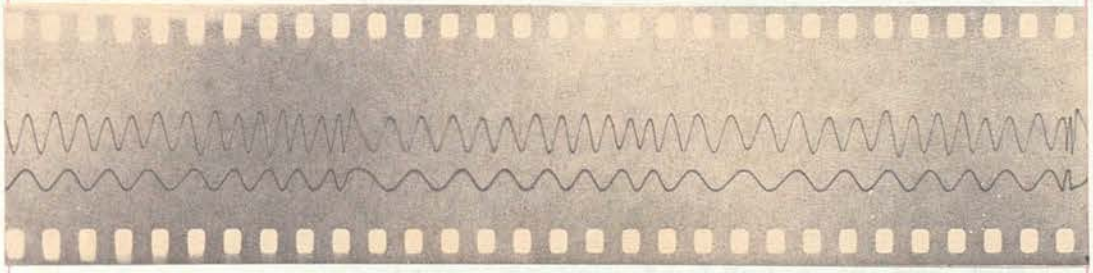

80 c/s.

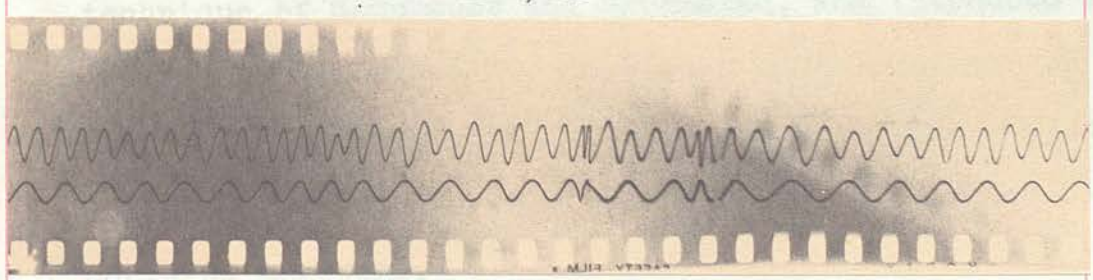

90 c/s.

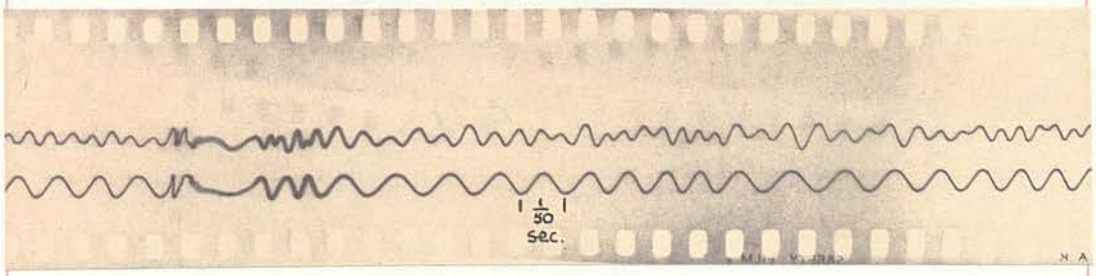

100 c/s.

FIG.56 Frequency Response of Vane for U_o = 55 ft/sec.

CHAPTER 5

RESULTS AND CONCLUSIONS

5.1. Preliminary Experiments

As the development of the vanes continued, the boundary layer was thoroughly investigated with each successive type. Although many vanes were used during this period, the existence of well defined laminar oscillations was still undetected.

The explanation of the apparent absence of the laminar oscillations was attributed to one of two causes. Either the free stream turbulence level was too high to permit theobservation of natural laminar oscillations, or else the vane itself was not sensitive enough to detect those present, if any. To settle this question, it was decided to adopt the technique of Schubauer and Skramstad, and introduce a disturbance of known frequency and amplitude into the boundary layer. By so doing, both the sensitivity of the vane and the theory of laminar oscillations could be assessed.

5.2.1. The Vibrating Ribbon

Before any reliance could be placed on observations with the vibrating ribbon, its own performance and also its effect on the boundary layer had to be investigated.

The ribbon consisted of a phosphor bronze strip,

0.10" broad, 0.001" thick, and the length varied from 6 cms to 15 cms depending on the resonant frequency required. It was excited by passing an alternating current through it, while under the influence of a magnetic field,and by supplying the current from a variable frequency oscillator or signal generator the frequency of vibration of the ribbon could be controlled. However due to the low power output of the signal generator used, the amplitude of the ribbon when far off resonance was very small, and to gain sufficient amplitude, it was necessary to adjust the resonant frequency of the ribbon, by varying the length or tension, to a frequency of 30 or 40 c/s. above that of the desired disturbance frequency. By varying the excitation voltage, control could then be obtained over the amplitude. A diagram of the ribbon arrangement is shown in Fig. 49. The bridges at the ends of the ribbon were made of 0.020" phosphor bronze, and the remaining dimensions made as small as possible, to avoid upsetting the flow.

Since the resonant properties of the ribbon were used, the frequency response was not flat, and the performance of the ribbon had to be fully calibrated. Fig. 57 shows the variation of voltage with frequency, required to excite the ribbon at constant amplitudes. This was measured using a telescope with an eyepiece scale, and the amplitude figures on the curves correspond to scale divisions on the eyepiece. Three

divisions on the eyepiece corresponding to an amplitude of 0.008". From the graph it can be seen that the response flattens off at frequencies well away from resonance, and whenever possible the ribbon was used at this part of the curve. But when larger amplitudes were required, the resonant frequency of the ribbon was adjusted to 30 or 40 c/s. above that of the required disturbance, and a corresponding increase in amplitude was obtained. For those reasons, further calibration was necessary.

The natural frequency of the vane could be varied by adjusting either the tension or the length. Fig. 58 shows a series of curves which gives the resonant frequency for any length of ribbon between 6 cms and 15 cms, for the three standard tensions used of 50 gms, 100 gms and 150 gms. Another series of curves were constructed to be used in conjunction with Fig. 58, and these are shown in Fig. 59. This gives excitation voltage against ribbon length required to maintain a constant amplitude of 0.008", for frequencies just off resonance. Thus from Fig. 58 the length and tension could be adjusted to give a resonant frequency, just above that of the required disturbance, and then from Fig. 59 the amplitude of 10 c/s., 20 c/s. etc. off resonance was known. A full knowledge of the movement of the ribbon was thereby obtained.

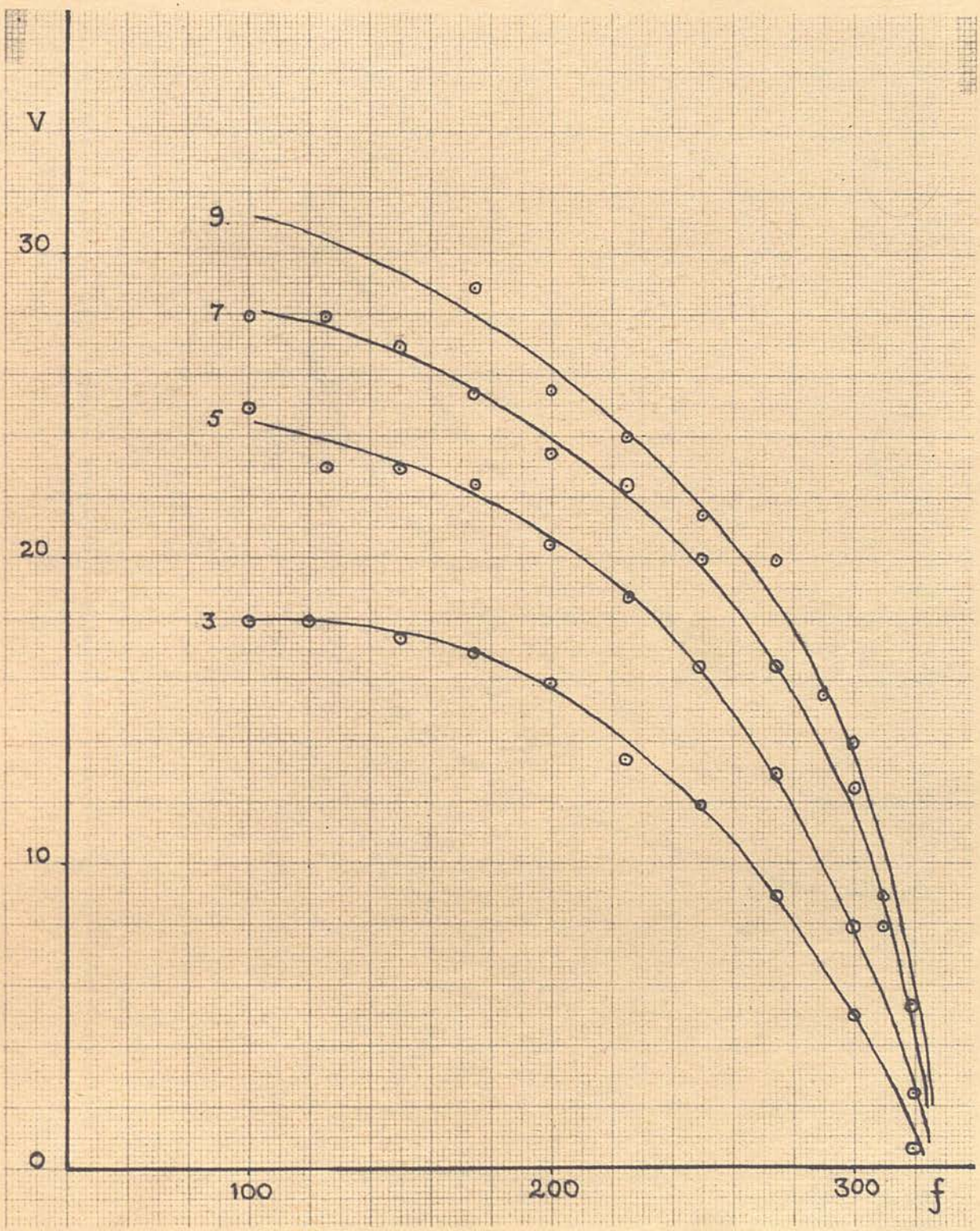

FIG.57 Voltages required to excite Ribbon at constant amplitude with variation of Frequency.

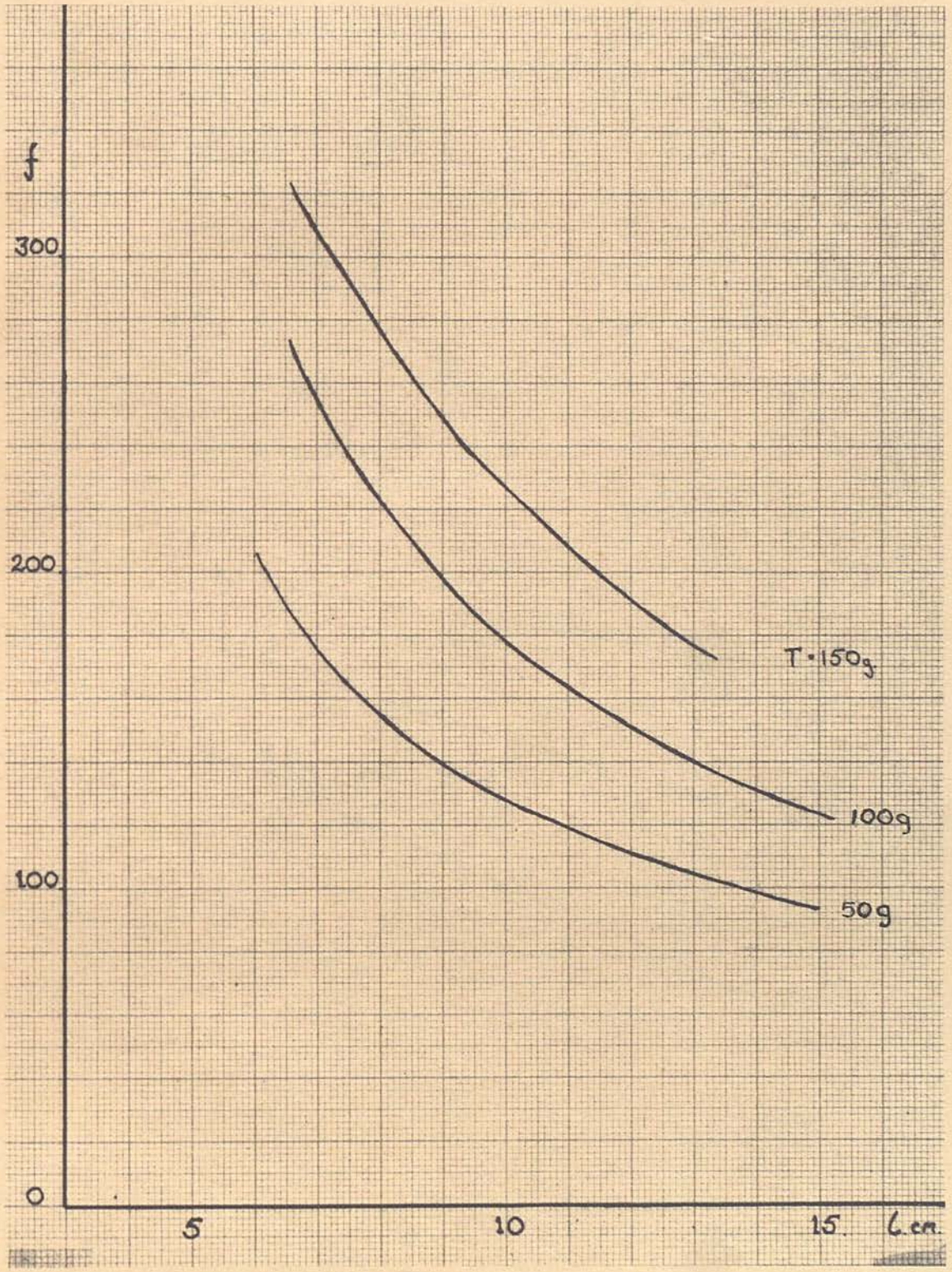

FIG.58 Variation of natural frequency of Ribbon (c/s) with length (cms.) and tension (gms.).

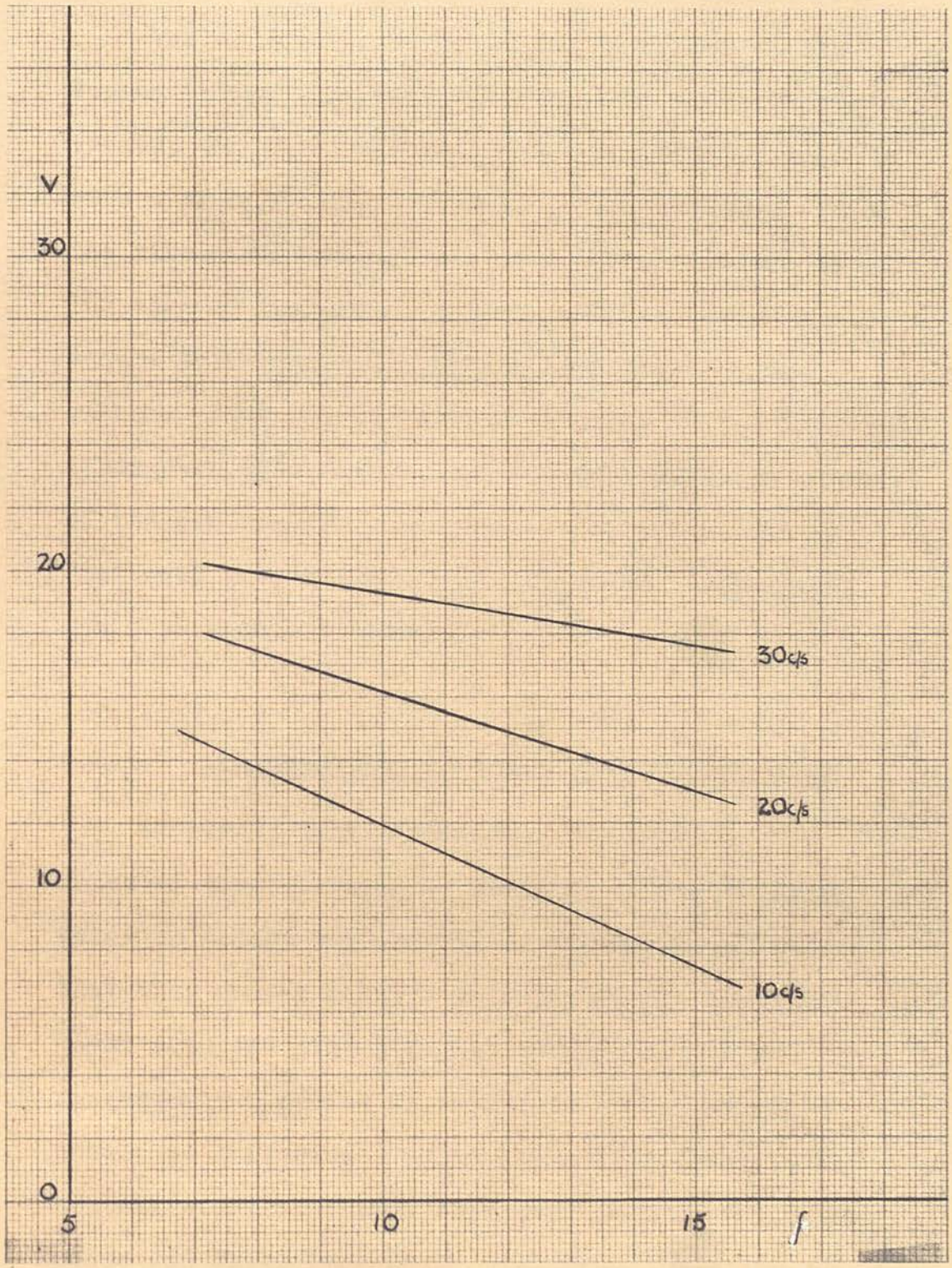

FIG.59 Voltage required to excite Ribbon at constant amplitude of 0·008", for δf = 10 c/s., 20 c/s., 30 c/s. off resonance.

5.2.2. Effect of Ribbon on the Boundary Layer

The effect of the vibration of ribbon on the boundary layer was next studied. The x position was varied, and the boundary layer downstream of the ribbon examined using a small total head tube. When the ribbon was placed less than 1 ft. from the leading edge of the plate, the flow was disturbed and became turbulent a few inches downstream of the ribbon. This was due to the thinness of the boundary layer over this region, causing the ribbon to vibrate of its own accord. When the ribbon was placed at distances greater than 1 ft. from the leading edge, the flow remained smooth.

5.3.1. The Detection of Artificial Disturbances

At first, little attention was given to the zones of amplification or damping, the only desire being to detect the artificial disturbances, and in fact they proved readily detectable. As the vane moved down the plate, it was obvious that some frequencies appeared to be damped whilst others grew. At this stage, no points on the theoretical neutral stability curve were obtained, as the technique was still imperfect. Sometimes the vane responded with varying amplitude over a considerable length

of the plate, and at other times the amplitude of the vane quickly increased to a maximum and no further increase was obtained. It was inferred from this that the sensitivity of the vane had an upper limit. The obvious way of overcoming this drawback was to reduce the amplitude of the ribbon to maintain a constant output signal as the vane was moved downstream. This technique was used to obtain the experimental points on the neutral stability curve.

A minimum level of disturbance amplitude, below which the vane could not detect was also observed and measured. From a knowledge of the ribbon response characteristics, an oscillation of known frequency and amplitude was injected into the boundary layer, and to obtain the lower limit of the vane's sensitivity, the amplitude was reduced until no output signal was recorded from the vane. Measurements were taken with the vane close to the ribbon, so that no preferential amplification or damping occurred. The amplitude of the disturbance, corresponding to the lower limit of the vane was then calculated from

$\frac{v_{rms}}{U_o} = \frac{0.7\omega a}{U_o}$ where 2a is the disturbance amplitude in ft. Measurements taken at 150 c/s., indicated a minimum amplitude of disturbance detectable by the vane, as $\frac{v}{U_o} = 0.5\%$. An important fact emerging from this experiment that had been overlooked up to this point, was that the percentage

disturbance injected into the boundary layer was frequency dependent. This fact explained some of the anomalous effects previously observed. A photograph of the general layout around the working section is shown in Fig. 60.

5.3.2. Experimental Points on the Neutral Stability Curve

Having completed the preliminary investigations on the performance of the vane, attempts were then made to obtain points on the neutral stability curve. The approximate position of the neutral point from the theoretical curve was first calculated and the ribbon placed 6" upstream of this. A disturbance of known frequency was then fed in, and excitation voltage varied to maintain a constant output signal from the vane as it was moved down stream. Hence in the curves shown of amplification and damping, amplification corresponds to a decrease in excitation voltage while damping corresponds to an increase.

Points on the low side of the curve were first obtained, and the variation of ribbon excitation voltage with x distance plotted for different frequencies and windspeeds. Two typical graphs are shown in Figs. 61 and 62. It can be seen that as the vane is moved down the plate at first the excitation voltage rises

slightly, then there is an essentially flat portion, followed by a marked decrease. The junction of the slope of the flat part with the slope corresponding to amplification, has been taken as the point of neutral stability, x_{crit}. The values of $\frac{\beta_r \nu}{U_o^2}$ and R for Figs. 61 and 62 are shown in the tables on the graphs.

By using this technique of varying the excitation voltage comparatively long traverses could be obtained, whereas to obtain photographic records of the type shown in Figs. 63 and 64, the neutral zone had to be predetermined, and the excitation voltage adjusted, so that the signal after the initial damping was just detectable by the vane at the neutral point. Even with these precautions only short traverses of about 6" could be made before the vane became "saturated".

To obtain points on branch 2 of the neutral stability curve, it can be seen from Fig. 65, that if amplification followed by damping is to be observed, then the frequency must be above 200 c/s., otherwise the turbulent regions, due to the wedge contamination will be encountered. This curve has been drawn for U_o = 70ft/sec., and by lowering the speed to 50ft/sec. amplification followed by damping could still be observed for frequencies down to 150 c/s. (see Fig. 30)

The technique employed was the same as before, and this time the excitation voltage of the ribbon had to be decreased until the neutral point had been crossed. Typical graphs are shown in Figs. 66 and 67. The point on the neutral curve, $x_{crit.}$, has been taken at the discontinuity in the slope of the curve. For the photographic record shown in Fig. 68 the conditions were adjusted carefully so that the maximum signal obtained at Branch 2 was within the upper limit of the vane's sensitivity. The experimental points have been plotted on the theoretical neutral stability curve and are shown in Fig. 69.

5.4.1. Discussion of Results

From the records of amplification in Figs. 61 and 62, it can be seen that as branch 1 of the neutral zone is crossed the two distinct gradients do not show damping followed by amplification. Rather do they show slight damping, as in Fig. 61, followed by a region of neutrality lasting for a distance of 3 or 4 inches, and then amplification. In Figs. 66 and 67 the amplification of the disturbance corresponding to the steep slope is followed by a region of lower amplification. The experimental points also lie slightly outside the theoretical neutral stability curve. In an attempt to explain these results, the

FIG.60 General View of Working Section and Associated Equipment.

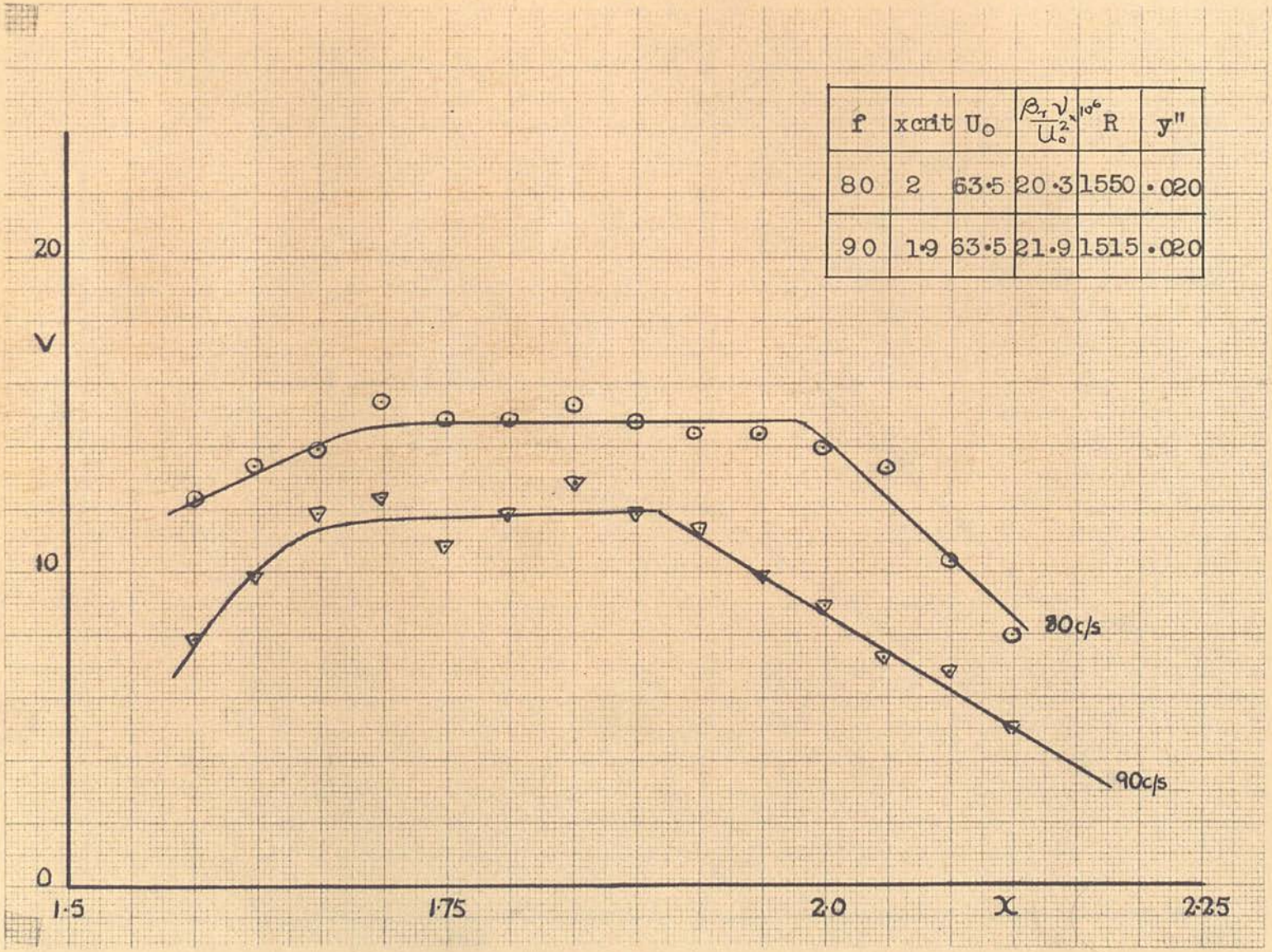

FIG.61 x traverse across Branch 2 of the Neutral Stability Curve.

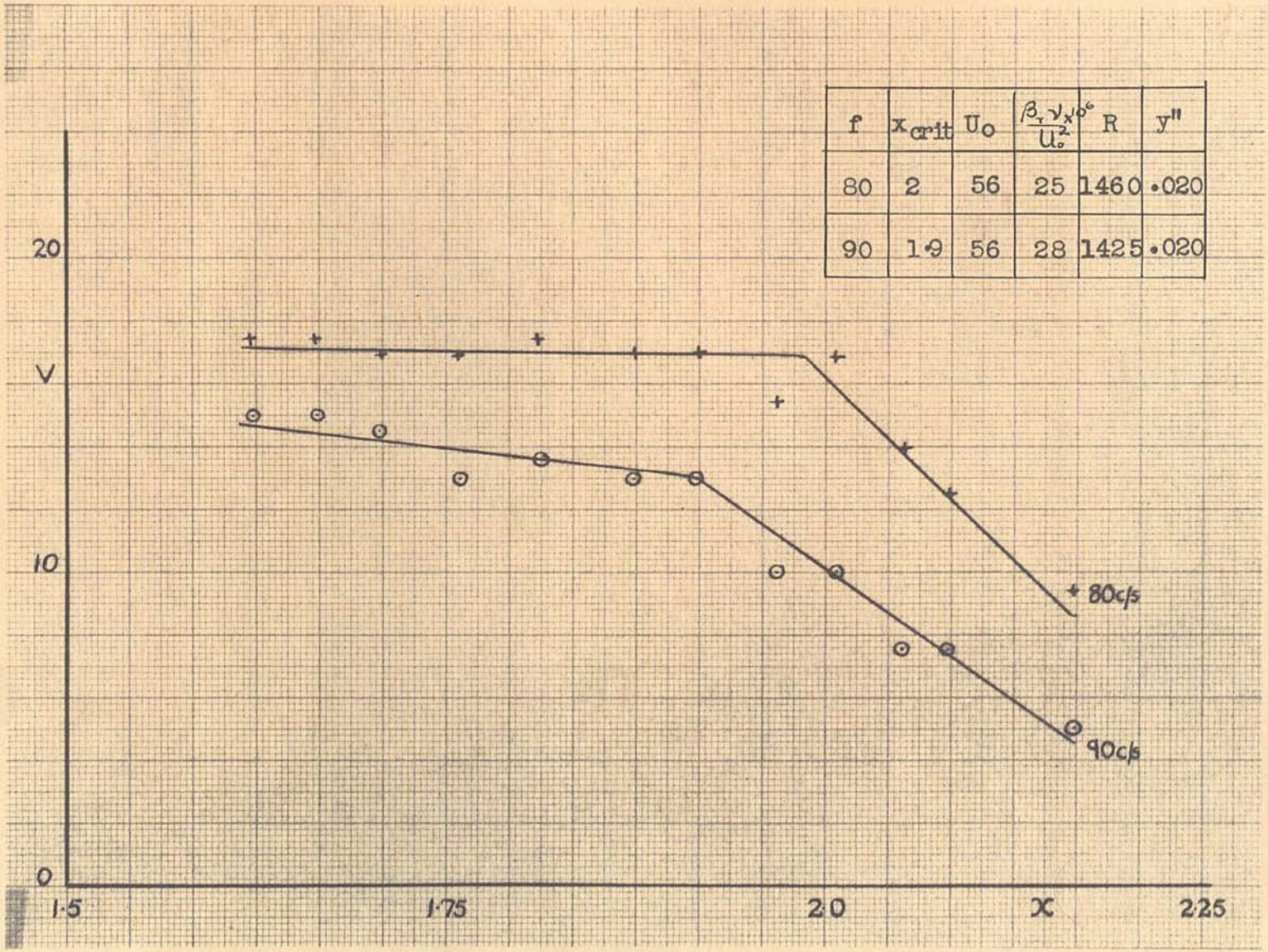

FIG.62 x traverse across Branch 2 of Neutral Stability Curve.

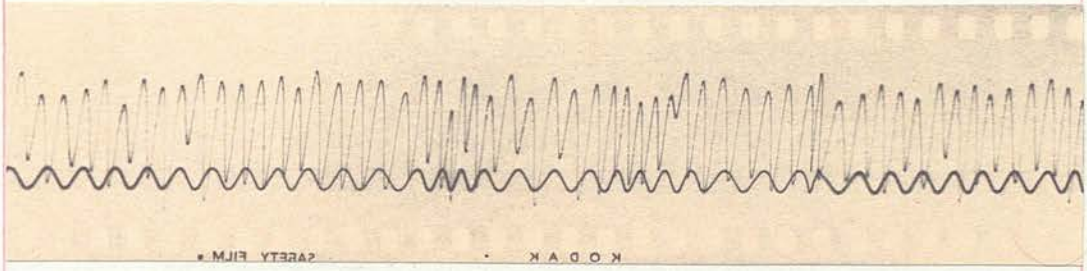

f = 85 c/s., U_o = 55 ft./sec. Rx = .59 x 10^6

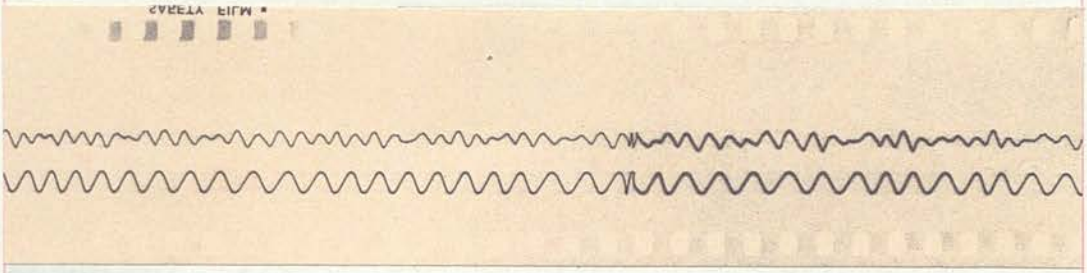

f = 85 c/s., U_o = 55 ft./sec. Rx = .65 x 10^6

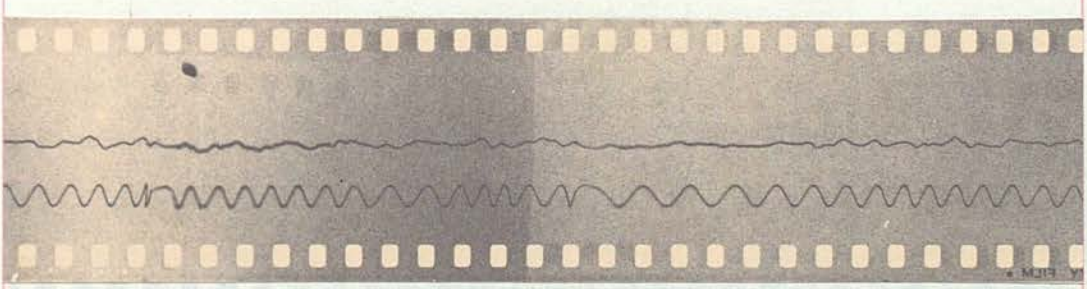

f = 85 c/s., U_o = 55 ft./sec. Rx = .68 x 10^6

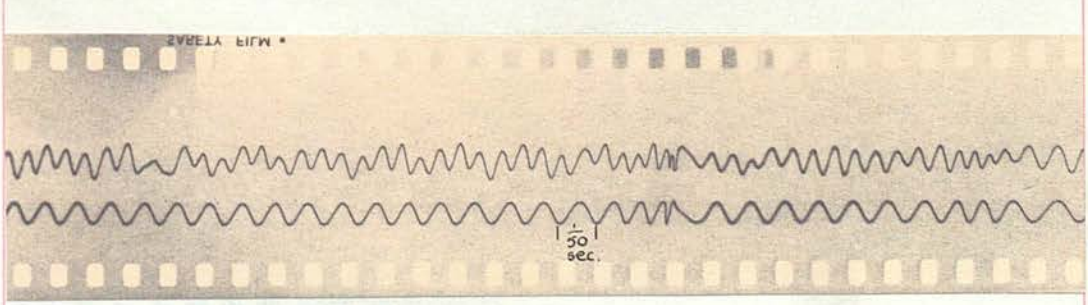

f = 85 c/s., U_o = 55 ft./sec. Rx = .74 x 10^6

FIG.63 Amplitude variation of Artificial Disturbance across Branch 1 of Neutral Curve.

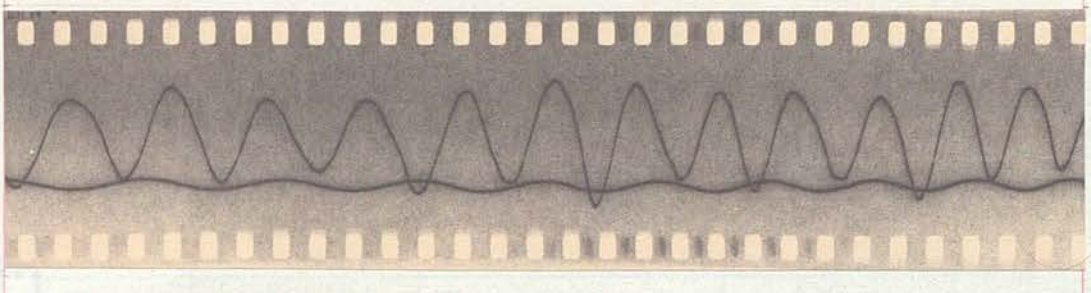

f = 70 c/s., U_o = 55 ft./sec. Rx = ·65 x 10^6

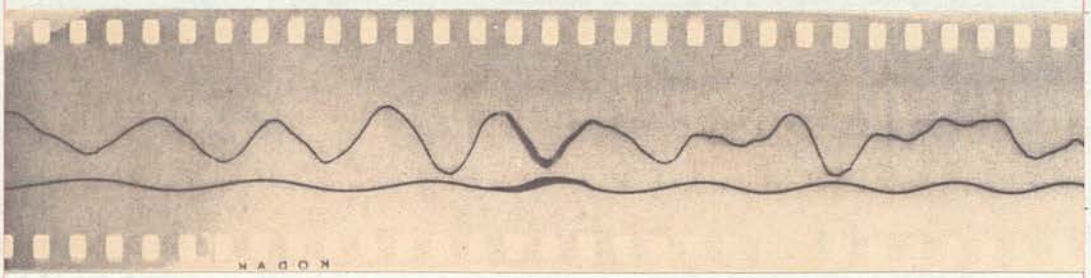

f = 70 c/s., U_o = 55 ft./sec. Rx = ·71 x 10^6

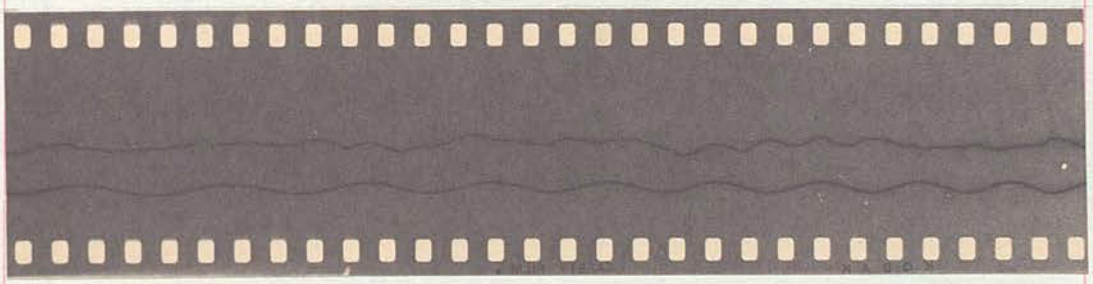

f = 70 c/s., U_o = 55 ft./sec. Rx = ·77 x 10^6

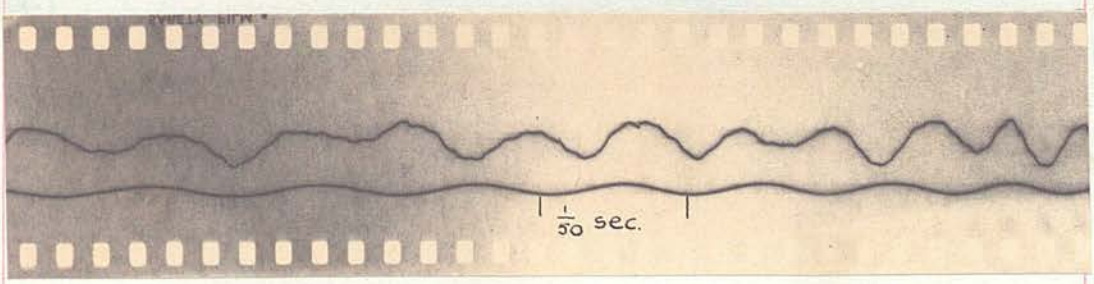

f = 70 c/s., U_o = 55 ft./sec. Rx = ·80 x 10^6

FIG.64 Amplitude variation of Artificial Disturbance across Branch 1 of Neutral Curve.

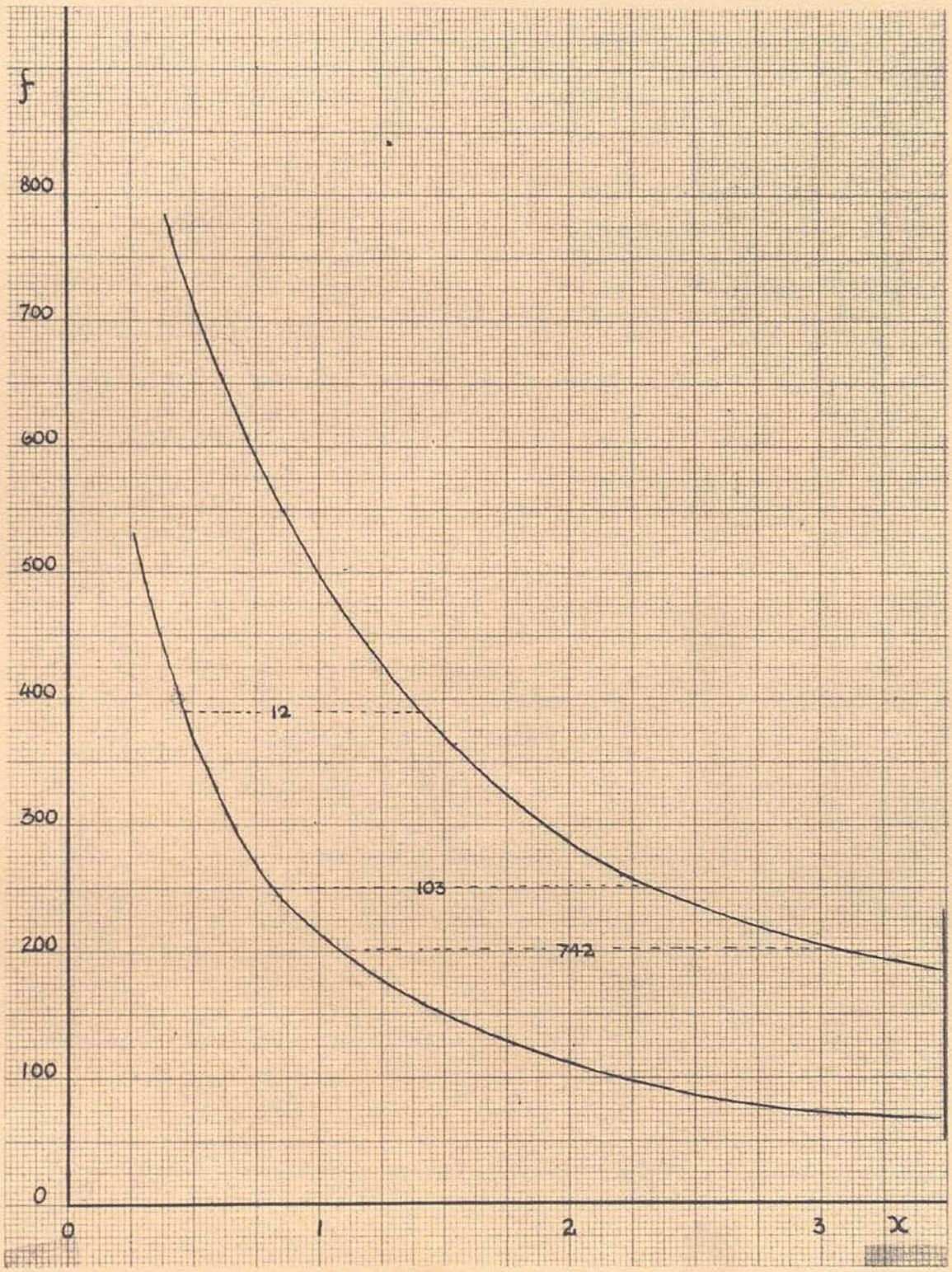

FIG.65 Neutral Stability Curve for $U_o = 70$ ft/sec. showing variation of total amplification with frequency.

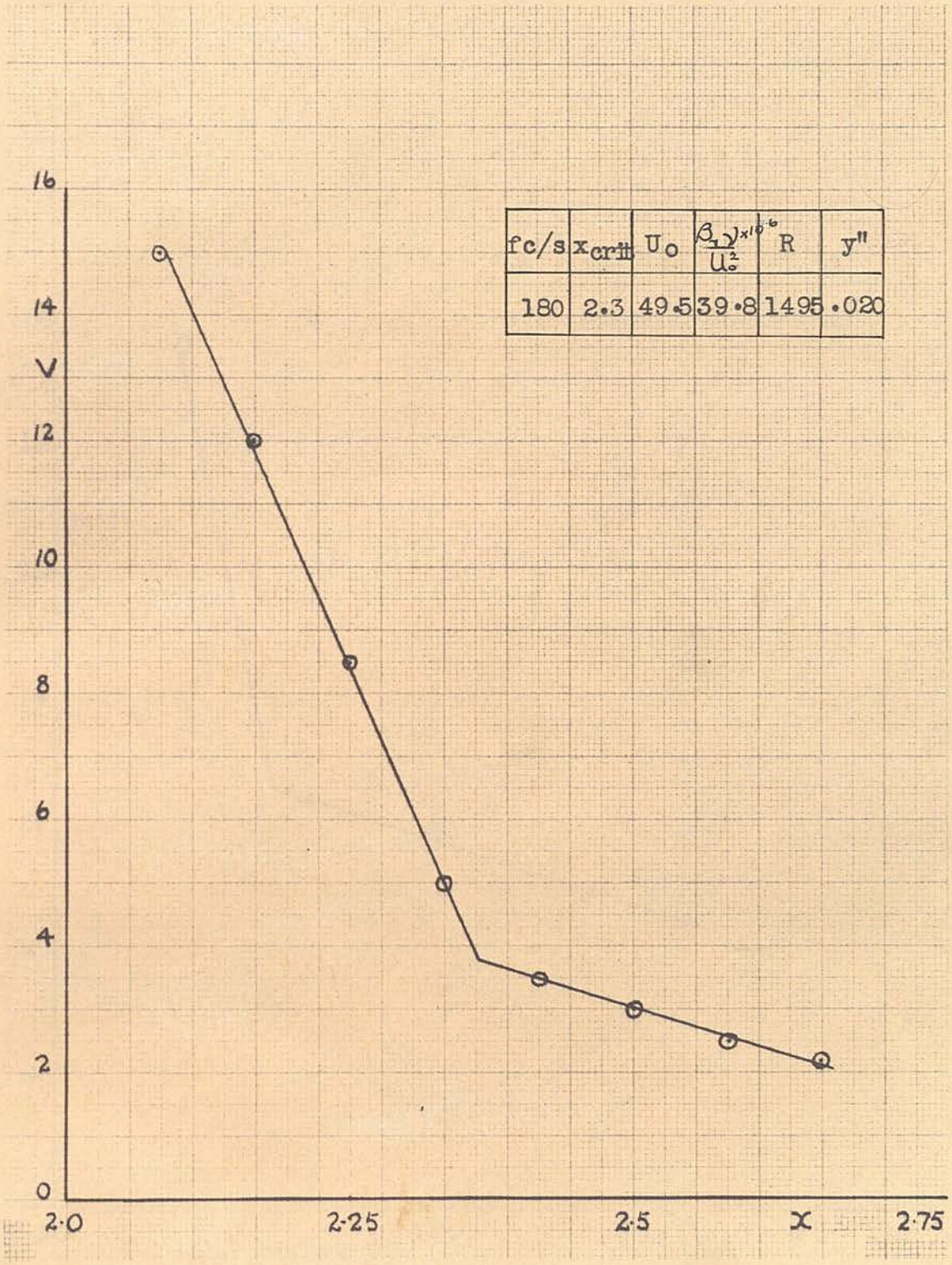

fc/s	x_{crit}	U_o	$\frac{\beta_1 \nu}{U_o^2} \times 10^6$	R	y''
180	2.3	49.5	39.8	1495	.020

FIG.66 x traverse across Branch 2 of Neutral Curve.

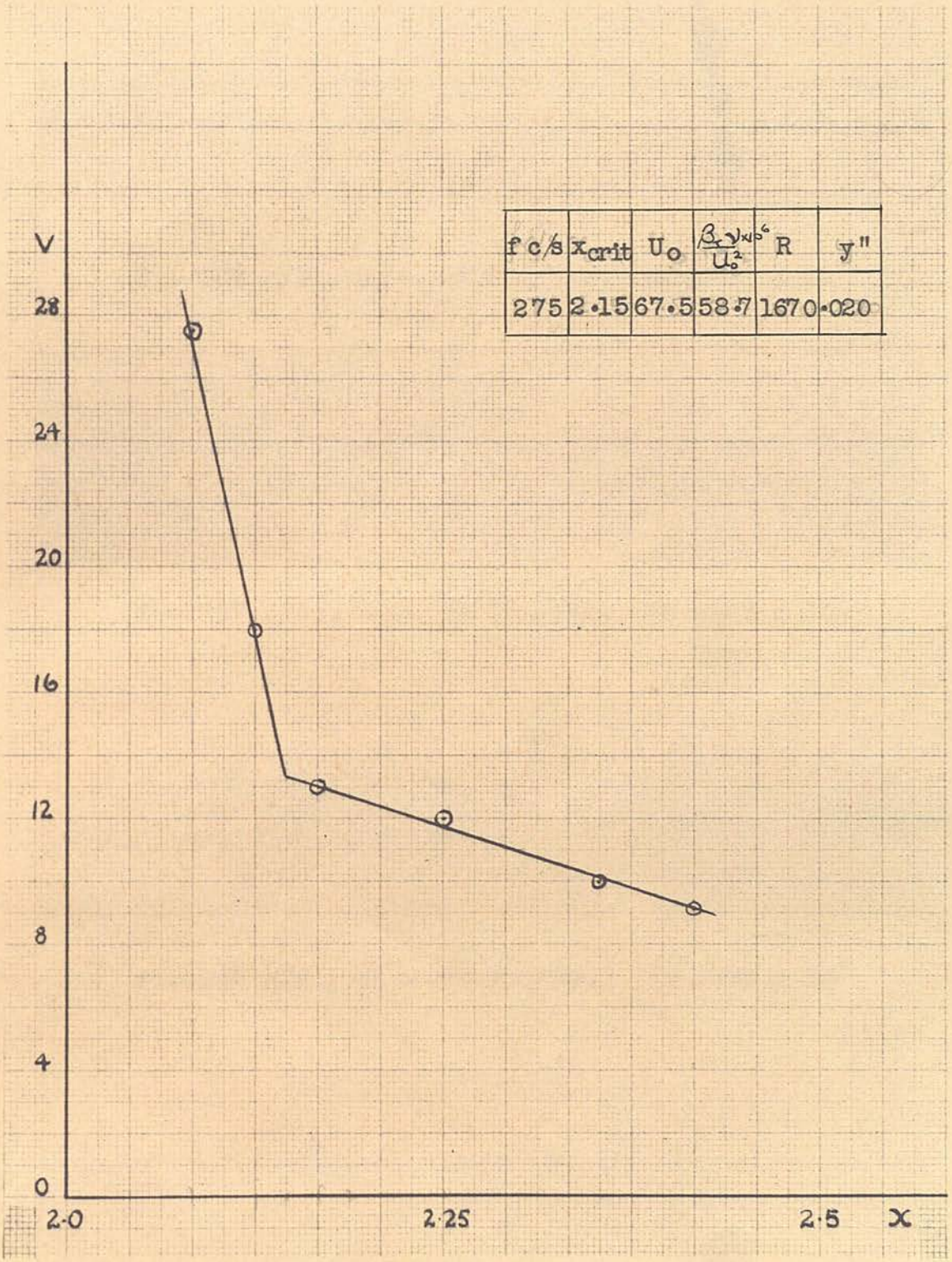

f c/s	x_{crit}	U_o	$\frac{\beta_x \nu \times 10^6}{U_o^2}$	R	y"
275	2·15	67·5	58·7	1670	·020

FIG.67 x traverse across Branch 2 of Neutral Curve.

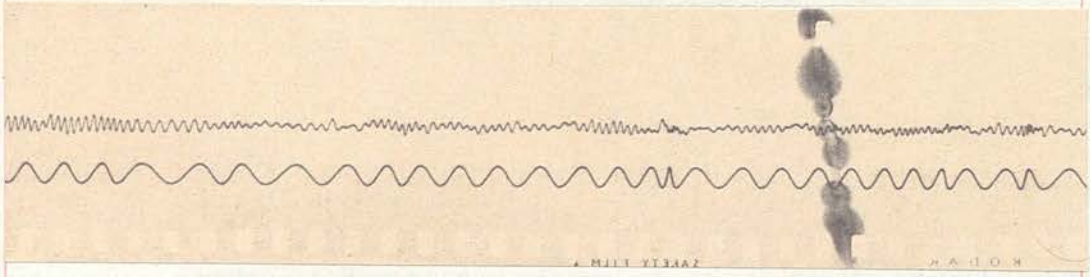

f = 267 c/s., U_o = 64 ft./sec. Rx = ·72 x 10^6

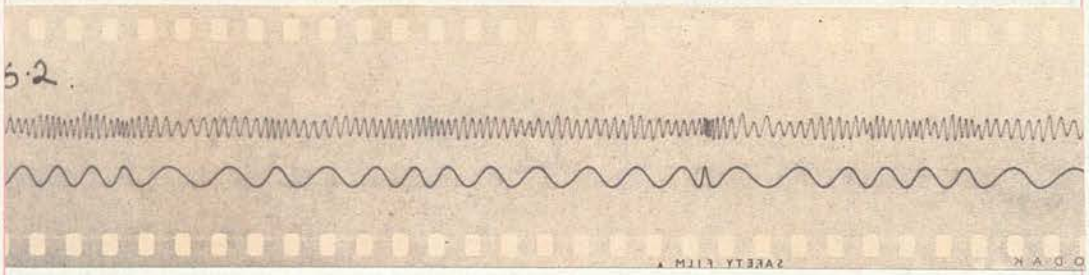

f = 267 c/s., U_o = 64 ft./sec. Rx = ·78 x 10^6

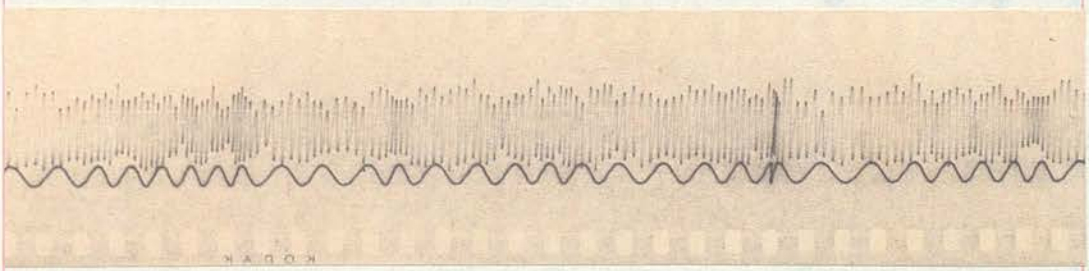

f = 267 c/s., U_o = 64 ft./sec. Rx = ·83 x 10^6

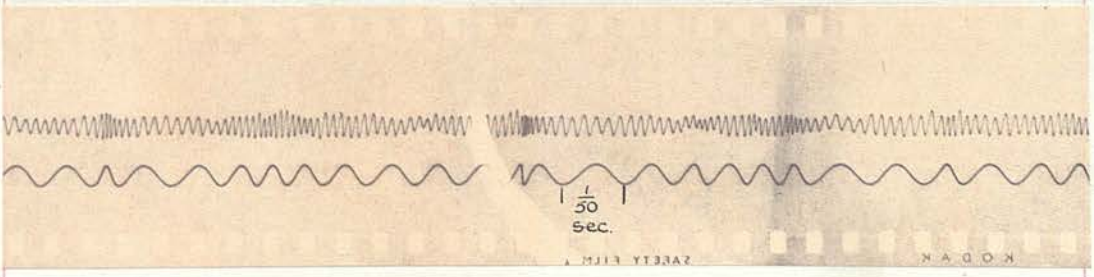

f = 267 c/s., U_o = 64 ft./sec. Rx = ·90 x 10^6

FIG.68 Amplitude variation of Artificial Disturbance across Branch 2 of Neutral Curve.

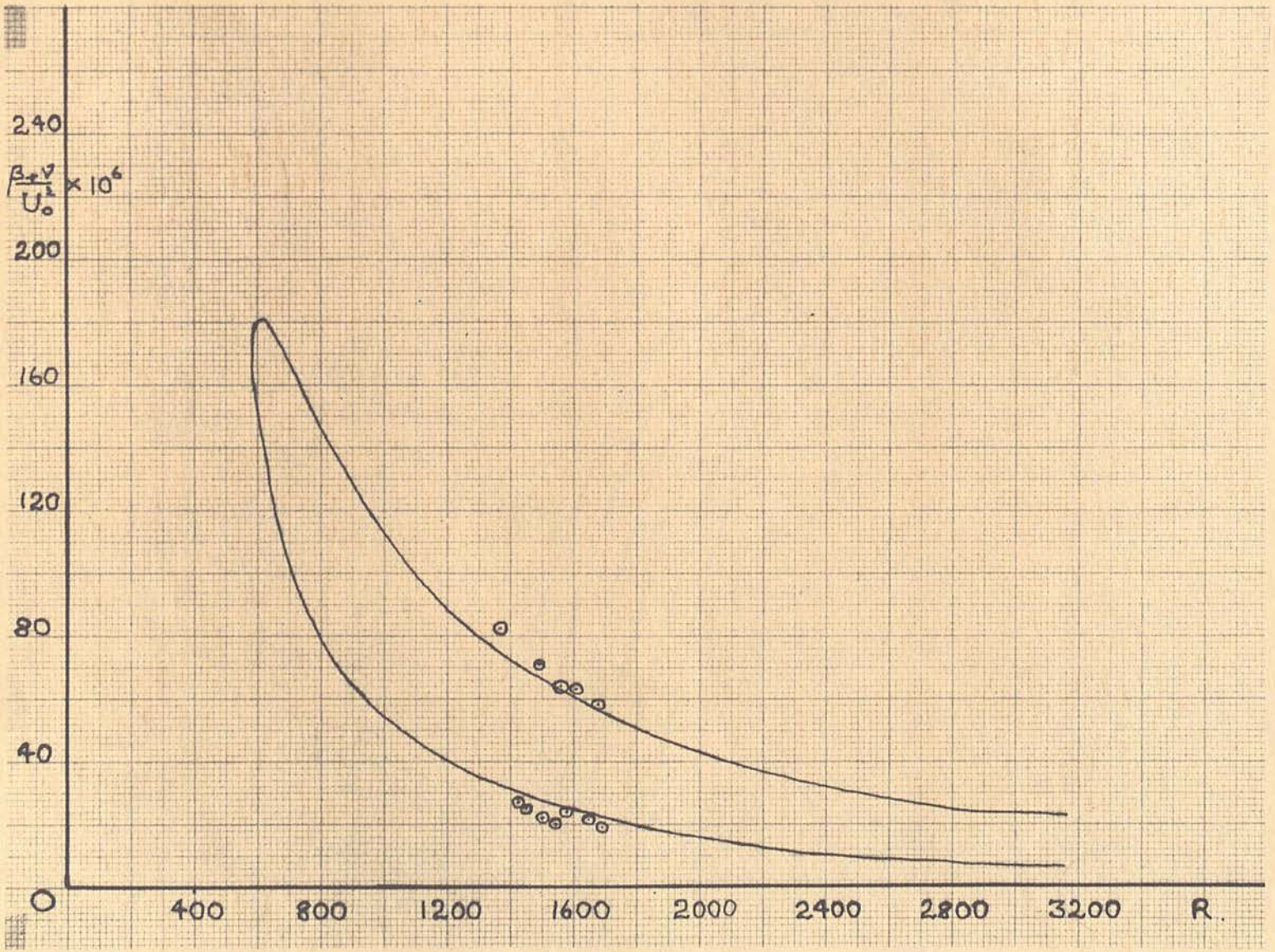

FIG.69 Experimental points on Neutral Stability Curve.

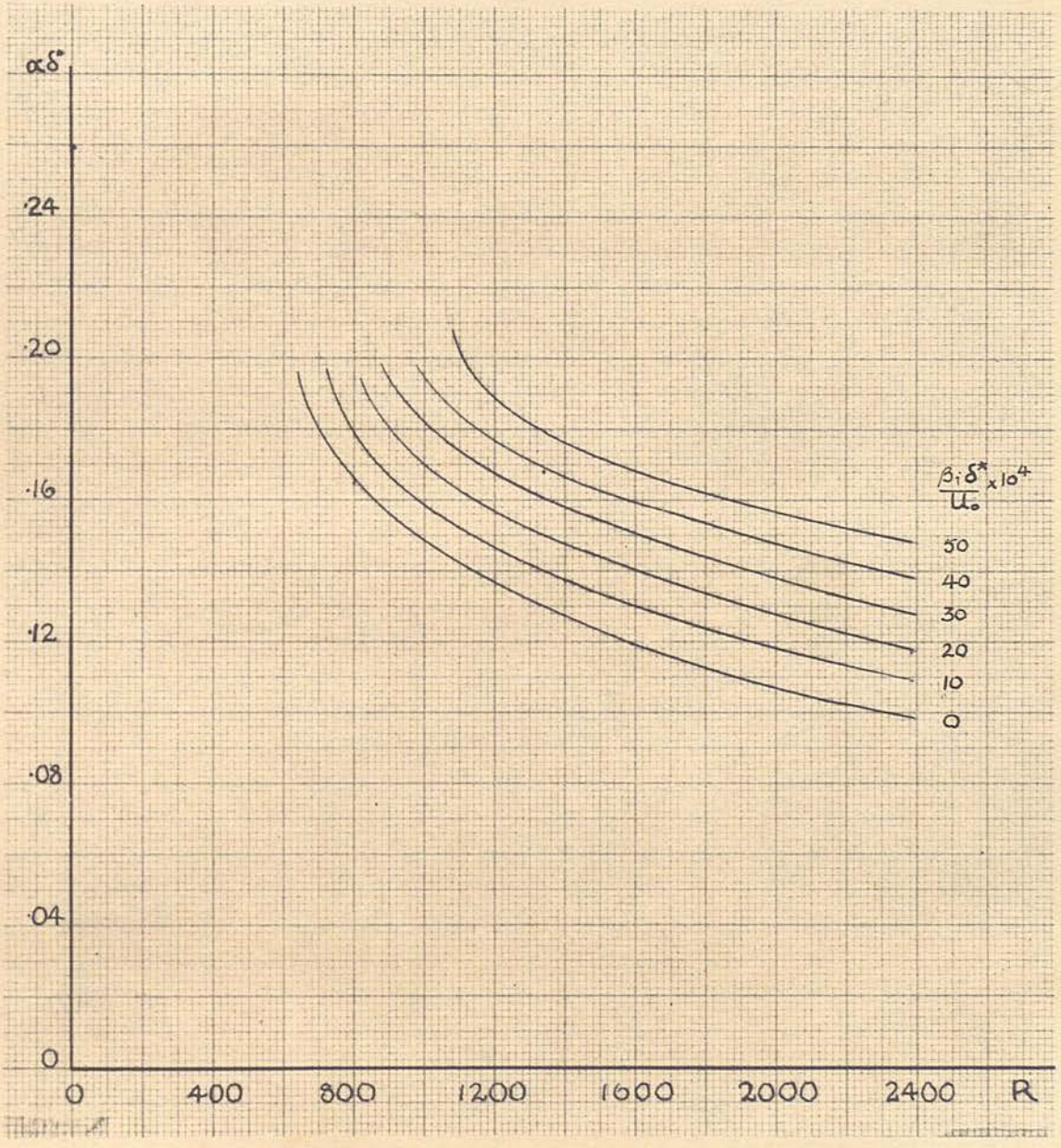

FIG.70 Contours of Equal Amplification according to Schlichting.

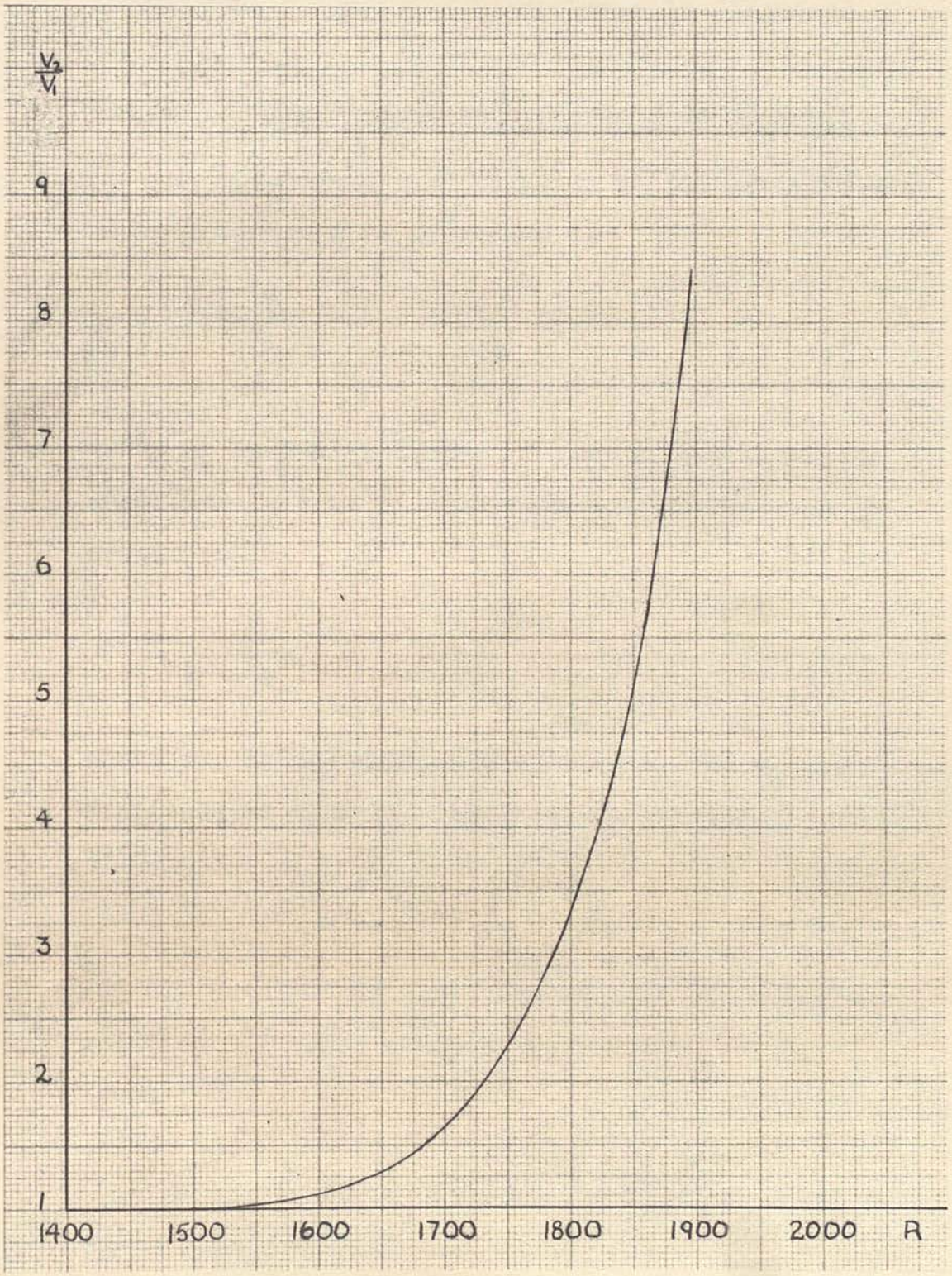

FIG.71 Theoretical amplification of disturbance at Branch 1 of Neutral Curve $U_o = 63$ ft/sec., $f = 90$ c/s.

effect of the high free stream turbulence on a theoretically amplified disturbance is discussed.

5.4.2. Theoretical Amplification at Branch 1

In accordance with equation 9 the amplification of a disturbance is expressed by

$$\frac{A_2}{A_1} = \exp \int_{t_1}^{t_2} \beta_i \, dt$$

where A_1 is the amplitude at time t_1, and A_2 is the amplitude at time t_2, and therefore in the case of disturbances,

$$\frac{V_2}{V_1} = \exp \int_{t(x_1)}^{t(x_2)} \beta_i \, dt$$

where v_1 is the amplitude at time t_1 and v_2 the amplitude at time t_2. This can be written

$$2.3 \log_{10} \frac{V_2}{V_1} = \int_{t(x_1)}^{t(x_2)} \beta_i \, dt$$

and differentiating with respect to t and using the relation $\frac{dx}{dt} = Cr$, where C_r is the wave velocity, gives

$$\beta_i = 2.3 \, C_r \frac{d\left(\log_{10} \frac{V_2}{V_1}\right)}{dx}$$

The wave velocity C_r is obtained from Fig. 50 and for the conditions U_o = 63 ft./sec., f = 90 c/s.,

C_r is 18.9 ft./sec. The variation of the coefficient of amplification β_i with Reynolds number is obtained from Fig. 70, which is a set of theoretical curves, of contours of equal amplification, according to Schlichting. The amplification of the disturbance can now be evaluated as it crosses the amplification zone, and the curve obtained for the above conditions is shown in Fig. 71. The curve is exponential and from R = 1500 to R = 1600 the amplification is very slight, and can be considered effectively constant over this region. After a Reynolds number of 1700 the amplitude begins to increase rapidly as the steep part of the exponential curve is approached. In other words, when the disturbance enters the amplification zone, for the first 4" effectively no amplification will take place, for the second 4" slight amplification will occur, and after this the amplitude will increase rapidly.

It is to be expected therefore that over the first few inches, the vane will be unable to detect any change in amplitude of the disturbance and for the next few inches the increase should be slight, finally followed by a significant increase in the output with increasing x distance. Why has the vane detected a sudden change of gradient rather than a gradual one as the neutral curve is crossed?

An explanation of this is found by examining the effect of the high free stream turbulence on the laminar oscillations. Due to the high turbulence level of the tunnel the percentage of total energy in the boundary layer, centred around the frequency being amplified is much less than at low levels of free stream turbulence. This is due to the fact that the rapidity with which the surrounding spectrum feeds off that being amplified, depends on the free stream turbulence. For high levels of turbulence this redistribution of energy is very rapid, and therefore the frequency response of the spectrum is much flatter than for low levels of turbulence.

Consider a disturbance of frequency f approaching Branch 1 of the neutral curve. As this disturbance leaves the ribbon the percentage of the total energy centred around f will be high. As the wave travels downstream however, as well as being damped the energy will be redistributed, and frequencies $f \pm \Delta f$ will now have an amplitude comparable with that of the original frequency f. Instead of considering just one dominant frequency f approaching Branch 1, a band of frequencies centred around f has now to be considered. From the slope of Fig. 65, it can be seen that when this band of frequencies encounter Branch 1, the frequency $f + \Delta f$ will be amplified first. The

amplitude of $f + \Delta f$ will begin to increase, but immediately this occurs, the energy will be redistributed and a part will be fed back to the original frequency f. This will tend to neutralize any natural damping, which the frequency f should undergo in the region preceding Branch 1 of the neutral curve. For a frequency of 90 c/s., and assuming a bandwidth $2 \Delta f$ of 20 c/s., then it can be seen from Fig. 65, that the frequency $f + \Delta f$, or 100 c/s., will commence to be amplified 6" upstream of the frequency of 90 c/s. Therefore by the time $f + \Delta f$ has travelled 6" into the amplification zone, the amplitude will be beginning to increase rapidly, and therefore the energy fed back to the frequency f will be considerable, and a sharp change in gradient will result, thus eliminating the gradual slope at the beginning of the amplification curve for the frequency f. The accuracy of the position of the point on the neutral curve depends on the breadth of the frequency spectrum, which in turn depends on the free stream turbulence. If the free stream turbulence is low, a large percentage of the total energy will be centred around the amplified frequency, accurate changes in gradient will be recorded and hence accurate points on the neutral stability curve will result. But with a broad bandwidth, corresponding to high

free stream turbulence, premature amplification will be recorded, with a consequent loss of accuracy of the point on the neutral curve.

For an explanation of the shape of the graphs and the position of points obtained on Branch 2 of the neutral curve, a similar argument can be applied. This time energy will continue to be fed in from frequency $f - \Delta f$ after the neutral curve has been crossed.

5.4.3. Position of Points on the Neutral Curve.

As can be seen from Fig. 69, the experimental points lie within a limited range of Reynolds number. The upper limit of this range is determined by the premature turbulence caused by the transverse contamination wedges, which occurs at a distance of 3'6" from the leading edge. To observe amplification followed by damping, without interference from the wedges of turbulence no reliance could be placed on measurements above about 3'3", and this formed the upper limit.

The Reynolds Number of the lower limit was determined by the position of the vibrating ribbon. It has already been stated at the beginning of this chapter that the nearest the ribbon could be placed to the leading edge of the plate was 1 foot, and this figure governed the lower Reynolds number limit.

5.5. Conclusions

From the results it can be seen that the vane can detect disturbances of the order of $\frac{v}{U_o} = 0.5\%$, and yet no pure natural laminar oscillations were observed. Hence either the turbulence level of the tunnel was too high to admit the observation of natural oscillations, or else they had not had sufficient amplification before being interrupted by the transverse contamination wedges.

The Neutral Stability Curve has been verified over a limited range of Reynolds number for v disturbances using artificial perturbations, induced in the flow by a vibrating ribbon. The experimental points do not lie directly on the curve but are displaced slightly, by an amount determined by the free stream turbulence.

In conclusion it may be said that if the turbulence level were lower and no transverse contamination wedges were present, laminar oscillations would be detected at greater Reynolds numbers, than were attainable in this tunnel. Increased accuracy of the position of the points on the Neutral Stability Curve, and also a larger range of experimental points, would result from a lower free stream turbulence.

GENERAL CONCLUSIONS

From the results of Chapter 5, it may be said that the vane has been successful in detecting v fluctuations of velocity. The Neutral Stability Curve has been verified over the region R = 1300 to R = 1700, the limitations of the tunnel preventing a greater range being investigated. Although the sensitivity of vanes in this report was of the order $\frac{v}{U_o} = 0.5\%$, with a lower turbulence level the signal/noise ratio of the disturbance will be greater, and it may be expected that the vane will become more sensitive.

The free stream turbulence could be reduced by having a larger contraction ratio and a finer honeycomb. For a worthwhile reduction of free stream turbulence, a contraction ratio of at least 15 : 1 would have to be built. However, if this were the case the inlet flare would then become so close to the ceiling that the inflow would be disturbed.

The ultimate aim of the project had been to extend the investigation into the natural transition and turbulent regions. However, it can be seen from the results of Chapter 2, that due to the transverse contamination wedges, it will only be possible to examine the fringe of the transition region. Hence it will be impossible to relate the spectrum of a natural turbulent burst, to the high amplitude laminar

oscillation from which it was formed.

Initial information on the performance of the vane in turbulence could be obtained by examining either the turbulent wedges, or a spot of turbulence formed in the boundary layer by means of a spark discharge. Perhaps the most useful experiment to adopt, would be to place the ribbon in the boundary layer, and to increase the amplitude of vibration until premature transition along a line resulted well forward from that of the contamination wedges. In this way control would be obtained over the transition front and the oscillations would contribute to transition.

REFERENCES

Batchelor, G.K. On the concept and properties of the idealized hydrodynamics resistance, A.C.A. 13 (1945)

Blasius, H. Grenzschichten in Flüssigkeiten mit kleiner Reibung. Z. Math. u. Phys., 56, 1 (1908). NACA Tech. Memo. No. 1256.

Burgers, J.M. The motion of a fluid in the boundary layer along a plane smooth surface. Proc. of the 1st Intern. Cong. App. Mech., 113, Delft (1924).

Charters, A.C. JR. Transition between laminar and turbulent flow by transverse contamination. NACA T.N., 891, (1943).

Clapp, J.K. An inductance - capacitance oscillator of unusual frequency stability, Proc. I.R.E. p. 356 (1948).

Dryden, H.L. Boundary layer flow near flat plates. Proc. 4th Intern. Cong. App. Mech. 175, Cambridge (1934).

Dryden, H.L. Turbulence and the Boundary Layer. J. Aero. Sci., 6, 85 and 101 (1939).

Dryden, H.L. Fifty years of Boundary-layer theory and Experiment. Sci., 121, 375-380 (1955).

Emmons, H.W. The laminar-turbulent transition in a boundary layer, Part 1 Journ. Aero. Sci., 18, No. 7, 490 (1951).

Hama, F.R. & Tani, I. Some experiments on the effect of a single roughness element on boundary layer transition. Journ. Aero. Sci. 20, No. 4, 289 (1953).

Howarth, L. On the solution of the laminar boundary layer equations. Proc. Roy. Soc. A, 164, 547 (1938).

Lin, C.C. On the stability of two-dimensional parallel flows. Quarterly App. Math., 3, 117 (1945); 3, 218 (1945); 3, 277 (1946).

McPhail, D.C. Turbulence changes in contracting and distorted passages. R. & M. 2437 (1944).

Nikuradse, J. Laminare Reibungsschichten an der längsangeströmten Platte. Monograph, Zentrale f. wiss. Berichtwesen, Berlin (1942).

REFERENCES (Contd.)

Prandtl, L. Über Flüssigkeitsbewegung bei sehr kleiner Reibung. Proc. 3rd Intern. Math. Cong., Heidelberg (1904). NACA Tech. Memo. No. 452, (1928).

Schlichting, H. ZAMM 13, 171 (1933).

Schlichting, H. ZAMM 15, 313 (1935).

Schlichting, H. 'Boundary layer theory.' (1951).

Schubauer, G.B. Rep. Nat. Adv. Ctee. Aero. Wash. No. 524 (1935).

Schubauer, G.B. & Klebanoff, P.S. Contributions on the mechanics of boundary layer transition. Paper No. 4 Symposium on boundary layer effects in aerodynamics. N.P.L. (1955).

Schubauer, G.B. & Skramstad, H.K. Jour. Res. Nat. Bur. Stand. RP. 1722, Vol. 38 (1947) NACA. Report No. 909.

Taylor, G.I. Statistical theory of turbulence V - Effect of turbulence on boundary layer. Proc. Roy. Soc. A, 156, No. 888, 307, (1936).

Taylor, G.I. Statistical Theory of turbulence. Proc. Roy. Soc. 151, 421 (1935).

Tollmien, W. NACA Tech. Memo. No. 609 (1931).

Tollmien, NACA Tech. Memo No. 792 (1936).

Whiddington, Radio micrometer. Phil. Mag. 15, 634, (1920).

ACKNOWLEDGMENTS

I thank Dr. M.A.S. Ross for suggesting the topic of this research, and for her constant advice and guidance throughout the course of the work. My thanks are also due to Professor W.H.J. Childs for his advice on the many problems occurring in connection with the wind tunnel.

I am indebted to Professor N. Feather, F.R.S., who assisted and encouraged the project in every possible way. I must also thank Mr. C.W. Davidson of the Engineering Department for his assistance in the design of the electronics, and Dr. E.J. Williams for his advice and careful scrutiny of the manuscript.